Dissertation zur Erlangung des Doktorgrades
der Fakultät für Chemie und Pharmazie
der Ludwig-Maximilians-Universität München

Structural and functional analysis of DNA binding by the Rad50 catalytic head from *Thermotoga maritima*

Anna Maria Rojowska
aus
Kraków, Polen

2013

Erklärung

Diese Dissertation wurde im Sinne von § 7 der Promotionsordnung vom 28. November 2011 von Herrn Prof. Dr. Karl-Peter Hopfner betreut.

Eidesstattliche Versicherung

Diese Dissertation wurde selbständig ohne unerlaubte Hilfe erarbeitet.

München, den 03. Dezember 2013

.....

Anna Maria Rojowska

Dissertation eingereicht am 19. September 2013

1. Gutachter: Prof. Dr. Karl-Peter Hopfner
2. Gutachter: Prof. Dr. Mario Halic

Mündliche Prüfung am 26. November 2013

This thesis has been prepared from September 2009 to September 2013 in the laboratory of Prof. Dr. Karl-Peter Hopfner at the Gene Center of the Ludwig-Maximilians-Universität München.

Publications

During the work on this thesis, following publication was published:

Strasser D., Neumann K., Bergmann H., Marakalala M. J., Guler R., Rojowska A., Hopfner. K.-P., Brombacher F., Urlaub H., Baier G., Brown G. D., Leitges M., Ruland J. (2011). **Syk kinase-coupled C-type lectin receptors engage protein kinase C-σ to elicit Card9 adaptor-mediated innate immunity.** *Immunity* 36 (1): 32-42.

During the work on this thesis, following publication was published:

Oral presentation at the EMBO Conference: DNA damage response in cell physiology and disease, 7-11 October 2013, Cape Sounio, Greece

Table of content

1. SUMMARY 1
2. INTRODUCTION 2
2.1. DNA damage and repair 2
2.2. Causes of double-strand breaks 4
2.2.1. Double-strand breaks of endogenous source 4
2.2.2. Double-strand breaks of exogenous source 4
2.2.3. Double-strand breaks in cell physiology 5
2.3. DSB repair 6
2.3.1. Homologous recombination 6
2.3.2. NHEJ 8
2.4. Repair pathway choice 11
2.5. Mre11-Rad50-Nbs1 complex: structural characterization 11
2.6. Mre11-Rad50-Nbs1 complex in cell physiology 17
2.6.1. HR in mitotic DSB 17
2.6.2. NHEJ 18
2.6.3. Telomeres 18
2.6.4. Meiosis 19
2.6.5. Signalling 19
2.6.6. Mre11-Rad50 complex in prokaryotes 20
2.7. Disease 22
2.8. Mre11-Rad50 complex from *Thermotoga maritima* and other prokaryotes 23
2.9. Aims of the project 24
3. MATERIALS AND METHODS 26
3.1. Materials 26
3.2. Molecular biology methods 33
3.3. Protein biochemistry methods 36
3.4. Structural biology methods 41
3.5. Yeast specific methods 43
3.6. *Xenopus laevis* specific methods 45
3.7. Bioinformatic methods 47
4. RESULTS 48
4.1. Preparation of the $Rad50^{NBD}$-$Mre11^{HLH}$ complex from *T. maritima* 48
4.1.1. Cloning and purification 48
4.1.2. Dimerization 49
4.2. Crystal structure of $tmRad50^{NBD}$-$Mre11^{HLH}$ with DNA 50
4.2.1. Crystallization and structure determination 50
4.2.2. Crystal structure of the $tmRad50^{NBD}$-$Mre11^{HLH}$-DNA 54
4.3. Characterization of the $tmRad50^{NBD}$-$Mre11^{HLH}$ *in vitro* 56
4.3.1. DNA binding properties of the wild-type $tmRad50^{NBD}$-$Mre11^{HLH}$ 56

4.3.2. Model of DNA binding and DNA-binding properties of the tmRad50^{NBD}-Mre11^{HLH} point mutants *58*
4.4. Structure-based characterization of Rad50 point mutations in *S. cerevisiae* 63
4.4.1. Response to DNA damage *64*
4.4.2. End-joining activity *68*
4.4.3. Telomere maintenance *68*
4.5. Establishment of the hMRN-induced ATM activation in *Xenopus laevis* interphase egg extract 70
4.5.1. Preparation of the recombinant hMRN *70*
4.5.2. Interphase X. laevis egg extracts *71*
4.5.3. DNA-induced ATM activation in interphase X. laevis egg extracts *72*
4.6. Rescue of ATM activation by the hMRN complex 73
5. DISCUSSION 75
6. REFERENCES I
7. ABBREVIATIONS XIII
8. CURRICULUM VITAE XVI
9. ACKNOWLEDGEMENTS XVII

1. Summary

Double-strand breaks are among the most deleterious DNA lesions, with a single unrepaired break capable of inducing apoptosis. This highly cytotoxic damage requires a fast and efficient cellular response. DSBs are repaired in two distinct repair pathways: homologous recombination or non-homologous end joining. Both of these repair systems ensure recognition of the damage site, activation of the cell-cycle checkpoint and repair of the lesion.

A key player in the DSB repair is the conserved Mre11-Rad50-Nbs1 complex. The enzymatic core of this assembly – Mre11-Rad50 – is highly conserved and found in all domains of life. Eukaryote-specific Nbs1 (Xrs2 in *S. cerevisiae*) is a signalling subunit transmitting the damage event to the ATM kinase.

Rad50 shares homology with the SMC protein family. Its dimer comprises two globular bipartite ATPase domains and two coiled-coil domains. The nuclease Mre11 also forms a dimer and associates with Rad50. This conserved catalytic head is believed to recognize DSB and form a DNA-binding interface. Moreover, the MR complex takes part in the initial processing of DNA ends and signals the lesion to the cell-cycle control machinery activated via Nbs1-ATM interaction. Nbs1 carries Mre11- and ATM-binding motifs and mediates damage recognition with checkpoint activation. The MRN complex is required not only for the repair of mitotic DSBs but also plays a role in meiotic recombination, telomere maintenance and adaptive immune system development. This multifaceted behaviour of the complex lies in its enzymatic activities, as well as DNA bridging and tethering function and activation of ATM-induced repair signalling.

This work attempted to characterize molecular principles of DNA recognition by the catalytic part of the bacterial Rad50. To this end, the enzymatic core of *T. maritima* Rad50 together with an interaction motif of Mre11 was crystallized with AMPPNP and a dsDNA molecule. In the structure, DNA binding is asymmetrical and involves residues on both the globular head of the Rad50 and the root of the coiled-coil domain. Further studies were performed to biochemically characterize the protein-DNA complex and the identified binding sites. The atomic model yielded a number of structural features that were analyzed *in vitro* and *in vivo*. Finally, significance of these features together with the current understanding of the DNA binding by the MRN complex are discussed.

2. Introduction

2.1. DNA damage and repair

Stability of the genetic information is one of the most crucial features of the cellular metabolism. However, a number of intra- and extracellular factors are able to compromise the composition or structure of the DNA, inducing either chemical modifications or direct breakage in the sugar-phosphate backbone. Resulting local DNA alterations may interfere with progression of transcription and replication and as a consequence pose a threat to DNA integrity.

A vast number of DNA lesions and modifications together with their respective repair mechanisms have been reported so far (Figure 1). Minor modifications (*e. g.* alkylations) that do not distort base-pairing and overall topology of the DNA can be readily repaired through direct DNA damage reversal (DDR). In most cases, DDR relies on the activity of a single enzyme, capable of removing UV-induced modifications without backbone incisions or base excisions (Eker et al. 2009).

More complex base modifications that cannot be repaired by DDR are often subjected to base-excision repair (BER) machinery. This pathway relies on a cross-talk between several co-factors of distinct enzymatic activities that ensure base excision, strand incision and removal of the sugar moiety. The resulting gap is refilled by BER-associated polymerases followed by ligation (Robertson et al. 2009). Both DDR and BER act on local modifications that do not affect the overall structure of the DNA and hence do not impede DNA metabolism. Hence, these repair pathways prevent small-scale deletions and sequence alterations during replication and transcription. More complex modifications, including inter- and intrastrand crosslinks locally distorting DNA structure, are mostly repaired by nucleotide-excision repair (NER) machinery (Nouspikel 2009). Damages subjected to this repair pathway arise mostly as a result of both intracellular and environmental stress, such as reactive oxygene species (ROS), ultraviolet (UV) radiation and genotoxic agents. Similarly to BER, the NER system employs a number of enzymatic factors that ensure sensing of the distorted DNA, local duplex melting and removal of the lesion-containing single-stranded fragment together with its flanking sequences. The missing segment is then filled by polymerase I and the newly synthesized polynucleotide chain is ligated with the remaining part of the strand. NER can occur co-transcriptionally and is then considered a separate repair pathway called transcription-coupled repair (TCR). DNA damage can severely

affect transcription progression, being harmful to the cell at two distinct levels: as a source of mutations and as an inducer of an altered gene expression profile. Therefore, TCR ensures that the lesions not repaired prior to transcription can be efficiently removed before they interfere with DNA metabolism. TCR and NER share the same overall scheme of the repair pathway and repair machineries except from the distortion-sensing step. In case of TCR, transcribing RNA polymerase II acts itself as a sensor of the DNA distortion, whereas NER employs other specialized protein complexes to sense the damage (Tornaletti 2009).

Another type of DNA modification are mismatches, occasionally introduced into the newly synthesized strand during replication. Mismatches consist of erroneous base pairing, instead of Watson-Crick A-T and G-C pairing. From structural point of view they do not interfere with DNA metabolism but may lead to sequence alterations. Mismatches are repaired in a mismatch repair (MMR) pathway; they are recognized by the replication proofreading machinery and removed together with an adjacent DNA fragment. Finally, the gap is refilled by polymerase III (Kunz, Saito, and Schar 2009).

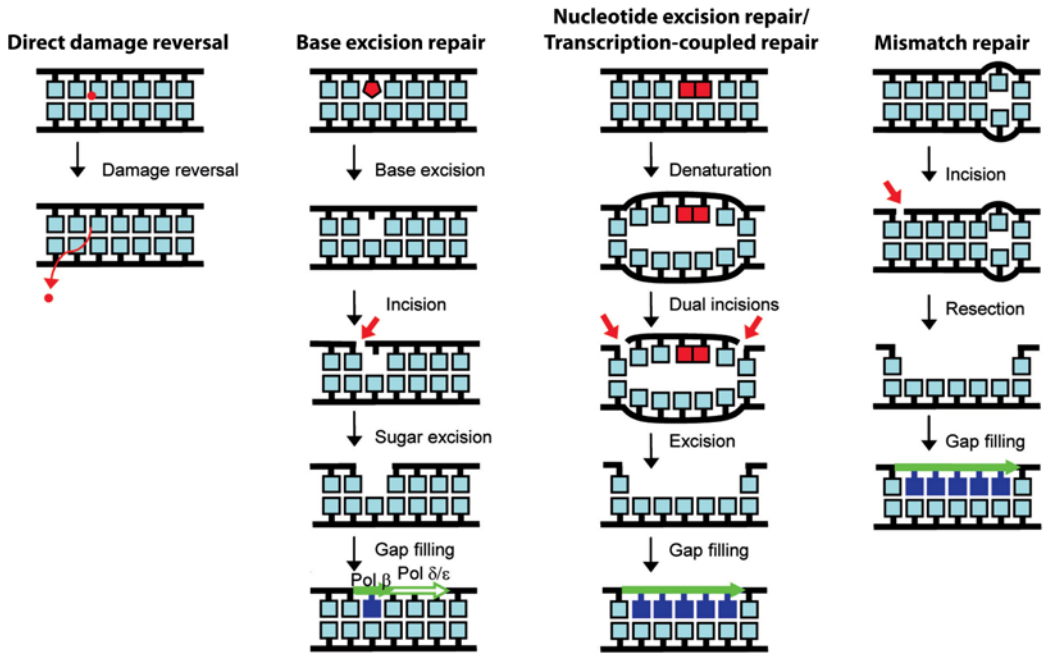

Figure 1. Overview of DNA repair pathways. DNA can be repaired by direct damage reversal, base excision repair, nucleotide excision repair, transcription-coupled repair and mismatch repair systems, depending on the nature of the lesion. Adapted from: (Nouspikel 2009).

This work focused on double-strand break repair (DSBR), a DNA repair system employed for damages involving breakage of the sugar-phosphate backbone on both DNA strands within a short-span distance. This type of damage is severely harmful and its detailed description is presented in the following paragraphs.

2.2. Causes of double-strand breaks

Double-strand breaks (DSBs) are considered one of the most deleterious DNA lesions and pose a severe threat to genomic stability, with a single unrepaired break being capable of inducing apoptosis. DSBs can arise spontaneously in a number of ways of both intra- and extracellular origin, but are also introduced in a programmed manner during certain cellular processes like meiosis or recombination of immunoglobulin genes. Both programmed and non-programmed DSBs depend on common repair pathways.

2.2.1. Double-strand breaks of endogenous source

The most prominent DSB source is replication. Many of physical and chemical DNA poisons discussed below do not introduce DSBs directly, but affect replication progression. This replicative stress leads to fork stalling and consequently to fork collapse, thereby exposing "naked" DNA ends (Costanzo et al. 2001; Kuzminov 2001). Another endogenous source of DSBs is products of cellular metabolism like reactive oxygen species. ROS are generated during cellular respiration and lipid peroxidation but can also arise as a result of ionizing radiation. A number of ROS-induced modifications of DNA has been reported, including protein-DNA adducts, base modifications, abasic sites, single-strand breaks (SSBs) and inter- and intrastrand crosslinks (Waris and Ahsan 2006). These lesions are repaired predominantly by BER and NER systems. However, if this repair fails, the damage imposes stress during replication and can elicit double-strand break response.

2.2.2. Double-strand breaks of exogenous source

Primary causes of DSBs of extracellular origin are ionizing radiation (IR), UV light and genotoxic agents. The most frequent DNA damage resulting from UV radiation are cyclobutane pyrimidine dimers (CPDs) and 6-4 photoproducts. These lesions contain covalent linkages between neighbouring thymines or cytosines (Goodsell 2001). UV-induced DNA modifications distort the structure of DNA and hence, are mostly repaired by the NER system. However, unless

repaired, they contribute to replicative stress, leading to fork stalling and collapse (Limoli et al. 2002).

Another environmental source of DSB is IR. The spectrum of damage caused by IR is very broad, including direct base and sugar moiety modifications. Moreover, IR generates ROS that in turn damage DNA (Mahaney, Meek, and Lees-Miller 2009). An example of IR-induced DSB is two single-strand breaks occurring on complementary strands and in close proximity to each other (Breen and Murphy 1995). Also, unrepaired SSB can interfere with replication progress, leading to fork stalling and collapse (Sutherland et al. 2000). IR potential of introducing modifications in DNA and triggering cell death is employed in some cancer treatment therapies (Ciccia and Elledge 2010).

A vast number of genotoxic agents that introduce severe DNA damage including DSBs have also been reported. Many of them cause inter- and intrastrand crosslinks, thereby interfering with transcription and replication (Bosco et al. 2004). A very specific group of chemical agents that damage DNA includes topoisomerase poisons like camptothecin, etoposide and their derivatives. These agents inhibit activity of topoisomerases and eventually cause defects in DNA structure. Distortions of DNA may in turn affect DNA metabolism, leading again to replication fork collapse. Equally harmful are alkylating agents attacking nitrogen atoms in base moieties and contributing to strand crosslinks (Singer 1986). Many of the genotoxic agents, including topoisomerase poisons, have found use as anti-cancer drugs.

2.2.3. Double-strand breaks in cell physiology

Introduced in a programmed manner and tightly regulated DSBs are a feature of certain cellular events. Such DSBs arise during meiosis and are fundamental to **crossing-over reaction**, allowing for exchange of genetic information between homologous chromosomes. This process takes place in prophase I of the meiotic division in sexually reproducing organisms. Crucial to meiotic DSB generation is Spo11 topoisomerase II that introduces an endonucleolytic cleavage on both DNA strands. This event fires off meiotic recombination, including crossing-over and break repair by homologous recombination (Keeney 2008).

Programmed DSBs are also fundamental to proper immunoglobulins (Ig) and T-cell receptors (Tcr) expression in B and T cells, respectively, and as such are prerequisite for the adaptive

immunity development in vertebrates. Genes coding Igs and Tcrs require a highly regulated processing that consists in excision, relocation and religation of distinct genetic segments. These genetic segments: variable (V), diversity (D) and joining (J) can be recombined in an endless number of configurations in a process called **V(D)J recombination**. V(D)J is a powerful tool for generating Igs and Tcrs recognizing a variety of antigens. The process requires a programmed formation of DSBs by RAG1/RAG2 (recombination-activating genes) nucleases (McBlane et al. 1995). Subsequently, the DSB site is processed by the non-homologous end joining repair machinery (Ma et al. 2002).

In yeast *Saccharomyces cerevisiae*, programmed DSBs are introduced during **mating-type switch**. Yeast haploid cells exhibit a simple sexual differentiation based on a single *MAT* locus denominated as type a or type α. During the mating-type switch, a sequence-specific HO endonuclease introduces a DSB at *MAT* locus, followed by resection of this locus and homology-governed repair. Homologous sequence involved in the repair process is a silent copy of the opposite *MAT* allele (Coic, Richard, and Haber 2006).

2.3. DSB repair

Unrepaired DSBs are among the most deleterious DNA lesions. Therefore, cells have developed a fast and efficient repair system, employing DSBs sensors, repair complexes and a signalling machinery. The two main DSB repair pathways are homologous recombination (HR) and non-homologous end joining (NHEJ). HR is a highly faithful pathway, in which a non-damaged homologous DNA segment (usually a sister chromatid) governs the repair of the lesion. NHEJ is more error-prone and involves a partial resection of the broken DNA ends followed by ligation. Since NHEJ is not accompanied by a large-scale polymerase gap filling, deletions and sequence alterations often arise in the religated DNA helix.

2.3.1. Homologous recombination

The process of homologous recombination starts with an extensive resection of the damage site in the 5'-3' direction, resulting in a generation of single-stranded 3' overhangs (Figure 2, panel A). Upon sensing the DNA damage, the Mre11-Rad50-Nbs1 (MRN) complex together with the Sae2 nuclease (*S. cerevisiae*; CtIP in human, Ctp1 in *S. pombe*) catalyzes removal of a short oligonucleotide from each 5' end. This short-term end processing is followed by a long-term

resection performed by ExoI or alternatively Dna2/Sgs1 complex. Resulting 3' overhang is recognized by a ssDNA-binding factor RPA (replication-protein A) (Gasior et al. 1998; Wolner et al. 2003), which is believed to play multiple roles in the initiation of HR. Firstly, RPA removes secondary structures on the overhang. It facilitates the following step of the repair reaction during which Rad51 associates with ssDNA (Sung et al. 2003), and regulates resection by stimulating activity of the Sgs1 helicase and the Dna2 nuclease (Cejka et al. 2010). Moreover, the RPA-ssDNA complex is a target for cell-cycle control kinases, eliciting a cycle arrest until the damage is repaired (Ball et al. 2007; Zou and Elledge 2003). In the course of HR, RPA is slowly displaced from the DNA and exchanged for one of the most crucial HR proteins Rad51 (RecA in *E.coli*). Since the affinity of RPA towards ssDNA is higher compared to Rad51, other protein factors contribute to the efficient cross-talk between RPA and Rad51. These recombination mediators in yeast include Rad52 and a two Rad51 paralogues: Rad55 and Rad57. Their role is to facilitate Rad51-DNA nucleofilament formation by loading Rad51 onto the RPA-coated ssDNA end, mechanistic stabilization of the filament and its protection from helicases (Liu et al. 2011; Shinohara and Ogawa 1998).

Rad51 coats tightly ssDNA, forming an extended presynaptic filament. The synaptic phase of the repair corresponds to the invasion of the filament into the homologous DNA fragment and its annealing to the homologous sequence into a structure called a D-loop. Next, Rad51 dissociates from the DNA, exposing the single-stranded 3' end for priming the DNA synthesis. From this point on, the downstream steps of the repair can follow several pathways (Figure 2, panels B, C and D). In the double-strand break repair model, the second end of the damaged DNA is engaged in the D-loop, forming a double Holiday-junction. Resolution of this Holiday structure can result in both crossover an non-crossover products (Orr-Weaver and Szostak 1983).

Alternatively, the invading strand can be displaced from the D-loop and annealed to a complementary strand associated with the other end of the break. This synthesis-dependent strand-annealing (SDSA) repair occurs preferentially during mitosis and results in non-crossover products (Ferguson and Holloman 1996).

The D-loop can also assemble into a replication fork, in which the homologous sequence serves as a template for a replication-dependent repair. This break-induced replication (BIR) is active on telomere ends where the second DNA end is missing (Davis and Symington 2004).

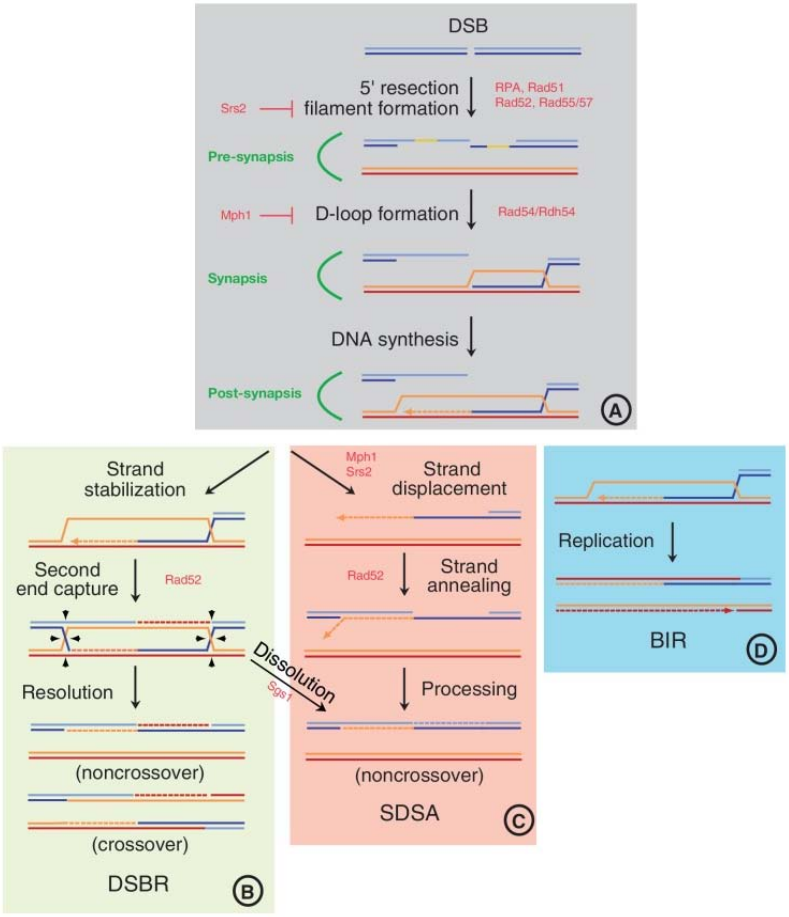

Figure 2. Homologous recombination pathway. After end resection followed by the Rad51-nucleofilament formation and D-loop generation (panel A), the break is repaired in double-strand break repair pathway (panel B), synthesis-depended strand annealing (panel C) or break-induced repair pathway (panel D). Adapted from: (Krejci et al. 2012).

Homologous recombination not only plays a role in the DSBR, but is also involved in the repair of other types of damage, including single-strand gaps and interstrand crosslinks. Hypomorphic mutations in genes involved in HR were recognized to be the cause of many cancer types (*e. g.* breast, prostate, colon and pancreas) and a cancer predisposition syndrome Fanconi anaemia (Halazonetis, Gorgoulis, and Bartek 2008).

2.3.2. NHEJ

Classical non-homologous end joining repair is governed by a conserved set of sensoring and enzymatic factors (Figure 3). The pathway starts with a DSB recognition by the Ku dimer (heterodimer of Ku70 and Ku80), one of the most abundant non-histone nuclear proteins. Ku

exhibits very high affinity to DNA and is therefore considered the sensor of the DNA damage. Ku associates with the DNA ends independently of other proteins, but is at the same time indispensable for the recruitment of all downstream NHEJ factors to the damage site (Walker, Corpina, and Goldberg 2001; Mari et al. 2006).

Ku and catalytic subunit of DNA-dependent protein kinase (DNA-PKcs) participate in forming the active holoenzyme of the DNA-dependent protein kinase (DNA-PK) (Gottlieb and Jackson 1993). DNA-PK carries a number of phosphorylation and autophosphorylation sites (Chan et al. 2002; Meek et al. 2007). Although the exact role of these sites has not been fully examined, some reports link the phosphorylation state of the DNA-PK to conformational changes of the complex, which would govern the dynamics of the NHEJ progression (Uematsu et al. 2007). DNA-PK is also responsible for tethering DNA ends at the damage site (DeFazio et al. 2002).

A bridging component XLF (also named Cernussos) links the recognition Ku-DNA-PK complex with the enzymatic core of NHEJ machinery: the XRCC4-LigIV complex. XLF was shown to stimulate ligation activity of the XRCC4-LigIV complex, in particular on mismatched or incompatible ends (Tsai, Kim, and Chu 2007; Gu et al. 2007).

Depending on the structure of the DNA ends, different downstream enzymatic factors are recruited to the damage site in order to ensure proper repair reaction. If DNA ends contain overhangs, the ligation reaction can only be performed after a short-term processing, leading to generation of blunt ends. Overhangs can be removed or serve as a template for a local replication. Removal of the overhangs depends on Artemis. This nuclease exhibits intrinsic 5'-3' exonuclease activity and a DNA-PK-dependent endonuclease activity (Ma et al. 2002). Alternatively, blunting of the overhangs can be performed by filling in the missing segment by the terminal deoxynucleotidyl transferase (Tdt) (Mahajan et al. 1999), polymerase μ and polymerase λ (Capp et al. 2006; Mahajan et al. 2002). Processing of the DNA ends also include addition of 5' phosphate groups by DNA-PK-XRCC4-dependent polynucleotide kinase (PNK) (Chappell et al. 2002).

In the end, processed DNA is ligated by the XRCC4-LigIV complex. Since the complex can associate with the Ku-DNA-PK assembly before the ends are fully processed, it is not clear at the moment how the ligation reaction is retarded and elicited in a timely-manner.

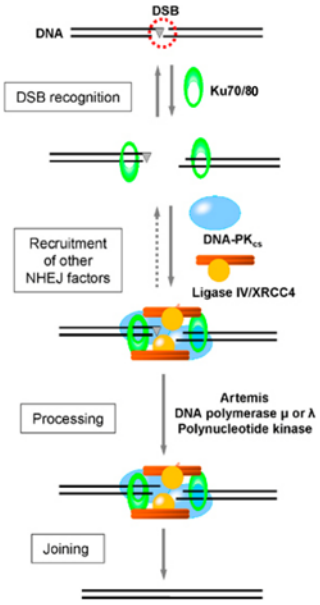

Figure 3. Classical non-homologous end joining pathway. Ku dimer recognizes DNA break and attracts downstream NHEJ-associated repair factors to the damage site. Prior to ligation, DNA ends are processed by Artemis nuclease and polymerases μ, λ and PNK. Adapted from: (van Gent and van der Burg 2007).

Microhomology-mediated end-joining

Microhomology-mediated end-joining **(**MMEJ) is concerned an alternative pathway of NHEJ. MMEJ can be elicited as a backup repair mechanism when short fragments of homology are available in the proximity of the break (so-called microhomologies) (Verkaik et al. 2002; Boulton and Jackson 1996). This rather error-prone pathway is believed to be little efficient in joining blunt DNA ends, but was found to be employed during Ig heavy chain class switch recombination in B cells (Yan et al. 2007). Both classical and alternative NHEJ pathways are supporting break repair at V(D)J recombination sites.

Hypomorphic or loss-of-function mutations in NHEJ subunits have been linked to several human genetic disorders, often accompanied by neurological defects, radiosensitivity, microcephaly and severe combined immunodeficiency (SCID) (Kerzendorfer and O'Driscoll 2009).

2.4. Repair pathway choice

NHEJ is a predominant repair pathway in mammalian cells, whereas yeast cells seem to employ mostly HR (Shrivastav, De Haro, and Nickoloff 2008). Since HR requires sister chromatid, its progression is limited to late S phase and G2 phase of the cell cycle. So far, the reason for the discrepancy in the repair pathway choice between lower and higher eukaryotes is not entirely clear and several hypotheses are under consideration. One postulates that the yeast NHEJ is less accurate and therefore less frequently employed. A few protein factors key to NHEJ in mammalian cells (*e. g.* DNA-PKcs, BRCA1 and Artemis) are missing in the the yeast NHEJ protein machinery. At the same time, mammalian genomes being far larger and structurally more complex than the yeast ones, pose an intrinsic difficulty for the HR machinery to find and recognize a homologous sequence within the vicinity of the damage.

Repair pathway choice is also regulated at the cellular level. HR is favoured in S/G2 phases and NHEJ is restricted mostly to the remaining phases of the cell cycle. In mammalian cells this balance is presumably accomplished by interplay of several regulatory factors, with 53BP1-RIF1 and BRCA1-CtIP being the most crucial complexes. 53BP1-RIF1 interacts with chromatin at DSBs sites and promotes further association of the downstream NHEJ machinery during G1 phase (Zimmermann et al. 2013; Escribano-Diaz et al. 2013). In late S phase and G2 phase, 53BP1-RIF1 interaction with chromatin is inhibited by the BRCA1-CtIP complex. Therefore, the BRCA1-CtIP assembly promotes HR. Moreover, the pathway choice is also regulated by cyclin dependent kinases (CDKs). In particular, phosphorylation of the yeast Sae2 nuclease occurring in the late S phase or G2 phase, stimulates resection activity of this protein required for HR (Huertas et al. 2008; Limbo et al. 2007). The phosphorylation state of the Sae2 also regulates its association with the MRN complex and BRCA1, hence favouring HR (Chen et al. 2008). Certainly, the regulatory network of the repair choice is highly complex. Many details of this fine-tuned regulation remain to be elucidated, especially in the light of the recent studies reporting more factors contributing to the HR/NHEJ balance.

2.5. Mre11-Rad50-Nbs1 complex: structural characterization

Rad50 and Mre11 are evolutionarily conserved and found in all domains of life, forming a very ancient DNA repair machinery. The MRN complex is essential for DSB sensing and repair but it

is involved in tethering broken ends and bridging distal DNA fragments, enzymatic processing of DNA ends and signalling the damage event with cell-cycle control machinery via Nbs1.

Rad50 gene was found among other alleles implicated in radiation sensitivity in yeast (Cox and Parry 1968). Many of these alleles were later found to be involved in meiosis (Game et al. 1980). Rad50 exhibits a typical structural maintenance of chromosome (SMC) protein structure, containing two globular domains at N- and C-termini with Walker A and Walker B nucleotide-binding motifs, respectively (Aravind, Walker, and Koonin 1999) (Figure 4).

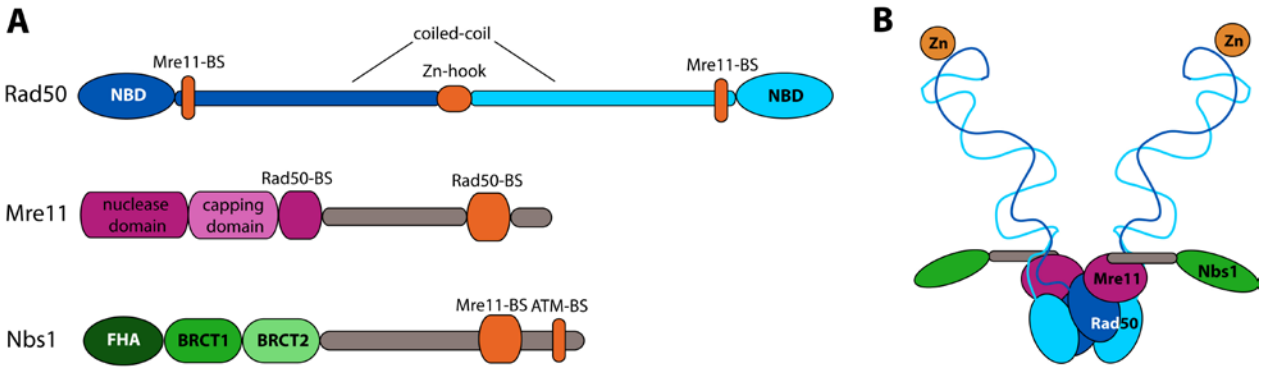

Figure 4. Mre11-Rad50-Nbs1 structure. A: domain structure of the subunits of the MRN complex, B: current understanding of the subunit arrangement in the MRN complex. BS: binding site.

A long and flexible (up to 60 nm) stretch of amino acids separating the two Walker domains forms a characteristic anti-parallel α-helical coiled-coil structure (van Noort et al. 2003; de Jager et al. 2001; de Jager et al. 2004). The coiled-coil folds back on itself, bringing the two globular domains together (Hopfner et al. 2000; Hopfner et al. 2001). In first atomic resolution structure of the archeal Rad50, these domains give shape to lobe I and lobe II (Figure 5) (Hopfner et al. 2000). Upon ATP and Mg^{2+} binding, Rad50 forms a homodimer. Remarkably, the ATP-binding interface involves nucleotide-binding domains (NBDs) of the opposite Rad50 monomers. In this head-to-tail arrangement, lobes 1 and 2 of one Rad50 monomer contact lobes 2 and 1 belonging to the opposite Rad50 molecule, respectively, and form two bipartite ATPase domains (Figure 5).

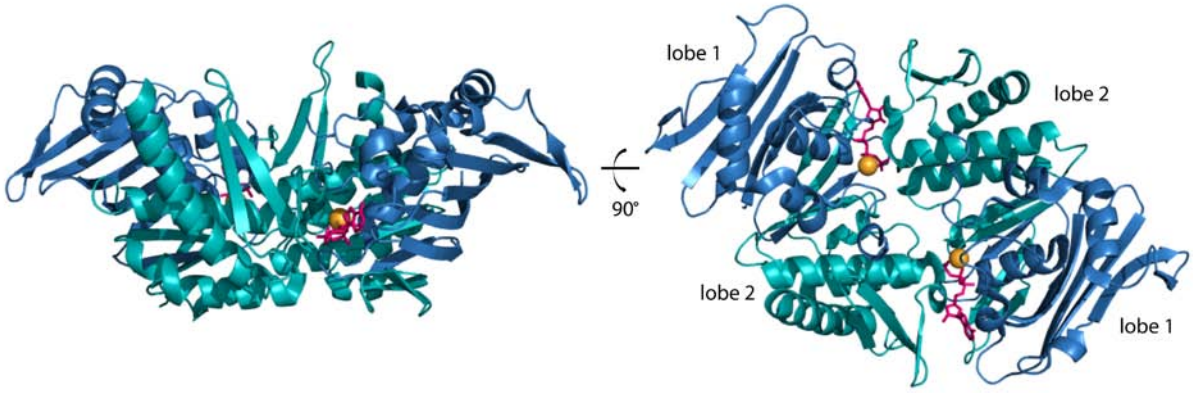

Figure 5. Catalytic head of the *P. furiosus* Rad50 dimer. Lobes 1 (dark blue) and 2 (teal blue) from opposite monomers sandwich Mg^{2+} (in orange) and AMPPNP (in pink). (PDB entry: 1F2T).

Essential for the ATP binding is the signature motif: a highly conserved sequence located in the vicinity of the Walker B motif. The signature motif is a sensor for γ-phosphate of the ATP molecule. Binding of the ATP changes relative position of lobe 2 towards lobe 1, promoting ATP sandwiching and tight dimer formation. Notably, mutations within the signature motif abolish Rad50 dimerization and MRN activity (Hopfner et al. 2000; Moncalian et al. 2004). Like all SMC proteins, Rad50 undergoes structural rearrangements upon ATP binding and hydrolysis. These rearrangements occur primarily at the ATPase domain and appear to be linked to the binding of other MRN assembly factors (Lammens et al. 2011; Lim et al. 2011; Mockel et al. 2012).

The apex opposite of the ATPase domain is known as a hook (or hinge) domain (Hopfner et al. 2002; Hopfner and Tainer 2003), with a conserved CXXC motif coordinating Zn^{2+}. The Zn-hook is involved in MRN intermolecular interactions during DNA bridging (Hopfner et al. 2002; de Jager et al. 2004) and mutations in this motif lead to the DSBR deficiency in yeast (Wiltzius et al. 2005). The long coiled-coil domain has been implicated in bridging distal DNA ends, as well as binding of the Mre11 (Hopfner et al. 2001; Lammens et al. 2011; Williams et al. 2011; Lim et al. 2011; Mockel et al. 2012).

Mre11 (meiotic recombination gene 11) was first identified in a genetic screen for meiosis-deficient yeast mutants (Ajimura, Leem, and Ogawa 1993). Its DNA-binding properties are attributed to the two C-terminal DNA-binding domains (D'Amours and Jackson 2002; Williams, Williams, and Tainer 2007), which, together with the nucleolytic activity of the protein, points

out the Mre11-Rad50 core to be responsible for the DNA recognition, DNA binding and processing of the damaged ends. *In vitro*, Mre11 is involved in hairpin opening and exhibits ssDNA endonuclease and dsDNA 3`→5` exonuclease activity dependent on Mn^{2+} (Paull and Gellert 1998; Hopkins and Paull 2008). Structural and biochemical data revealed that the archeal Mre11 can bind different DNA substrates and provided evidence for the Mre11 3`→5` exonuclease activity (Usui et al. 1998; Hopfner et al. 2001; Williams et al. 2008).

From early on, one of the most puzzling questions in the field of DSB repair was lack of the 5`→3` exonuclease activity in Mre11, required for the DNA end resection prior to HR. It was therefore assumed that Mre11 activity is somehow reversed *in vivo*. However, recent studies show clearly that Mre11 is only one of many nucleases involved in DNA end processing and that 5'-3' resection is performed by other factors. A number of these nucleases has been identified and exhaustively investigated, including Sae2, Dna2 and Exo1.

Mre11 forms a homodimer and associates with the Rad50 dimer, binding to its coiled-coils (Hopfner et al. 2002; Lammens et al. 2011) (Figure 4). First structural insight into the Mre11 architecture showed a dimeric protein with two active sites coordinating in total four Mn^{2+}. Each monomer is formed by two distinct domains: the N-terminal domain containing phosphodiesterase motifs that build up the active site and the C-terminally located capping domain in the vicinity of the active site, partially closing the substrate binding cleft (Figures 4 and 6). Dimerization occurs along a conserved patch of hydrophobic residues located in the N-terminal segment of each monomer.

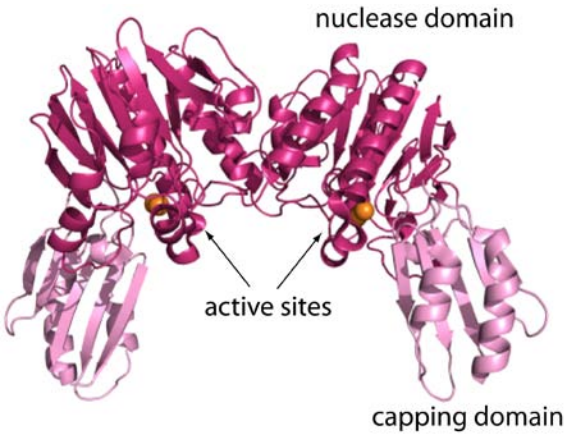

Figure 6. Structure of the *P. furiosus* Mre11. Mre11 dimerizes along conserved hydrophobic motifs. Each monomer coordinates two Mn^{2+} (in orange) in its active site (PDB entry: 1II7).

Archeal Mre11 was also crystallized with two different DNA substrates mimicking broken DNA end or branched DNA (Williams et al. 2008). These substrates were chosen to gain structural insight into two distinct MR complex features: tethering broken ends (synaptic feature) and recognition of the stalled replication fork. The overall architecture of both DNA-free and DNA-bound pfMre11 is almost identical, without significant conformation change induced by DNA binding. Understanding of the DNA-bound Mre11 models poses some difficulties since more recent Mre11-Rad50 atomic structures clearly argue against the location of the DNA-binding interface on Mre11. In principle, the position occupied by the DNA molecule in the DNA-bound Mre11 structure is sterically secluded in the Mre11-Rad50 dimer (Lim et al. 2011; Mockel et al. 2012) (Figure 7).

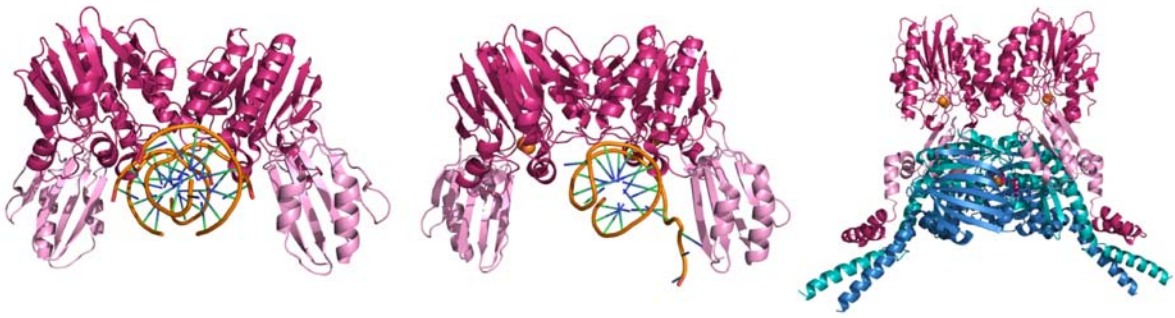

Figure 7. Structures of prokaryotic Mre11-DNA and Mre11-Rad50 complexes. Left panel: DNA mimicking DSB (PDB entry: 3DSC), middle panel: DNA mimicking stalled replication fork (PDB entry: 3DSD). DNA-bound Mre11 structures became difficult to interpret when confronted with the Mre11-Rad50 model from *T. maritima* (right panel, PDB entry: 3THO). Rad50 dimer clearly closes the proposed DNA-binding pocket on Mre11.

Recent studies shed light on the eukaryotic Mre11 structure (Park et al. 2011; Schiller et al. 2012). Most notably, yeast Mre11 model with Nbs1 peptide revealed first insights into Nbs1 binding by the Mre11 and the involvement of Mre11 structural features in the outbreak of ataxia-telangiectasia-like disease (ATLD). *S. pombe* Mre11 forms a flexible dimer with asymmetrically bound Nbs1 stabilizing the dimer interface. Furthermore, despite sharing the overall 3D architecture with prokaryotic orthologues, eukaryotic structures possess a large loop insertion at one end of the dimer interface and an additional helix in the capping domain (Schiller et al. 2012). Interestingly, some of the ATLD mutations map to this regions, suggesting its involvement in the DSB-induced signalling.

Less functional and structural information is available about **Nbs1** (Xrs2 in *S.cerevisiae*) – the only MRN subunit to be found exclusively in eukaryotes. Xrs2 was first reported to belong to the recombinational genes involved in the DNA repair in *S. cerevisiae* (Suslova, Fedorova, and Zhelezniakova 1975). The human orthologue was found during a genetic analysis of the cells derived from patients suffering from the Nijmegen breakage syndrome (NBS) (Varon et al. 1998). Back then, the protein had alternative names nibrin and p95; later Nbs1 annotation was accepted and this name is used in this work as well.

In general, Nbs1 orthologues show a very poor sequence conservation, except from Mre11- and ATM-binding motifs. Nbs1 carries an N-terminal forkhead associated (FHA) and tandem BRCA1 C-terminus (BRCT) domains, both commonly known for binding phosphoproteins (Figures 4 and 8) (Xu et al. 2008; Lloyd et al. 2009; Williams et al. 2009). This N-terminal segment forms an extended fold conserved from yeast to human, which is highly phosphorylated at a number of residues. Phosphorylation state of Nbs1 regulates the recruitment of downstream DNA damage and checkpoint proteins.

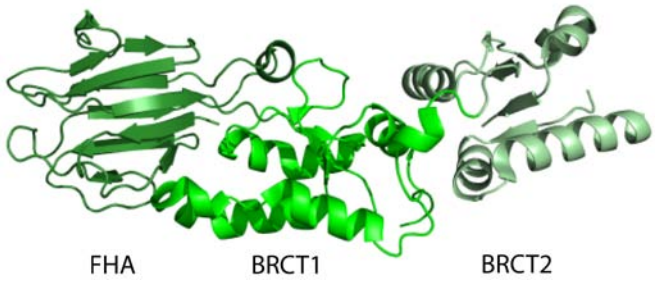

Figure 8. Structure of the N-terminal segment of Nbs1 from *S. pombe*. Nbs1 carries FHA and tandem BRCT domains clustered at the N-terminus of the protein. (PDB entry: 3HUE).

The poorly structured C-terminal part of the Nbs1 carries conserved ATM- and Mre11-binding sites. Therefore, it was suggested that Nbs1 is the signalling subunit of the MRN complex. Indeed, Nbs1/Xrs2 plays a role in mediating the DSB recognition and repair with the cell-cycle checkpoint machinery (Falck, Coates, and Jackson 2005; You et al. 2005; Lloyd et al. 2009; Williams et al. 2009). Nbs1-ATM interaction is also crucial for the induction of apoptosis (Stracker et al. 2007). However, recent structural and biochemical studies showed that in *S. pombe* Nbs1 also interacts with Ctp1 and promotes nuclease activity of the MR complex, thereby being involved in DNA processing (Lee et al. 2003). Nbs1 also possesses a nuclear localization

signal (NLS), responsible for transportation of the MRN complex from the cytoplasm to the nucleus (Desai-Mehta, Cerosaletti, and Concannon 2001). These reports clearly show that Nbs1 plays a multifunctional role in the context of the MRN complex.

Considering extended architecture of the N-terminal part of Nbs1, indispensable for the recruitment of downstream DSBR factors, and the long and flexible C-terminus interacting with the MR complex and ATM kinase, a model of clustering of the primary and secondary DSBR proteins through the Nbs1 has been proposed (Williams et al. 2009).

2.6. Mre11-Rad50-Nbs1 complex in cell physiology

The MRN complex is a multifunctional machinery: it is involved in the DSB recognition and repair, nucleolytic processing of the DSB ends, DNA tethering at the damage site, as well as cell-cycle checkpoint activation. As discussed below, MRN is crucial not only in the repair of mitotic DSBs, but also in the development of the adaptive immune system, damage signalling, repair of collapsed replication fork, telomere maintenance and repair of meiotic DSBs. The importance of the MRN complex is demonstrated by the fact that null mutations in any of the three subunits of the complex are lethal during embryogenesis in mice (Xiao and Weaver 1997; Luo et al. 1999; Zhu et al. 2001) whereas polymorphic mutations are linked to Nijmegen breakage syndrome and ataxia-telangiectasia-like disease, severe genomic human disorders. Many years of research have contributed to the better understanding of the multifaceted behaviour of the complex but some key questions still remain to be answered.

2.6.1. HR in mitotic DSB

Mre11-Rad50-Nbs1 complex was implicated in the repair of mitotic DSBs as the major sensor of the DNA damage. Its role in homologous recombination is important to several aspects of this repair pathway and so far has been best described in yeast. Firstly, the endonucleolytic and not the exonucleolytic activity of Mre11 is indispensable for the 5’ resection prior to HR in yeast (Williams et al. 2008). Mre11, together with the Sae2 nuclease, was shown to perform the short-term resection on broken DNA ends, facilitating further processing by ExoI or the Sgs1-Dna2 complex. Also, MRX enhances recruitment of ExoI and the Sgs1-Dna2 complex to the damage site and therefore stimulates long-term resection (Shim et al. 2010).

This model seems not to be entirely true in mammals, where endonuclease-deficient Mre11 is embryonically lethal in mice (Buis et al. 2008). The same strong phenotype is observed in endonuclease-deficient Mre11 in *S. pombe*. Also, *S. pombe* and mammalian orthologues of Sae2 (Ctp1 and CtIP, respectively) show very poor sequence conservation and, in contrast to Sae2, do not exhibit nuclease activity *in vitro*. However, CtIP was shown to interact with Mre11, which would suggest the stimulatory effect of CtIP on Mre11 (Limbo et al. 2007; Sartori et al. 2007). Certainly, the protein landscape in HR is far more complex in mammals and therefore the details of the mammalian resection still remain to be elucidated.

Beside its enzymatic activity, the MRN/X complex plays a scaffolding function. Due to the intermolecular interactions via Zn-hooks, MRN/X complexes bound to distally located DNA molecules could perform bridging function important in preventing sister chromatid separation during repair (Hopfner et al. 2002; Borde and Cobb 2009).

2.6.2. NHEJ

From early on, role of the MRN complex in NHEJ/MMEJ was rather puzzling. Since Ku showed much higher affinity for DNA, the MRN complex was no longer a candidate for a damage sensor. However, studies reported that the MRN complex is indeed involved in NHEJ (Zhuang et al. 2009) and MMEJ (Xie, Kwok, and Scully 2009; Rahal et al. 2010). Mre11 knockdown reduces both NHEJ and MMEJ efficiency in mammalian cells. In *S. cerevisiae*, end-joining defects caused by Mre11 deletion are rescued by nuclease-deficient Mre11, which would suggest that the MRN complex plays rather a structural and not enzymatic role in NHEJ (Zhang and Paull 2005). Also, the MRN response in classical NHEJ does not seem induce ATM activation. Certainly, the exact nature of the MRN roles in NHEJ/MMEJ remains to be elucidated, together with the employment of the complex in yeast versus vertebrate NHEJ.

2.6.3. Telomeres

Structurally, telomeres represent one part of a double-strand break. Therefore, it was intriguing to find several factors involved in the DNA-damage response to be associated with telomeres. In *S. cerevisiae*, the MRX complex associates with telomeres in the late S-phase and is needed for the recruitment of the telomerase Cdc13-Stn1-Ten1 (CST) complex to the telomeres (Takata, Tanaka, and Matsuura 2005). Deletion or disruption of the individual MRX subunits results in telomere shortening and subsequent cell senescence (Kironmai and Muniyappa 1997; Boulton

and Jackson 1998). In the absence of the functional MRX, the CST complex loses its affinity to telomeres. At the moment it is not clear how the MRX affects the association of the CST with telomeres. One hypothesis postulates that the MRX complex and/or its associated co-factors (*e. g.* Sae2) process telomeric DNA and generate short 3' overhangs recognizable by Cdc13. Cdc13 is a ssDNA-binding protein, mediating association of the CST complex with telomeres. Alternative explanation suggests that the MRX forms a structural scaffold for the CST complex on the telomere.

DSBR machinery is also involved in vertebrate telomere maintenance. MRN complex can be found on telomeres and associated with shelterin complex responsible for protecting "naked" DNA ends (Lombard and Guarente 2000; Zhu et al. 2000). At the same time, telomeres devoid of the protective shelterin cap cannot recruit telomerase. Consequently, the exposed uncapped telomere end leads to the ATM-induced checkpoint activation characteristic for DSB-induced signalling (Takai, Smogorzewska, and de Lange 2003; Karlseder et al. 1999).

2.6.4. Meiosis

Spo11-generated DSBs during meiosis are characterized by covalently attached topoisomerase to each of the 5' ends of the break. These protein-DNA adducts need to be removed prior to further resection. Removal of the Spo11 together with a short oligonucleotide is catalyzed by Mre11/Sae2 and enhanced by ExoI (Neale, Pan, and Keeney 2005; Garcia et al. 2011). Remaining single-stranded 3' overhangs are then subjected to downstream steps of the HR. However, repair of these breaks requires a set of specialized factors involved exclusively in the repair of meiotic DSBs.

2.6.5. Signalling

Every DNA damage event has to be rapidly signalled to the cell-cycle control machinery, so that the cell gains time for repair and recovery and does not retain potentially mutagenic DNA rearrangements. The MRN complex actively participates in signal transduction of the DNA damage to the major DSB kinase ATM. Together with the genotoxic stress kinases DNA-PKcs and ATR (ataxia-telangiectasia and Rad3-related), ATM belongs to the phosphatidylinositol 3-kinase-related kinase family (PIKKs), mediating a number of various stress responses (Lempiainen and Halazonetis 2009). ATM resides mostly in the nucleoplasm in a form of an inactive dimer that dissociates into monomers upon activation. The very first hallmark of the

ATM activation is its autophosphorylation on serine 1981 (in human), followed by the autophosphorylation of other residues. All these modifications are required to retain ATM at the damage site (Bakkenist and Kastan 2003; Lee and Paull 2004; Dupre, Boyer-Chatenet, and Gautier 2006).

The exact nature of the ATM activation is not clear. However, the MRN complex, together with other sensor proteins BP531 and BRCA1, is required for this activation. In particular, a direct interaction between specific motifs on the ATM kinase and Nbs1 was shown to be indispensable for the ATM-induced signalling (Falck, Coates, and Jackson 2005; Stracker et al. 2007; Difilippantonio et al. 2007). ATM is a very promiscuous kinase and once activated, it phosphorylates a number of substrates. Those related to DSB-repair pathway include *e. g.* H2AX histone, checkpoint kinases Chk1 and Chk2, mammalian recombination mediator BRCA1, transcription regulator p53, DNA-PKcs, Artemis and all subunits of the MRN complex. Phosphorylation of p53 signals the DNA damage event to transcriptome regulatory network, including activation of both cell cycle checkpoint factors and apoptotic proteins (Choi et al. 2012; Sullivan et al. 2012). By activating the checkpoint, the cell is given time to repair the break and recover from the damage event. Continuous signalling from the lesion site that cannot be repaired, leads to a metabolic shutdown and programmed cell death. Both responses are considered the cellular defense against genomic instability.

2.6.6. Mre11-Rad50 complex in prokaryotes

Best described prokaryotic Mre11-Rad50 orthologues is the SbcCD complex from *E. coli* (SbcD for Mre11 and SbcC for Rad50). The complex was first cloned and sequenced in 1989 (Naom et al. 1989). Sequence analysis revealed that *sbcD* and *sbcC* were related to the bacteriophage T4 genes gp46/gp47 and bacteriophage T5 genes gpD13/gpD12, which in turn share homology with the eukaryotic Mre11 and Rad50 proteins (Leach, Lloyd, and Coulson 1992). Later, it was also shown that the SbcCD complex is mechanistically similar to the eukaryotic Mre11-Rad50 complex (Sharples and Leach 1995).

Both *sbcCD* genes are transcribed from the same promoter. The SbcCD complex was first implicated in preventing replication of long palindromic DNA segments. Palindromes tend to form secondary structures and contribute to replication fork stalling and collapse, thereby posing a threat to genome stability. Studies showed that mutations in *sbcCD* enhance palindrome

propagation (Chalker, Leach, and Lloyd 1988; Gibson, Leach, and Lloyd 1992). It was later found that the RecABC complex involved in prokaryotic homologous recombination is required for viability in *sbcCD+* genetic background and in the presence of palindromes. This finding suggested that the initial SbcCD action on palindromic DNA is a prerequisite to the subsequent recombinational processing.

SbcCD proteins were recombinantly expressed and biochemically characterized (Connelly and Leach 1996; Connelly et al. 1997; Connelly, Kirkham, and Leach 1998; Connelly, de Leau, and Leach 1999). SbcCD co-purified together; however, during gel filtration the complex fell apart and the reversion of this could be achieved by addition of Mn^{2+}. The complex exhibited ATP-dependent 3'-5' exonuclease activity on dsDNA and ATP-independent endonuclease activity on ssDNA. It could also cleave hairpins, leaving 3'-hydroxyl and 5'-phosphate ends. Enzymatic activities required Mn^{2+} and were independent of the DNA sequence. All these findings, together with the *in vivo* evidence of the SbcCD localization on the chromosomal sites containing palindromic sequences supported the role of the complex in inhibiting replication of potentially harmful DNA segments (Eykelenboom et al. 2008). The same report showed that the ends of the SbcCD-cleaved DNA were required to promote resection and HR.

Despite high similarities in sequence and predicted secondary structure between prokaryotic and eukaryotic MR complexes, there are some key differences between these orthologues. Firstly, the eukaryotic complex is bigger and contains additionally Nbs1. Differences are also observed at the level of quaternary structure arrangement. As reported so far, the eukaryotic MR complex always forms heterotetramers and higher oligomeres of heterotetrameric complexes. In contrast, prokaryotic MR complexes are stable as heterodimers, with possibility of forming higher-order oligomeres (de Jager et al. 2004). The MRN complex plays a much more complex role in the cellular physiology compared to its prokaryotic orthologue. However, since the overall secondary structure prediction together with tertiary structure seem to be very similar for both prokaryotic and eukaryotic MR orthologues, many biochemical and structural characteristics of the prokaryotic MR complex have served a great help elucidating the roles of the complex in eukaryotic DNA metabolism.

2.7. Disease

A number of deficiencies are linked to the mutations in the MRN complex, all sharing molecular and phenotypical similarities with the ataxia-telangiectasia (AT) disorder, in which ATM gene is mutated (ataxia-telangiectasia mutated). AT is a neurodegenerative disease, caused by a defective DNA damage signalling (Savitsky et al. 1995). On a molecular level, AT is linked to a partial or complete loss of the ATM kinase activity due to distinct mutations (Gilad et al. 1998; Becker-Catania et al. 2000), and is manifested in decreased Ig levels (Sanal et al. 1999), chromosomal aberrations, telomere shortening (Metcalfe et al. 1996) and sensitivity to the DNA damaging agents (Taylor et al. 1975; Gatti 2001). AT patients not only suffer from uncoordinated movements (ataxia) and have dilated blood vessels (telangiectasia), but also show radiosensitivity, immune dysfunction and predisposition to cancer.

In 1999, the first patient with symptoms close to AT was reported (Stewart et al. 1999). However, no telangectasia and immunodeficiency were observed and the progression of the disease was slower compared to AT. The new disorder was called ataxia-telangiectasia-like disease (ATLD) and linked to a point mutation in the Mre11. Since then, a number of other Mre11 mutations have been reported (Delia et al. 2004; Fernet et al. 2005; Uchisaka et al. 2009), all causing ATLD.

Similarly, mutations in Nbs1 cause Nijmegen breakage syndrome (NBS) (Carney et al. 1998; Varon et al. 1998; Maser, Zinkel, and Petrini 2001), yet another disorder related to AT. Again, no telangiectasia was observed and in contrast to both AT and ATLD, NBS patients do not exhibit neurodegeneration. A characteristic symptom of NBS, uncommon for AT and ATLD, is microcephaly.

So far, only one Rad50 mutation associated with a human disease has been described, with clinical characteristics similar to the NBS. The new disorder was annotated NBS- like disease (NBSLD) (Waltes et al. 2009).

Subtle differences between disorders caused by the hypomorphic mutations in the MRN subunits clearly point out their related but also specialized function in the DNA damage response. In particular, the divergent effect on the development of the nervous system for AT, ATLD and NBS is so far not well understood. Details underlying the molecular and functional characteristics of the MRN subunits will certainly contribute to better understanding of the MRN-related disorders.

2.8. Mre11-Rad50 complex from *Thermotoga maritima* and other prokaryotes

Recent studies have greatly advanced our understanding of the structural features in the prokaryotic Mre11-Rad50 complex. I particular, ATP-induced conformational changes within the complex have been mechanistically and functionally described (Lammens et al. 2011; Lim et al. 2011; Williams et al. 2011; Mockel et al. 2012). These studies shed light on the ATP-driven cross-talk between Rad50 and Mre11, giving a detailed insight into how ATP binding and hydrolysis influences the function of the complex (Moncalian et al. 2004; Bhaskara et al. 2007).

Notably, it turned out that in the absence of ATP or its analogs, the Mre11-Rad50 complex from *Thermotoga maritima*, encompassing full-length Mre11 and the catalytic head of the Rad50 with the adjacent coiled-coil domains exhibits an elongated shape (Figure 9). The two monomers of the Rad50 are far apart, with the coiled-coils pointing out towards almost opposite directions (120°). Mre11 and Rad50 interact at two conserved interfaces, one formed between the Mre11 capping domain and the Rad50 lobe 1 and the other involving a short helix-loop-helix motif of Mre11 and a hydrophobic patch in the Rad50 coiled-coils.

Further SAXS and cross-linking studies showed that upon ATP□S the structure becomes more compact due to ATP□S-induced dimerization of the Rad50. At the same time, AMPPNP-driven engagement of the Rad50 globular domains was shown in structure of the Rad50 catalytic core with the helix-loop-helix motif of Mre11 (Lammens et al. 2011; Williams et al. 2011) (Figure 9).

Figure 9. Mre11-Rad50 complexes from *T. maritima*. Left panel: in the absence of ATP analogs, the complex has an elongated shape with Rad50 monomers located far apart from each other (PDB entry: 3QG5). Right panel: upon ATP binding, Rad50 dimerizes (PDB entry: 3QF7).

Further atomic models of the archeal and bacterial full-length Mre11 co-crystallized with the catalytic core of the Rad50 in ATP/ADP bound state provided more details about the ATP-induced conformational changes (Lim et al. 2011; Mockel et al. 2012). ATP-induced Rad50 dimerization leads to changes at the Mre11 dimer interface, rendering the dimer more compact

and suggesting that the ATP binding and subsequent hydrolysis might be transmitted to the signalling component of the complex Nbs1 via Mre11. Interestingly, the relative Rad50-Mre11 arrangement clearly obstructs the active site of Mre11 and contradicts previous results showing archeal Mre11 bound to DNA (Williams et al. 2008) (Figure 7). It remains to be elucidated how the entire complex coordinates DNA binding and how this binding, together with the ATP hydrolysis, contributes to the activation of the cell cycle control machinery.

Considering structural and to a degree functional conservation between prokaryotic and eukaryotic Mre11/Rad50 orthologues, as well as the number of already reported prokaryotic crystal structures, the Rad50-Mre11 complex from *Thermotoga maritma* is a good starting point for structural investigations of the complex-DNA assembly. Having the structure in hand, biochemical and functional studies could be performed, including structure-based *in vivo* approach.

2.9. Aims of the project

Certainly, the MRN/MRX complex plays a pivotal role in various aspects of the DSB repair. Not only does it serve as a molecular sensor of the damage, but also actively participates in the repair process, exhibiting enzymatic activities. Furthermore, the complex forms a structural scaffold required for the recruitment and assembly of the downstream repair and signalling factors, thereby being a key component of the repair machinery. The importance of the Nbs1-regulated damage signalling manifested in severe phenotypes of AT- and NBS-related disorders further confirms the crucial role of the complex. Lastly, the broad spectrum of cellular events employing the MRN/MRX complex: telomere maintenance, meiotic recombination, immune system development to mention a few, gives this complex a particular importance in cell physiology.

Although many years of extensive research have greatly contributed to dissecting the role and activity mechanism of the MRN complex, a number of fundamental questions is still a matter of debate. Certainly, the divergence in the requirement of the Mre11 nuclease activity in distinct MRN-dependent cellular events is still unclear. Furthermore, details of the subtle cross-talk between structural and enzymatic features of the complex and Nbs1-dependent ATM signalling require in-depth studies. Finally, the mechanism of DNA recognition and the regulation of the interplay between DNA binding and downstream repair and signalling events remain to be elucidated.

The aims of this thesis were to determine how the complex senses and binds DNA. To this end, the enzymatic core of the Rad50 from *T. maritima* comprising the nucleotide-binding domain (tmRad50^{NDB}) together with a short interaction helix-loop-helix peptide of Mre11 (tmMre11^{HLH}) was crystallized in a dimeric form with AMPPNP and a short dsDNA molecule. Moreover, significance of structural features of this model was analyzed *in vitro* in DNA-binding assays. Further attempts were undertaken to functionally characterize the importance of structure-based features of Rad50 in the DNA damage response, repair and telomere maintenance *in vivo* in *S. cerevisiae* and in ATM signalling *in vitro* in *Xenopus laevis* egg extract system with the recombinant hMRN complex.

3. Materials and methods

3.1. Materials

Chemicals used in this work were purchased from Sigma-Aldrich (Deisenhofen), Carl Roth (Karlsruhe) or Merck (Darmstadt). Enzymes used for molecular biology methods were obtained from Fermentas (St.Leon-Rot) or New England Biolabs (Frankfurt).

Desalted oligonucleotides for molecular cloning were purchased from Metabion International AG (Martinsried), HPLC purified oligonucleotides for *in vitro* activity assays were obtained from Biomers.net (Ulm) and Thermo Fisher Scientific (Ulm). RP-HPLC and PAGE-purified oligonucleotides for crystallization were purchased from Biomers.net (Ulm) and Thermo Fisher Scientific (Ulm), respectively.

Chromatographic media and columns were purchased from GE Healthcare (Munich). For crystallization experiments commercial screens and tools from Hampton Research (Laguna Niguel, USA), NeXtal (QIAGEN, Hilden) and Jena Bioscienes (Jena) were used.

Oligonucleotides

Table 1 lists oligonucleotides used for molecular cloning and mutagenesis relevant to this work.

Table 1. Oligonucleotides used for molecular cloning and mutagenesis.

oligonucleotide	5'-3' sequence	purpose
hM11_Sma_F	TTTCCCGGGATGAGTACTGCAGATG	Fw primer, human Mre11 FL
hM11_Kpn_R	TTTGGTACCTCATCTTCTATTTCTTCTTAAAGAACTAGTG	Rv primer, human Mre11 FL
hR50_BamH_F	TTTGGATCCATGTCCCGGATCGAAAAG	Fw primer, human Rad50 FL
hR50His_Xba_R	TTTTCTAGATTAGTGGTGATGGTGATGGTGC	Rv primer, human Rad50 FL, 6xHis at C-terminus
hR50_Xba_R	TTTTCTAGATTAATGAACATTGAATCCCAGGGAGC	Rv primer, human Rad50 FL
hN_Sal_F	TTTGTCGACATGTGGAAACTGCTGCC	Fw primer, human Nbs1 FL
hNHis_Not_R	TTTGCGGCCGCTTAGTGGTGATGGTGATGGTGTCTTCTCCTTTTTAAATAA	Rv primer, human Nbs1 FL, 6xHis at C-terminus
hN_Not_R	TTTGCGGCCGCTTATCTTCTCCTTTTTAAATAAG	Rv primer, human Nbs1 FL
tmR50_R2Q_For	CTTTAAGAAGGAGATATACATATGCAGCCTGAACGCCTCACCGTTAG	R2Q mutation in tmRad50
tmR50_R2Q_Rev	CTAACGGTGAGGCGTTCAGGCTGCATATGTATATCTCCTTCTTAAAG	R2Q mutation in tmRad50
tmR50_R5Q_For	GAGATATACATATGCGCCCTGAACAATCACCGTTAGAAACTTTCTCG	R5Q mutation in tmRad50
tmR50_R5Q_Rev	CGAGAAAGTTTCTAACGGTGAGTTGTTCAGGGCGCATATGTATATCTC	R5Q mutation in tmRad50
tmR50_R9E_For	CCTGAACGCCTCACCGTTGAAAACTTTCTCGGACTGAAAAACG	R9E mutation in tmRad50
tmR50_R9E_Rev	CGTTTTTCAGTCCGAGAAAGTTTTCAACGGTGAGGCGTTCAGG	R9E mutation in tmRad50
tmR50_N10D_For	CTGAACGCCTCACCGTTAGAGACTTTCTCGGACTGAAAAACGTC	N10D mutation in tmRad50
tmR50_N10D_Rev	GACGTTTTTCAGTCCGAGAAAGTCTCTAACGGTGAGGCGTTCAG	N10D mutation in tmRad50
tmR50_R94E_For	GAGAGATAAATGCCCTGCAGGAAAAACACAACGCGAAGCTCTC	R94E mutation in tmRad50
tmR50_R94E_Rev	GAGAGCTTCGCGTTGTGTTTTTCCTGCAGGGCATTTATCTCTC	R94E mutation in tmRad50
tmR50_K95E_For	GAGATAAATGCCCTGCAGAGAGAACACAACGCGAAGCTCTC	K95E mutation in tmRad50
tmR50_K95E_Rev	GAGAGCTTCGCGTTGTGTTCTCTCTGCAGGGCATTTATCTC	K95E mutation in tmRad50
tmR50_K99E_For	CAGAGAAAACACAACGCGGAGCTCTCCGAGATACTGGAAAAC	K99E mutation in tmRad50

tmR50_K99E_Rev	GTTTTCCAGTATCTCGGAGAGCTCCGCGTTGTGTTTTCTCTG	K99E mutation in tmRad50
tmR50_K108E_For	GAGATACTGGAAAACGGAGAGAAAGCGGCCATAGCTGCAAAAC	K108E mutation in tmRad50
tmR50_K108E_Rev	GTTTTGCAGCTATGGCCGCTTTCTCTCCGTTTTCCAGTATCTC	K108E mutation in tmRad50
tmR50_K109E_For	GAGATACTGGAAAACGGAAAGGAAGCGGCCATAGCTGCAAAAC	K109E mutation in tmRad50
tmR50_K109E_Rev	GTTTTGCAGCTATGGCCGCTTCCTTTCCGTTTTCCAGTATCTC	K109E mutation in tmRad50
tmR50_K115E_For	GAAAGAAAGCGGCCATAGCTGCAGAACCTACCAGTGTTAAGC	K115E mutation in tmRad50
tmR50_K115E_Rev	GCTTAACACTGGTAGGTTCTGCAGCTATGGCCGCTTTCTTTC	K115E mutation in tmRad50
tmR50_K175E_For	GAAACACTCGAAAAGCTGGAAGAACTCCTCAAAGAGAAAATGAAAAAGCTG	K175E mutation in tmRad50
tmR50_K175E_Rev	CAGCTTTTTCATTTTCTCTTTGAGGAGTTCTTCCAGCTTTTCGAGTGTTTC	K175E mutation in tmRad50
tmR50_K182E_For	GAAAAACTCCTCAAAGAGAAAATGGAAAAGCTGGAGAACGAGATATCC	K182E mutation in tmRad50
tmR50_K182E_Rev	GGATATCTCGTTCTCCAGCTTTTCCATTTTCTCTTTGAGGAGTTTTTC	K182E mutation in tmRad50
tmR50_R765E_For	GGTATCGAAAGACCAGCGGAGGGACTTTCCGGTGG	R765E mutation in tmRad50
tmR50_R765E_Rev	CCACCGGAAAGTCCCTCCGCTGGTCTTTCGATACC	R765E mutation in tmRad50
tmR50_S768R_For	GACCAGCGAGGGGACTTCGCGGTGGGGAAAGAGCTC	S768R mutation in tmRad50
tmR50_S768R_Rev	GAGCTCTTTCCCCACCGCGAAGTCCCCTCGCTGGTC	S768R mutation in tmRad50
tmR50_E798Q_For	GGACGCGTTCTTCATCGATCAAGGGTTTTCCAGTCTCGACACG	E798Q mutation in tmRad50
tmR50_E798Q_Rev	CGTGTCGAGACTGGAAAACCCTTGATCGATGAAGAACGCGTCC	E798Q mutation in tmRad50
scR50_K103E_For	CAGAAATATTCAGTTGCTAATGGAAAAGACTACTACTACATTTAAGAC	K103E mutation in scRad50
scR50_K103E_Rev	GTCTTAAATGTAGTAGTAGTCTTTTCCATTAGCAACTGAATATTTCTG	K103E mutation in scRad50
scR50_K104E_For	CAGAAATATTCAGTTGCTAATGAAAGAGACTACTACTACATTTAAGAC	K104E mutation in scRad50
scR50_K104E_Rev	GTCTTAAATGTAGTAGTAGTCTCTTTCATTAGCAACTGAATATTTCTG	K104E mutation in scRad50
scR50_Q115E_For	CATTTAAGACTTTAGAAGGCGAGTTGGTCGCTATAAATAATAGTGGTG	Q115E mutation in scRad50
scR50_Q115E_Rev	CACCACTATTATTTATAGCGACCAACTCGCCTTCTAAAGTCTTAAATG	Q115E mutation in scRad50
scR50_R131E_For	GACCGCAGTACTTTGTCCACCGAGTCTCTGGAATTAGACGCAC	R131E mutation in scRad50
scR50_R131E_Rev	GTGCGTCTAATTCCAGAGACTCGGTGGACAAAGTACTGCGGTC	R131E mutation in scRad50
scR50_N190E_For	GAAATTTACAAAGGCTCTAGACGAGTTAAAATCCATAAAGAAAGACATGTCCG	N190E mutation in scRad50
scR50_N190E_Rev	CGGACATGTCTTTCTTTATGGATTTTAACTCGTCTAGAGCCTTTGTAAATTTC	N190E mutation in scRad50
scR50_R1201E_For	GCAGGATGTTGAATTGGATATGGAGGGACGATGTTCCGCGG	R1201E mutation in scRad50
scR50_R1201E_Rev	CCGCGGAACATCGTCCCTCCATATCCAATTCAACATCCTGC	R1201E mutation in scRad50
scR50_S1205R_For	GAATTGGATATGAGAGGACGATGTCGCGCGGGTCAAAAAGTTCTTGCATC	S1205R mutation in scRad50
scR50_S1205R_Rev	GATGCAAGAACTTTTTGACCCGCGCGACATCGTCCTCTCATATCCAATTC	S1205R mutation in scRad50
scR50_E1235Q_For	GTGGCGTAATTGCACTAGACCAACCTACCACCAATTTAGATGAAG	E1235Q mutation in scRad50
scR50_E1235Q_For	CTTCATCTAAATTGGTGGTAGGTTGGTCTAGTGCAATTACGCCAC	E1235Q mutation in scRad50

Oligonucleotides used for preparing short dsDNA to crystallize with tmRad50^{NBD}-Mre11^{HLH} are listed in Table 2.

Table 2. Oligonucleotides used in the preparation of the DNA for crystallization experiments.

oligonucleotide	5'-3' sequence	purpose
Palin15_For	GGTCGGTGACCGACC	Fw primer, 15 bp palindromic DNA
Palin15_Rev	GGTCGGTCACCGACC	Rv primer, 15 bp palindromic DNA
13mer_for	GGCGAGCCGTGGC	Fw primer, 13 bp DNA
13mer_rev	GCCACGGCTCGCC	Rv primer, 13 bp DNA
15mer_for	GCTGCGAGCCGTGGC	Fw primer, 15 bp DNA
15mer_rev	GCCACGGCTCGCAGC	Rv primer, 15 bp DNA
17mer_for	GCTGCGAGCCGTGGCCG	Fw primer, 17 bp DNA
17mer_rev	CGGCCACGGCTCGCAGC	Rv primer, 17 bp DNA
19mer_for	GCTGCGAGCCGTGGCCGTG	Fw primer, 19 bp DNA
19mer_rev	CACGGCCACGGCTCGCAGC	Rv primer, 19 bp DNA
21mer_for	ATAGGGCTATAAAAGGGGGTG	Fw primer, 21 bp DNA
21mer_rev	CACCCCCTTTTATAGCCCTAT	Rv primer, 21 bp DNA
15mer[TT]_for	TTGGCGAGCCGTGGC	Fw primer, 15 bp DNA with 1 nt overhang
16mer_rev	TGCCACGGCTGCCAA	Rv primer, 15 bp DNA with 1 nt overhang
16merBr_rev	U^{Br}GCCACGGCTGCCAA	Rv primer, 15 bp DNA with 1 nt overhang of bromouracil

Oligonucleotides used for preparing fluorescently labelled dsDNA for DNA binding assays with the recombinant tmRad50^{NBD}-Mre11^{HLH} are listed in Table 3.

Table 3. Oligonucleotides used in the preparation of the DNA for the *in vitro* activity assays.

oligonucleotide	5'-3' sequence	purpose	label/ modification
ss30_F	CCGGAAAGCATCTAGCATCCTGTCAGCTGC	Fw primer, 30 bp DNA	6-FAM at 5'
ss30_R	GCAGCTGACAGGATGCTAGATGCTTTCCGG	Rv primer, 30 bp DNA	
ss60_F	GCTAATGCCGCGTGCCTTGTCTCACCTTCGATTTAGCATGGTATC AGCAGAGCAAGCCTC	Fw primer, 60 bp DNA	6-FAM at 5'
ss60_R	GAGGCTTGCTCTGCTGATACCATGCTAAATCGAAGGTGAGACAA GGCACGCGGCATTAC	Rv primer, 60 bp DNA	
ss60_2_5'P	CGAAGGTGAGACAAGGCACGCGGCATTAGC	Rv primer, 60 bp nicked DNA	phosphate group at 5'
ss60_1	GAGGCTTGCTCTGCTGATACCATGCTAAAT	Rv primer, 60 bp nicked DNA	

Blunt-ended 200 bp DNA used for eliciting DNA damage response in *Xenopus laevis* egg extracts was prepared in a PCR with pBluescript II SK+ as DNA template and following primers:

pBlue_For: 5'- GGGGGATCCACTAGTTCT-3' (forward primer)

pBlue200_Rev: 5'- TTTCACTCATTAGGCACCCC-3' (reverse primer)

Constructs

Constructs of the human MRN complex and its subunits are listed in Table 4. All these constructs contain full-length wild-type ORFs.

Table 4. pFBDM-based constructs of the human MRN complex and its subcomplexes.

construct	ORF	tag	restriction sites
pFBDM:hMre11_hRad50$^{6His/C}$_hNbs1	hMre11	-	SmaI/KpnI
	hRad50	6xHis at C-terminus	BamHI/XbaI
	hNbs1	-	SalI/NotI
pFBDM:hMre11	hMre11	-	SmaI/KpnI
pFBDM:hRad50	hRad50	-	BamHI/XbaI
pFBDM:hNbs1$^{6His/C}$	hNbs1	6xHis at C-terminus	SalI/NotI
pFBDM:hMre11_hRad50	hMre11	-	SmaI/KpnI
	hRad50	-	BamHI/XbaI
pFBDM:hMre11_hRad50$^{6His/C}$	hMre11	-	SmaI/KpnI
	hRad50	-	BamHI/XbaI

Construct pET29b:tmRad50^{NBD}_Mre11^{HLH} containing segments of the wild-type Rad50 and Mre11 from *T. maritima* was a gift from A. Schele (Hopfner group):

pET29b: tmRad50 [aa 1-190-GGAGGAGG-686-852; NdeI/NotI] tmMre11$^{6His/C\text{-}term}$ [aa 343-385; NotI/ Bpu1102I].

Construct pRS313:scRad50 containing the wild-type Rad50 from *S. cerevisiae* with 477 bp upstream (promoter) and 291 bp downstream (terminator) regions:

pRS313: scRad50 [full-length; XhoI/EcoRI].

Constructs derived from pET29b:tmRad50^{NBD}-Mre11^{HLH} and pRS313:scRad50 containing equivalent mutations in the Rad50 ORF are listed in Table 5.

Table 5. Equivalent point mutations introduced into the Rad50 gene in pET29b:tmRad50^{NBD}-Mre11^{HLH} and pRS313:scRad50 constructs.

Mutation in tmRad50	Mutation in scRad50
R2Q	-
R5Q	-
R9E	-
N10D	-
R94E	K103E
K95E	K104E
K99E	Q115E
K108E	-
K109E	-
K115E	R131E
K175E	N190E
K182E	-
R765E	R1201E
S768R	S1205R
E798Q	E1235Q
R94E+K115E	K103E+R131E
K95E+K115E	K104E+R131E

Construct for the end-joining activity assay containing kanMX cassette with 456 bp upstream (promoter) and 270 bp downstream (terminator) regions:

pRS315:kanMX [full-length; SalI/BamHI].

Prior to end-joining experiments, 3 μg of pRS315:kanMX construct was linearized with 30 U of NcoI for 2 h at 37°C, followed by 20-minute enzyme inactivation at 80°C.

DNA used in *in vitro* assays

Circular supercoiled and nicked plasmids (ΦX174 RF I and ΦX174 RF II, respectively) for EMSA were purchased from New England Biolabs. In order to prepare a circular relaxed species of the plasmid DNA, 1 μg of ΦX174 RF II was ligated with 10 U of T4 ligase for 12 hours at 22°C. The ligase was then inactivated by 10-minute incubation at 65°C. Linearized plasmid species was prepared by enzymatic digest of 1 μg ΦX174 RF I with 20 U of EcoRI restrictase for 2 h at 37°C and subsequent 20-minute enzyme inactivation at 65°C.

Blunt-ended dsDNA was prepared by annealing adequate oligonucleotides listed in Table 3. To this aim, oligonucleotides were mixed with annealing buffer (40 mM Tris pH 7.5, 100 mM NaCl, 10 mM $MgCl_2$), at 1.2 molar excess of fluorescently labelled oligonucleotide, preheated to 94°C and cooled down to 4°C at the rate of 0.1°C/s.

Blunt-ended 200 bp DNA used for eliciting DNA damage response in *Xenopus laevis* egg extract was prepared in a PCR and purified by extraction from agarose gel. Samples were prepared according to the following protocol, with Phusion Flash Master Mix (Finnzymes, Espoo, Finnland), containing polymerase and deoxyribonucleotides:

pBluescript SK+ II (template)	50-100 ng	98°C	1 min
pBlue_For 50 μM	0.5 μl	98°C	30 s
pBlue_Rev 50 μM	0.5 μl	52°C	20 s
Phusion master mix	10 μl	72°C	5 s
H_2O	ad 20 μl	72°C	5 min
		4°C	∞

dsDNA used in crystallization experiments was prepared by annealing adequate oligonucleotides listed in Table 2. To this aim, oligonucleotides were mixed with annealing buffer (40 mM Tris pH 7.5, 100 mM NaCl, 10 mM $MgCl_2$), at 1:1 molar ratio, preheated to 94°C and cooled down to 4°C at the rate of 0.1°C/s.

Strains (*E. coli* and *S. cerevisiae*) and cell lines

Escherichia coli, *Saccharomyces cerevisiae* strains and insect cell lines used in this work are listed in Tables 6, 7 and 8, respectively.

Table 6. *Escherichia coli* strains used for molecular cloning and protein expression.

***E. coli* strain**	**genotype**	**source**
XL1 Blue	recA1 endA1 gyrA96 thi-1 hsdR17 supE44 relA1 lac [F´ proAB lacIqZΔM15 Tn10 (Tetr)]	Stratagene, Heidelberg
Rosetta (DE3)	F^- ompT $hsdS_B(r_B^- m_B^-)$ gal dcm (DE3) pRARE2 (CamR)	Novagen, Madison, USA
DH10MultiBac	F^- mcrA Δ(mrr-hsdRMS-mcrBC) Φ80lacZΔ M15 lacX74 recA1 endA1 araD139 (ara, leu)7697 galU galK Δ– rpsL nupG /pMON14272 / pMON7124	Dr. Imre Berger Redbiotech, Schlieren, Switzerland

Table 7. *Saccharomyces cerevisiae* strains used in *in vivo* assays.

***S. cerevisiae* strain**	**genotype**	**source**
W303-1a	Mat**a** ade2-1 ura3-1 trp1-1 his3-11,15 leu2-3,112 can1-100 rad5-535	Dr. Boris Pfander, Max-Planck Institute for Biochemistry, Martinsried
W303-1a Δrad50	rad50Δ:TRP1 Mat**a** ade2-1 ura3-1 trp1-1 his3-11,15 leu2-3 112 can1-100 rad5-535	Dr. Stephen Jackson, Gurdons Institute, Cambridge

Table 8. Insect cell lines used for baculovirus generation and protein expression.

insect cell line	**origin**	**source**
Sf21	clonal isolate derived from *S. frugiperda*	Invitrogen, Karlsruhe
HighFive	clonal isolate derived from *T. ni*	Invitrogen, Karlsruhe

Media and antibiotics

Escherichia coli cultures (XL1 Blue and Rosetta) were grown in liquid LB (lysogeny broth) medium (1% (w/v) bacto-tryptone, 0.5% (w/v) yeast extract, 1% (w/v) NaCl) or on LB plates containing 1.5% (w/v) agar. Respective antibiotics were added to media to final concentrations: 100 μg/mg ampicilin, 50 μg/ml kanamycin, 34 μg/ml chloramphenicol.

Escherichia coli cultures (DH10MultiBac) were grown in 2xYT medium (yeast extract tryptone) (1.6% (w/v) bacto-tryptone, 1% (w/v) yeast extract, 0.5% (w/v) NaCl, pH 7.0) or on LB plates containing 0.1 mM IPTG, 50 μg/ml kanamycin, 10 μg/ml tetracycline, 10 μg/ml X-Gal and 7 μg/ml gentamycin.

Saccharomyces cerevisiae cultures (strains W303-1a and W303-1a Δrad50) were grown in liquid YPD medium (yeast extract peptone dextrose; 1% (w/v) bacto-peptone, 1% (w/v) yeast extract,

2% (w/v) glucose) or on YPD plates containing 2% agar. These same strains transformed with pRS313 constructs were grown in synthetic SDC(-His) medium (Formedium, Hunstanton, UK) (0.675% (w/v) yeast nitrogen base without aminoacids, 0.06% (w/v) complete synthetic mix with all aminoacids except the auxotrophy marker histidine) or on SDC(-His) plates containing 2% agar.

Sf21 insect cells were grown in Sf-900 III (GIBCO/Invitrogen, Karlsruhe) serum-free medium supplemented with 10 μg/ml gentamycin.

HighFive insect cells were grown in Express Five (GIBCO/Invitrogen, Karlsruhe) serum-free medium prepared according to the manufacturer's instruction and supplemented with 10 μg/ml gentamycin and 9.5 mM L-glutamine (GIBCO/Invitrogen, Karlsruhe).

Antibodies

Primary and secondary antibodies and their respective concentration used for immune-based detection of proteins are listed in Tables 9 and 10, respectively.

Table 9. Primary antibodies and serum used for the immune-based protein detection and immuno-depletion.

primary antibody	origin	dilution	source
anti-Rad50, *S.cerevisiae*	rabbit, polyclonal	1:4000	Dr. John Petrini, Memorial Sloan-Kettering Cancer Center, New York, USA
anti-β-actin, human	mouse, monoclonal	1:4000	Abcam (ab8224), Cambridge, UK
anti-Mre11 serum, *X. laevis*	rabbit, polyclonal	1:2000	Dr. Jean Gautier, Columbia University Medical Center, New York, USA
anti-phosphorylated-ATM (anti-P-ATM), human	rabbit, polyclonal	1:1000	Abcam (ab979891) Cambridge, UK
anti-α-tubulin, *R. norvegicus*	mouse, monoclonal	1:6000	Sigma Aldrich (T8203), Munich

Table 10. Secondary antibodies used for the immune-based protein detection.

secondary antibody	origin	dilution	source
anti-rabbit IgG-HRP	goat, polyclonal	1:5000 (in blots against xlMre11) 1:10000 (in blots against scRad50)	Biorad (17-6515), Munich
anti-mouse IgG-HRP	sheep, polyclonal	1:5000	GE Healthcare (NA9310V), Munich

3.2. Molecular biology methods

Molecular biology procedures were carried out according to standard protocols unless otherwise stated. Commercially available kits and enzymes were used according to the manufacturer's instructions.

Molecular cloning

Constructs carrying ORFs of single subunits of the human MRN complex were a gift from Dr. T. Paull (University of Texas, Austin, USA) and are listed in Table 11.

Table 11. Constructs of the human MRN subunits (gift from T. Paull).

construct name	encoded ORF	tag
pTP hMre11$^{6His/C}$	full-length	6xHis at C-terminus
pTP hRad50$^{6His/C}$	full-length	6xHis at C-terminus
pTP hNbs1	full-length	-

These constructs were used to prepare pFBDM-based constructs for protein expression in insect cells. Primers listed in Table 1, introducing restriction sites and 6-histidine tag in case of the Nbs1$^{6His/C}$ construct, were used to amplify full-length ORFs of Mre11, Rad50$^{6His/C}$, Nbs1 and Nbs1$^{6His/C}$ according to the following PCR protocol:

template	50-100 ng	98°C	1 min
Forward primer 50 µM	0.5 µl	98°C	30 s
Reverse primer 50 µM	0.5 µl	56°C	20 s
Phusion master mix	10 µl	72°C	1 min/3 kb s
H_2O	ad 20 µl	72°C	5 min
		4°C	∞

PCR products and pFBDM vector were digested with adequate restriction enzymes. To prevent religation, the vector was dephosphorylated with 2 U of alkaline phosphatase per 1.5 μg vector for 30 min at 37°C. Ligation was performed with 2.5 U of T4 ligase at vector : insert molar ratio of 1:5 or 1:10, with 50-100 ng of vector, for 12 h at 22°C. Prior to transformation the ligase was inactivated for 20 min at 65°C.

pFBDM:hMre11_hRad50 and pFBDM:hMre11_hRad50$^{6His/C}$ constructs were prepared according to the above protocol by ligating pFBDM_hRad50 or ligating pFBDM_hRad50$^{6His/C}$ with the digested PCR product of hMre11.

pFBDM:hMre11_hRad50$^{6His/C}$_hNbs1 was prepared, using the multiplication cassette of the pFBDM vector. pFBDM:hNbs1 was digested with restrictases SpeI and BstZ17I and dephosphorylated. hMre11/hRad50$^{6His/C}$ segment was excised from pFBDM: hMre11 _hRad50$^{6His/C}$ construct with PmeI and AvrII enzymes and ligated with pFBDM:hNbs1 due to compatibility of cohesive SpeI- and AvrII-generated ends and PmeI-/BstZ17I-generated blunt ends. Ligation was performed as described before at vector : insert molar ratio of 1:2.

pET29b:tmRad50^{NBD}_Mre11^{HLH} construct was previously prepared by A. Schele (Hopfner group). *Tm*Rad50^{NBD} was engineered by fusing the N-terminal (aa 1-190) and C-terminal (aa 686-852) segments of Rad50 with an 8-aminoacid linker (GGAGGAGG) in a single ORF and cloning into pET29b with NdeI/NotI. *Tm*Mre11^{HLH} motif (aa 343-385) with a 6-histidine tag at the C-terminus was cloned downstream of the Rad50^{NBD} with NotI/Bpu1102I.

pRS313:scRad50 construct was prepared by subcloning wild-type scRad50 ORF with promoter and terminator regions from pRS426:scRad50 construct (gift from H. Feldmann, Genzentrum LMU) to pRS313 vector with XhoI/EcoRI.

pRS315:kanMX construct was prepared by subcloning kanMX cassette containing 456 bp upstream (promoter) and 270 bp downstream (terminator) regions from pRS314:kanMX construct (gift from H. Feldmann, Genzentrum LMU) to pRS315 vector with SalI/BamHI.

Site-directed mutagenesis

In order to obtain point mutations in pET29b:tmRad50^{NBD}_Mre11^{HLH} and pRS313:scRad50 constructs, site-directed mutagenesis was performed in a single-step PCR with polymerase Pfu Ultra (Agilent, Waldbronn), according to the following protocol:

template	100-200 ng	94°C	5 min
Forward primer 2 μM	0.5 μl	94°C	1 min
Reverse primer 2 μM	0.5 μl	56°C	1 min
Pfu Ultra 10-fold buffer	5 μl	68°C	2 min/1 kb
dNTPs 10mM	1 μl	68°C	10 min
Pfu Ultra 2.5 U/ μl	1 μl	4°C	∞
H_2O	ad 50 μl		

After PCR, 20 U of DpnI restrictase was added to mutagenesis reaction, incubated 2 h at 37°C and inactivated 20 min at 80°C. 5 μl of the sample was the used to transform *E. coli* competent cells. Single colonies were picked for DNA amplification and purification. Mutations were confirmed by DNA sequencing (Eurofins MWG Operon, Ebersberg).

Escherichia coli **transformation**

Chemically competent *E. coli* (XL1 Blue and Rosetta strains) cells were transformed with 50-100 ng of purified plasmid, 20 μl ligation sample or 5 μl mutagenesis sample. After 20-minute incubation on ice, cells were heat-shocked 45 s at 42°C and cooled down 2 min on ice. 600 μl of fresh LB medium was added and the cell suspension was incubated 1 h at 37°C. In case of transformation with purified DNA, 150 μl of cell suspension was plated on LB-agar medium containing appropriate antibiotic. In case of transformation with a ligation sample or mutagenesis sample, cells were first pelleted by brief centrifugation (4000 rcf, 2 min, RT), resuspended in 150 μl of LB medium and plated. Colonies grew 12-16 h at 37°C.

Chemically competent *E .coli* DH10MultiBac cells were transformed with 1.5 ug of purified plasmid and incubated 20 min on ice. Cells were heat-shocked 60 s at 42°C and cooled down 2 min on ice. 1 ml of fresh 2xYT medium was added and the cell suspension was incubated 16 h at 37°C. 20-100 μl of the cell suspension were next plated and incubated for 48-72 h at 37°C. In order to confirm that the colonies contained recombinant backmid (baculoviral DNA), white cells were restreaked on fresh plates and if the white color was preserved (*i. e.* recombination of the ORFs of interest into bacmid was successful), used further for backmid isolation.

3.3. Protein biochemistry methods

Protein expression in *E. coli*

Recombinant protein expression was performed in *E. coli* Rosetta (DE3) strain transformed with pET29b:tmRad50^{NBD}_Mre11^{HLH} carrying wild-type or mutated Rad50 ORF. Cells were grown in LB media under aerobic conditions (150 rpm, 37°C) to an OD_{600} of 0.6-0.8. Protein expression was induced with 0.2 mM IPTG and carried out at 18°C overnight. Cells were harvested by centrifugation (5000 rcf, 15 min, 4°C) and submitted to further purification steps or frozen in liquid nitrogen and stored at -80°C until further use.

Protein expression baculovirus-infected insect cells

Baculovirus preparation in Sf21 cells

Bacmids containing ORFs of the MRN complex or its subunits were used to generate baculovirus particles able to infect and drive protein expression in insect cells. First, 2 ml of Sf21 cells at density 0.4x10^6 cells/ml were incubated at 27.5°C in 6-well culture plate. Transfection solution was prepared by mixing 200 µl medium, 3 µl transfection agent (FuGene, Promega, Mannheim) and 1-2 µg bacmid DNA. After the cells had attached to the bottom of the culture well, transfection solution was added. As a control, cells mixed with a transfection solution without bacmid was also prepared. Cells were further incubated for 72-84 h at 27.5°C, giving rise to the first generation of the baculovirus (P1). 1 ml of medium containing P1 virus was added to 10 ml Sf21 cell suspension at density 1x10^6 cells/ml and cultured for 72-84 h (95 rpm, 27.5°C). After incubation, cells were monitored under a light microscope (viability, morphology). In case of evident infection, cells were pelleted (3000 rcf, 10 min, RT), virus-containing medium was filtered (generation P2) and used to rise final P3 generation. To this end, 100 µl of P2 virus were added to 100 ml of Sf21 cell suspension at density 0.4x10^6 cells/ml and incubated for 72 h (95 rpm, 27.5°C). After incubation, the culture was again monitored for viability and morphology. Infected cells were pelleted (3000 rcf, 10 min, RT), virus-containing medium was filtered (generation P3) and stored at 4°C.

Protein expression in HighFive cells

In order to determine the amount of the virus required for efficient protein expression, small-scale expression tests were performed. To this end, 10 ml HighFive cell suspension at density

$1x10^6$ cell/ml were infected with 0 (control culture), 10, 20 50 and 200 µl of P3 baculovirus. After 72-hour incubation (95 rpm, 27.5°C) cells were monitored for viability and morphology. Protein expression was determined by whole-cell SDS-PAGE analysis. The optimal amount of P3 baculovirus for subsequent large-scale experiments was the lowest volume that still induced protein expression.

hMRN complex was expressed in 500 ml fresh cell suspension. Cells were cultured for 72 h (95 rpm, 27.5°C), pelleted (3000 rcf, 15 min, RT), frozen in liquid nitrogen and stored at -20°C until further use.

Protein purification

tmRad50^{NBD}-Mre11^{HLH}

Cells were resuspended in Lysis buffer and disrupted by sonication. Lysate was cleared by centrifugation (20000 rcf, 30 min, 4°C), incubated 10 min at 65°C to denature *E. coli* endogenous proteins and again cleared by centrifugation (15000 rcf, 15 min, 4°C). Lysate was applied on Ni-NTA affinity chromatography resin in a gravity-flow column. Resin was washed with 2 CV of Lysis buffer and 1 CV of Wash buffer. Protein was eluted with Elution buffer, concentrated and subjected to gel filtration. Fractions corresponding to the monomeric species were collected, concentrated to 60-80 mg/ml, frozen in liquid nitrogen and stored at -80°C. All mutants of tmRad50^{NBD}-Mre11^{HLH} were purified according to this protocol. Table 12 lists buffers used in tmRad50^{NBD}-Mre11^{HLH} preparation.

Table 12. Buffers for purification of the recombinant tmRad50^{NBD}-Mre11^{HLH} complex.

Lysis buffer	Wash buffer	Elution buffer	Gel filtration buffer
25 mM Tris pH 8.0	25 mM Tris pH 8.0	25 mM Tris pH 8.0	5 mM Tris pH 7.8
300 mM NaCl	1.5 M NaCl	100 mM NaCl	200 mM NaCl
10 mM imidazole	20 mM imidazole	150 mM imidazole	

hMRN

Recombinant human MRN complex was purified similarly to the previously reported protocol (Paull and Gellert 1998, 1999). Cell pellet was resuspended in Lysis buffer supplemented with complete mix of protease inhibitors (Roche, Penzberg). Cell suspension was brefly sonified and centrifuged (25000 rcf, 45 min, 4°C). Cell lysate was sonified again, filtered and applied on Ni-NTA resin. After complete migration of the lysate through the column upon gravity flow, the

resin was washed with 2 CV of Lysis buffer and 5 CV of Wash buffer. The complex was eluted with Elution buffer, dialysed to Buffer A, applied on MonoQ column and eluted with 12 CV gradient of 50-500 mM NaCl. Fractions containing MRN complex were pulled together, concentrated and applied on gel filtration column Superose 6. Fractions containing MRN complex were again pulled together, concentrated to approximately 5 mg/ml, frozen in liquid nitrogen and stored at -80°C. Table 13 lists buffer used in hMRN preparation.

Table 13. Buffers for purification of the recombinant hMRN complex

Lysis buffer	Wash buffer	Elution buffer	Buffer A	Gel filtration buffer
50 mM Na phosphate pH 7.0 500 mM NaCl 10 mM imidazole 0.5% (v/v) Tween20 10% (v/v) glicerol 20 mM 2-ME	50 mM Na phosphate pH 7.0 500 mM NaCl 20 mM imidazole 0.5% (v/v) Tween20 10% (v/v) glicerol 20 mM 2-ME	50 mM Na phosphate pH 7.0 500 mM NaCl 100 mM imidazole 0.5% (v/v) Tween20 10% (v/v) glicerol 20 mM 2-ME	20 mM Tris pH 8.0 50 mM NaCl 0.05% (v/v) Tween20 10% (v/v) glicerol 1 mM DTT	20 mM Tris pH 8.0 500 mM NaCl 0.1% (v/v) Tween20 10% (v/v) glicerol 1 mM DTT

SDS-PAGE analysis

Protein samples were analyzed in vertical SDS-polyacrylamide gel electrophoresis system according to Laemmli (Laemmli 1970). 15% acrylamide in the separating gel was used for analysis of tmRad50^{NBD}-Mre11^{HLH} samples, whereas hMRN samples were separated in 10% acrylamide gels.

Samples were mixed with Sample buffer and incubated 5 min at 90°C. Electrophoresis was performed at 200-220 V in Running buffer. Next, gels were stained in Staining solution and destained with deionised water. To determine approximate protein weight, a molecular weight marker was used (PageRuler Prestained 26616 and PageRuler Unstained 26614 from Thermo Scientific for analyses of hMRN and tmRad50^{NBD}-Mre11^{HLH}, respectively; PageRuler Prestained 26616 from Thermo Scientific and Dual Color 161-0374 from Biorad for Western blot analyses of yeast samples and *X. laevis* egg extract samples, respectively). Table 14 lists buffers used for sample preparation and SDS-PAGE electrophoresis.

Table 14. Buffers used for the SDS-PAGE analysis.

4-fold Sample buffer	Running buffer	Staining solution
110 mM Tris pH 6.8 16% glycerol 4% (w/v) SDS 5% 2-ME 0.6% bromphenolblue	25 mM Tris 192 mM glycine 0.1% (w/v) SDS	7% (w/v) acetic acid 50% (w/v) EtOH 0.2% (w/v) Coomassie Brilliant Blue R-250

Dimetrization of tmRad50^{NBD}-Mre11^{HLH}

Dimerization of the monomeric tmRad50^{NBD}-Mre11^{HLH} complex was initiated by addition of AMPPNP. Protein was mixed with AMPPNP to final concentration of 20 mg/ml protein and 5 mM AMPPNP in dimerization buffer and incubated at 8°C. Dimerization was monitored by analytical gel filtration after 1, 5, 24, 48 and 72 h after reaction start. The process was very fast (for wild-type protein and most mutants it reached the maximal dimerization efficiency already between 1-5 h) but for practical reasons protein was always dimerized for 24 h prior to *in vitro* activity assays. Table 15 lists stocks and buffers used for preparation of dimerized tmRad50^{NBD}-Mre11^{HLH} species.

Table 15. Stocks and buffer used for tmRad50^{NBD}-Mre11^{HLH} dimerization.

monomeric protein stock	ANPPNP stock	Dimerization buffer
60-80 mg/ml	50 mM in 100 mM Tris pH 7.5	5 mM Tris pH 7.8 100 mM NaCl 5 mM $MgCl_2$

Analytical gel filtration

Protein homogeneity and dimerization efficiency was monitored by analytical gel filtration. Dimerization mix was first diluted to protein final concentration of 8 mg/ml, injected on Superdex s200 5/150 column and eluted in the running buffer containing 5 mM Tris pH 7.8, 100 mM NaCl and 5 mM $MgCl_2$.

Western blot analysis

S. cerevisiae samples

TCA-precipitated whole-cell yeast lysates were first subjected to SDS-PAGE analysis in 8% acrylamide gels and then blotted onto nitrocellulose membrane (Roth) in Transfer buffer with 20% EtOH and 0.1% (w/v) SDS. Transfer was carried out at 200 mA for 1 h at 8°C. The

membrane was then blocked in TBST buffer supplemented 5% milk for 1 h at RT. Incubation with the primary antibody (anti-Rad50 and anti-α-actin as loading control) was performed overnight at 8°C in TBST buffer with 5% milk. Next, the membrane was washed with TBST buffer (3 x 10 min) and incubated with a HRP-conjugated secondary antibody in TBST for 1 h at RT. Finally, the membrane was washed in TBST buffer (3 x 15 min) and immunostained proteins were detected by adding HRP substrate solution and subsequent exposure with a light sensitive Hyperfilm™ ECL™ (GE Healthcare).

X. laevis samples

Xenopus laevis egg extract samples were first subjected to SDS-PAGE analysis in 4-12% gradient Bis-Tris gel (Criterion, Biorad) in XT buffer (Biorad) and blotted onto PVDF membrane (Millipore) in 2-fold Transfer buffer with 20% EtOH and 0.05% (w/v) SDS. Transfer was performed at 250 mA for 2 h at 8°C. The membrane was next blocked in TBST supplemented with 5% milk for 1 h at RT, washed with TBST (3 x 15 min) and incubated with the primary antibody (anti-P-ATM and anti- α-tubulin as loading control) in TBST overnight at 8°C. After washing with TBST (3 x 15 min), the membrane was incubated with HRP-conjugated secondary antibody in TBST for 1 h at RT and washed again with TBST (3 x 15 min). Immunostained proteins were detected by adding HRP substrate solution and subsequent exposure with a light sensitive Hyperfilm™ ECL™ (GE Healthcare). Table 16 lists buffers and solutions used for Western blot analysis.

Table 16. Buffers for the Western blot analysis.

Transfer buffer	TBST buffer	HRP substrate solution
25 mM Tris	20 mM Tris pH 7.4	100 mM Tris pH 8.5
195 mM glycine	150 mM NaCl	225 uM coumaric acid
	0.1% (v/v) Tween20	1.25 mM luminol
		0.009% (w/v) H_2O_2

Electrophoretic mobility shift assay

With plasmid DNA

DNA-binding properties of the wild-type tmRad50^{NBD}-Mre11^{HLH} were analysed in electrophoretic mobility shift assay (EMSA). Increasing amount of dimerised protein (0, 71.5 nM, 357.5 nM, 715 nM, 1.43 μM, 3.57 μM, 7.15 μM, 14.3 μM, 28.6 μM and 57.2 μM) was

incubated with plasmid DNA (7.15 nM) in 5 mM Tris pH 7.8, 100 mM NaCl, 5 mM $MgCl_2$ in a total volume of 20 μl for 15 min on ice. The reaction samples were next mixed with loading buffer (6-fold loading buffer: 10 mM Tris pH 7.8, 16% (v/v) glycerol, 0.03% (w/v) bromphenol blue, 0.03% (w/v) xylene cyanol) and separated in 0.5% agarose gel in TA buffer (40 mM Tris, 20 mM acetic acid) for 3.5 h at 80 V and 8°C. Protein-DNA complexes were stained with DNA-intercalating agent GelRed and visualized by UV Imaging System (Intas). Four different plasmid species were used in that assay: circular nicked relaxed ΦX174 RF II, circular intact relaxed ΦX174 RF II, circular supercoiled ΦX174 RF I and linearized ΦX174 RF I.

DNA-binding by mutants of tmRad50^{NBD}-Mre11^{HLH} was analyzed with circular nicked relaxed ΦX174 RF II, according to the above protocol.

With short dsDNA

Increasing amounts of dimerised tmRad50^{NBD}-Mre11^{HLH} (0, 125 nM, 250 nM, 375 nM, 625 nM, 1.25 μM, 2.5 μM, 5 μM and 12.5 μM) were incubated with 25 nM 30 and 60 bp blunt-ended and fluorescently labelled DNA in 5 mM Tris pH 7.8, 100 mM NaCl, 5 mM $MgCl_2$ in a total volume of 10 μl for 15 min on ice.

Reaction samples were next mixed with loading buffer (6-fold loading buffer: 10 mM Tris pH 7.8, 16% (v/v) glycerol, 0.03% (w/v) bromphenol blue, 0.03% (w/v) xylene cyanol) and separated in 8% poliacrylamide native gel in TA buffer (40 mM Tris, 20 mM acetic acid) for 1-1.5 h at 100 V and 8°C. Protein-DNA complexes were visualized with a Typhoon System (Amersham Biosciences) using the green-excited (488 nm) fluorescence mode.

Similar reaction was performed with 60 bp intact and 60 bp nicked DNA, but at DNA concentration of 50 nM and increasing protein concentrations of 0, 1.25 μM, 2.5 μM, 5 μM, 10 μM, 12.5 μM, 25 μM, 50 μM and 100 μM.

3.4. Structural biology methods

Crystallization and crystal freezing

Prior to screening and refinement, tmRad50^{NBD}-Mre11^{HLH} protein was mixed with ANPPNP and DNA stocks, giving crystallization mix of 12 mg/ml protein, 5 mM AMPPNP and 3.5-5 molar excess of DNA. First screenings were performed in 96-well plates, using commercially available crystallization screens. Refinements of the initial condition (0.15 M D-maleic acid, 20% (w/v)

PEG3350) were performed in 24-well plates by the hanging drop vapor diffusion method, diluting 1 µl of the crystallization mix with 1 µl of the mother liquor and closing the drop over 400 µl-reservoir with the mother liquor. During refinement varying pH values and PEG3350 content were used. Crystals of tmRad50^{NBD}-Mre11^{HLH}-DNA were grown at 20°C. They appeared after 24 h and grew further for the next 7-10 days. At that point, they were fished and frozen in liquid nitrogen under cryoprotective conditions, containing mother liquor with 20-25% (v/v) glycerol or 15% (v/v) L-(+)-2,3-butanediol.

Data collection

Diffraction data were collected at beamlines ID-29 and BM-30 at European Synchrotron Radiation Facility (ESRF, Grenoble, France) or at X06SA beamline at Swiss Light Sourse synchrotron (SLS, Villigen, Switzerland). Most crystals formed space group P2(1) with one dimeric molecule per asymmetric unit and cell dimensions: a=49.8 Å, b=106.0 Å, c=93.9 Å, α=90°, β=98.3°, γ=90°. Crystal that yielded the final structure formed space group P1 with two dimeric molecules per asymmetric unit and cell dimensions: a=50.2 Å, b=107.6 Å, c=97.1 Å, α=90.6°, β=98.3°, γ=89.4°. Data processing was performed with XDS software (Kabsch 1993).

Structure determination, model building and refinement

The structure was determined first by molecular replacement with Phaser (McCoy et al. 2007), using the tmRad50^{NBD}-Mre11^{HLH} apo structure as a search model (PDB entry: 3QF7). The initial model was rebuilt manually in COOT (Emsley and Cowtan 2004) and refined in Phenix (Adams et al. 2002). At early stage of manual building and refinement, a 15 bp DNA molecule was manually build into the difference density and the model was subjected to rigid-body refinement constrained to the built-in DNA. Further refinements included interative cycles of bulk solvent corrections, overall *B*-values, positional and B-factor, TLS refinement and manual building. Prior to refinement, 5% of the reflections were randomly omitted to monitor the R_{free} value.
All figures of structural models were prepared with PyMOL (DeLano Scientific).

3.5. Yeast specific methods

Yeast transformation with pRS313:scRad50 constructs

3 ml of YPD medium were inoculated with one loop of *S. cerevisiae* W303-1a (wild-type) or W303-1a Δrad50 and grown overnight (155 rpm, 30°C). In the morning next day cultures were diluted 1:5 or 1:10 in 3 ml of fresh medium and grown further for 3-4 h until OD_{600} of 1-2 was reached. Cells were pelleted by centrifugation (4000 rcf, 1 min, RT) and resuspended in 100 µl Solution 1 (10 mM Tris pH 7.4, 100 mM lithium acetate). 3 µg of respective construct was premixed with 10 µl of salmon sperm DNA (10 mg/ml stock) and added to the cell suspension. Next, 500 µl of Solution 2 (10 mM Tris pH 7.4, 100 mM lithium acetate, 50% (w/v) PEG3350) was added, vortexed and rotated 30 min at RT on a turning wheel. Cell suspension was next subjected to 10-minute heat-shock step at 42°C. After a 2-minute incubation on ice, cells were pelleted by centrifugation (4000 rcf, 1 min, RT), resuspended in 100 µl of deionised water and plated on SDC(-His)-agar medium. Plates were incubated 72 h at 30°C.

Plate survival assay

3 ml of SDC(-His) medium were inoculated with a single colony of *S. cerevisiae* W303-1a or W303-1a Δrad50 transformed with pRS313 constructs and grown overnight (155 rpm, 30°C). Cultures were diluted in deionised water to OD_{600} of 1 and serial 10-fold dilutions in water were prepared (10^0-10^{-5}). 4 µl of each dilution were plated on SDC(-His)-agar medium supplemented with DNA-damaging agents: 0.005% MMS or 1 µg /ml CPT or 50 mM HU. Cells were incubated at for 72 h at 30°C. Experiment was performed in triplicates.

Sample preparation for Western blot analysis

TCA-precipitated whole-cell yeast lysates for Western blot analysis were prepared according to a modified protocol based on Yaffe and Schatz (Yaffe and Schatz 1984). 20 OD units of an overnight yeast culture were centrifuged and the cell pellet was washed with 1 ml deionised water. Cells were lysed at RT with 1.5 ml Solution 1 (200 mM NaOH, 1% 2-ME) and vortexing. 150 µl 50% (w/v) TCA was added, cell were vortexed again, incubated for 10 min on ice and centrifuged (16000 rcf, 10 min, 4°C). Pellet was washed with 1.5 ml acetone and incubated 5 min on ice. After centrifugation (16000 rcf, 5min, 4°C), pellet was resuspended in 25 µl of 2-fold Sample buffer (Table 13), sonified in a bath sonicator for 2 min and incubated 5 min at 90°C.

The samples were centrifuged again (16000 rcf, 5min, 4°C) and 6 µl of the supernatant was submitted to SDS-PAGE and subsequent Western blot analysis.

Analysis of end-joining activity

20 ml of SDC(-His) medium were inoculated with a full loop of *S. cerevisiae* W303 1a-WT (wild-type) or W303-1a Δrad50 transformed with pRS313 constructs and grown overnight (155 rpm, 30°C). Next day morning cultures were diluted in 100 ml of fresh YPD medium to OD_{600} of 0.1-0.2 and grown further for 4-6 h until OD_{600} of 0.6-0.8 was reached. Cells were pelleted (3000 rcf, 20 min, RT), washed with 50 ml of deionised water, pelleted again (3000 rcf, 20 min, RT) and resuspended in 2 ml of 100 mM lithium acetate. Cells were again harvested by centrifugation (16000 rcf, 15 s, RT) and resuspended in 200 µl of 100 mM lithium acetate. 100 µl of this cell suspension was centrifuged (5000 rcf, 1 min, RT), supernatant was discarded and the cells were mixed with 240 µl of 50% (w/v) PEG3350, 36 µl 1 M lithium acetate, 54 µl deionised water and 3 µg of supercoiled or linearized pRS315:kanMX construct, vortexed and incubated 30 min at 30°C prior to 25-minute heat-shock step at 42°C. After brief incubation on ice, cells were pelleted (6000 rcf, 1 min, RT), resuspended in 1 ml of deionised water. 100 µl of the cell suspension were plated on SDC(-His, -Leu)-agar medium and incubated for 72 h at 30°C. Experiment was performed in triplicates.

Colonies were counted; the average number of colonies formed by cells transformed with the linearized plasmid was normalized against the average number of transformants with the supercoiled plasmid. Error was calculated using the relative standard deviation method.

Analysis of telomere length (assay performed by Dr. H. Feldmann, Gene Center, Munich)

Genomic DNA was isolated from 100 ml overnight *S. cerevisiae* culture at OD_{600}=1.5-2.0. 1 µg of the DNA was digested with 10 U XhoI overnight at 37°C and analysed on 1% agarose gel in TAE buffer (Tris-acetate-EDTA buffer; 40 mM Tris, 20 mM acetic acid, 1 mM EDTA). DNA was subsequently blotted onto nitrocellulose membrane and hybridized with a [^{32}P]-labelled poly$(GT)_{20}$ probe in Church buffer (7% SDS, 1% BSA, 250 mM Na_2HPO_4, 1 mM EDTA) overnight at 60°C. Blots were washed in 0.2-fold SSC buffer (saline-sodium citrate buffer, 1-fold: 15 mM trisodium citrate pH 7.0, 150 mM NaCl) supplemented with 0.1 % SDS for 20 min at RT. DNA was visualized by autoradiography.

3.6. *Xenopus laevis* specific methods

Egg extract preparation and monitoring

Interphase *Xenopus laevis* egg extracts were prepared according to a modified protocol based on Kubota (Kubota and Takisawa 1993). Eggs derived from hormonally primed female frogs were collected and washed with 100 mM NaCl. Approximately 50 ml of eggs were used to prepare one batch of egg extract. Eggs were dejellied in 50 ml Buffer D supplemented with 5 mM DTT (10 min, RT), washed with 1/4 MMR buffer (3 x 50 ml) and activated with 2 µl calcium ionophore for 5 min. Eggs were washed again with 1/4 MMR buffer (3 x 50 ml) and then with ice-cold buffer S (3 x 50 ml) supplemented with 10 µg/ml leupeptin in the last step. Washed eggs were transferred to 2 ml eppendorf tubes and packed by brief centrifugation (2000 rcf, 45 s, 4°C). Buffer excess was discarded and eggs were crushed by centrifugation (16000 rcf, 12 min, 4°C). Cytoplasmatic fraction was collected, mixed with cytochalasin B to final concentration of 40 µg/ml and centrifuged again (70000 rcf, 12 min, 4°C). Cytoplasmatic and membrane fractions were collected, mixed with glycerol to final concentration of 1%, frozen in 20 µl aliquots in liquid nitrogen and stored in liquid nitrogen.

In order to check if prepared extracts were indeed arrested in interphase, replication activity was monitored. To this end, 20 µl of the extract was mixed with creatin phosphate (final concentration 30 mM), creatin phosphor kinase (final concentration 150 µg /ml), cyclohexamide (final concentration 40 µg/ml), Cy3-dCTP (final concentration 1 µM) and demembrated sperm nuclei (final concentration 3000 nuclei/ µl) and incubated at 23°C. 3 µl of this reaction were mixed with 3 µl FIX buffer and monitored for replication at time point 0, 30 and 60 min. Extract that supported replication were used for subsequent experiments. Table 17 lists buffers and reagent stocks used for egg extract preparation and handling.

Table 17. Buffers and stocks used for *X. laevis* egg extract preparation.

Buffer D	Buffer MMR	Buffer S	FIX buffer
10 mM Tris pH 8.5 110 mM NaCl	20 mM Hepes-KOH pH 7.5 400 mM NaCl 2 mM KCl 1 mM $MgSO_4$ 2 mM $CaCl_2$ 0.1 mM EDTA	50 mM Hepes-KOH pH 7.5 50 mM KCl 2.5 mM $MgCl_2$ 250 mM sucrose	25 mM Hepes-KOH pH 7.8 25 mM KCl 1.25 mM $MgCl_2$ 18% glycerol 3 µg/ml Hoechst

calcium ionophore	10 mM stock in DMSO
cytochalasin B	10 mg/ml stock in DMSO
creatin phosphate	1 M stock in deionised water
creatin phosphor kinase	10 mg/ml stock in deionised water
cyclohexamide	10 mg/ml stock in deionised water

Immunodepletion of MRN complex

In order to remove endogenous MRN complex from egg extract, anti-xlMre11 serum was used (gift from J. Gautier). 25 µl of the serum was first incubated with 40 µl 50% (v/v) Protein-A Sepharose slurry (GE, Healthcare) in PBS for 1 h at RT on a turning wheel (15 rpm). The beads were then washed (3 x 400 µl of PBS), divided and transferred to 3 new eppendorf tubes for subsequent 3 round of immundepletion. Protein-A beads for mock depletion were prepared as described above but PBS was used instead of the serum. 50 µl of egg extract was incubated three times with aliquots of antibody bound beads (or free beads for mock extract preparation). Incubation was performed for 45, 30 and 30 min at 4°C on a turning wheel (4 rpm). Extract was separated from the beads and the efficiency of immunodepletion was monitored by Western blot analysis.

DNA-induced ATM phosphorylation

Immunodepleted and mock extracts were used to check DNA damage response. To this end, 9.5 µl of the extract was mixed with 0.5 µl DNA stock (200 bp blunt-ended DNA, 35 ng/µl) and incubated at 23°C for 0, 2, 5, 10, 15 and 30 min. At each time point, 0.5 µl of the reaction was taken to prepare an SDS-PAGE sample. Subsequently, samples were separated in SDS-PAGE (Criterion, Biorad), blotted and immunostained against phosphorylated ATM.

Rescue of ATM signalling in MRN-depleted extract

Recombint hMRN complex, expressed in insect cells was previously shown to rescue DNA damage response in MRN-depleted egg extracts (Costanzo et al. 2001). In this work, an attempt to reproduce this experiment was undertaken, using wild-type hMRN preparation and in case this was successful, further experiments were to be performed with hMRN mutants.

Immunodepleted and mock-depleted extracts were preincubated with 1 or 2 µl of recombinant hMRN (5.8 mg/ml) for 15 min at 23°C. As a control, extract were also mixed with hMRN

storage buffer. Next, 0.5 µl of DNA was added and samples for SDS-PAGE were prepared at timepoints 0, 15, 30 and 60 min. ATM-phosphorylation was monitored as the readout of DNAdamage response.

3.7. Bioinformatic methods

Sequence alignments of Rad50 orthologues were performed with the program ClustalOmega, available online: http://www.ebi.ac.uk/Tools/msa/clustalo/ (Sievers et al. 2011).

4. Results

4.1. Preparation of the Rad50^{NBD}-Mre11^{HLH} complex from *T. maritima*

Previous attempts of crystallizing longer *T. maritima* and *P. furiosus* MR complexes with DNA were unsuccessful (work of C. Möckel, Hopfner group). For this reason, a minimal part of the protein complex, containing the Rad50 ATPase domain (NBD, nucleotide-binding domain) together with a short helix-loop-helix Rad50-interacting motif of Mre11 (tmRad50^{NBD}-Mre11^{HLH}), was used for further studies and crystallization trials.

4.1.1. Cloning and purification

Construct containing catalytic head of tmRad50 and a short peptide of tmMre11 was a gift from A. Schele (Hopfner group). In this construct, the bipartite N- and C-terminal segments of the Rad50 NBD together with the adjacent coiled-coil domain (residues 1-190 and 687-852) were fused via a flexible linker GGAGGAGG. A short helix-loop-helix motif of Mre11 (residues 347-385), encompassing the very C-terminal part of the protein and carrying a polyhistidine C-terminal tag was cloned downstream to the Rad50 ORF. It was shown before that one of the interaction interfaces between Mre11 and Rad50 relies on a strong hydrophobic interaction between the root of the coiled-coil domain and the HLH motif of Mre11 (Lammens et al. 2011). This hydrophobic patch on the Rad50 coiled-coil, if remained unoccupied, could potentially influence solubility of the recombinant protein. Therefore, the construct design included the helix-loop-helix motif of Mre11, assuming it would render Rad50 more stable and soluble (Figure 10).

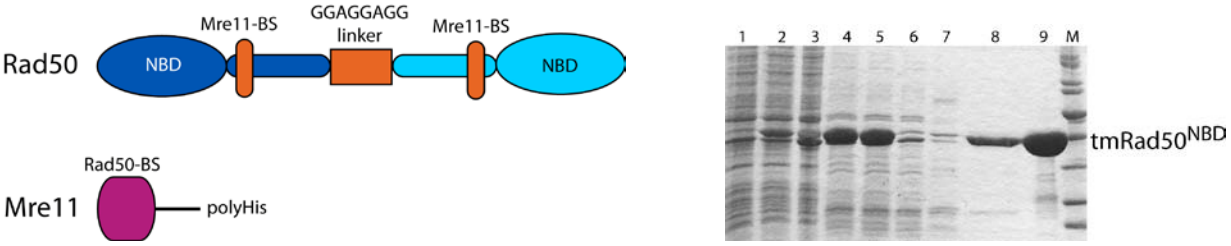

Figure 10. Construct preparation and purification of tmRad50^{NBD}-Mre11^{HLH}. Left panel: construct design of the tmRad50^{NBD}-Mre11^{HLH} catalytic head; BS: binding site. Right panel: SDS-PAGE analysis of the tmRad50^{NBD}-Mre11^{HLH} purification on Ni-NTA resin (1: cells before induction, 2: cells after induction, 3: pellet, 4: cleared cell lysate, 5: cleared lysate after heat step, 6: flow-through, 7: wash 1, 8: wash 2, 9: elution). Due to the small size of Mre11^{HLH} only Rad50^{NDB} is detectable.

The complex was recombinantly co-expressed in *E. coli*. Subsequent purification and crystallization revealed that both proteins were interacting very stably, even if high concentrations of salt were used (up to 1.5 M NaCl during purification). The MR complex eluted from the Ni-NTA resin was directly applied on the gel filtration column. Interestingly and in contrast to recombinant eukaryotic orthologues, the gel filtration profile showed that the complex migrated predominantly as a monomeric species (including one Rad50 molecule and one Mre11 HLH motif), with only a minor fraction forming a dimer (Figure 11).

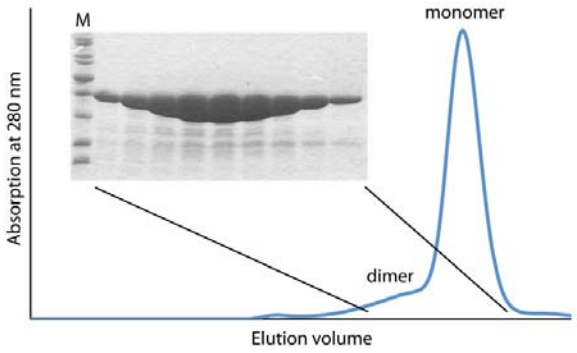

Figure 11. Elution profile of tmRad50^{NBD}-Mre11^{HLH} in gel filtration. Small fraction of the protein forms a dimer, the rest remains in a monomeric form. Due to the small size of tmMre11^{HLH} only tmRad50^{NDB} is detectable on the SDS-PAGE gel.

Heterologous expression of the tmRad50^{NBD}-Mre11^{HLH} complex was very efficient, with an average yield of 12 mg of protein per 1 g of cells.

4.1.2. Dimerization

Prior to crystallization and biochemical analyses, the monomeric tmRad50 carrying the tmMre11 HLH motif was dimerized, to assure correct formation of the bipartite ATPase domains. To this end, tmRad50^{NBD}-Mre11^{HLH} was incubated with AMPPNP. The reason to use AMPPNP was to avoid subsequent hydrolysis and opening of the complex as it was suggested before (Lammens et al. 2011).

Dimerization efficiency was monitored over time with gel filtration. As expected, the protein dimerized very efficiently; most of the protein formed a dimeric species between 1-5 h after addition of AMPPNP, with an average efficiency of approximately 85%. This dimeric form was stable over time at least until 96 h after addition of AMPPNP. Even though a high excess of

AMPPNP was used to induce dimerization, the protein was never completely dimerized, leaving about 15% in a monomeric state (Figure 12).

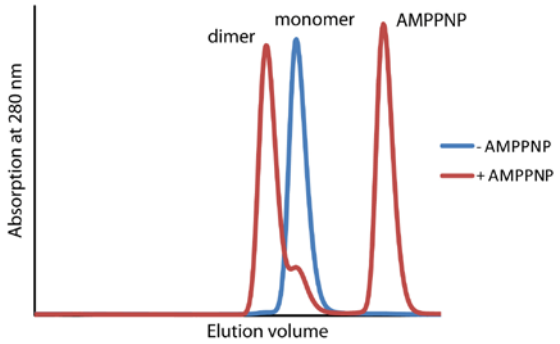

Figure 12. **AMPPNP-induced dimerization of tmRad50^{NBD}-Mre11^{HLH}.** As monitored in gel filtration, in the absence of AMPPNP the protein remains in a monomeric form (blue line). Addition of AMPPNP and Mg^{2+} results in a dimer formation (red line).

4.2. Crystal structure of tmRad50^{NBD}-Mre11^{HLH} with DNA

4.2.1. Crystallization and structure determination

In order to gain structural insight into the Rad50-DNA complex formation, tmRad50^{NBD}-Mre11^{HLH} was crystallized with DNA. To this end, monomeric tmRad50^{NBD}-Mre11^{HLH} was mixed with short dsDNA of varying lengths (13 bp, 15 bp, 15 bp with 1 nt overhang, 17 bp and 21 bp) and AMPPNP and screened against various conditions. AMPPNP was used instead of ATP in order to prevent hydrolysis and subsequent dimer dissociation (Lammens et al. 2011). Other non-hydrolyzable ATP analogs were not tested, as it had been observed before that the protein behaviour was better with AMPPNP than with ATPγS (C. Möckel, personal communication).

Four initial hits were further optimized in the refinement steps and macroscopically good-quality crystals were subjected to X-ray diffraction experiments. Initial data analysis, including structure determination by molecular replacement with the apo tmRad50^{NBD}-Mre11^{HLH} model (PDB entry: 3QF7) showed that most of these crystals did not contain DNA and therefore were not further refined and processed.

DNA-containing crystals appeared with 15 bp-DNA with 1 nt overhang in a crystallization condition containing 150 mM D-malic acid pH 7.0 and 20% (w/v) PEG3350. They were refined

against pH and PEG3350 concentration. It turned out that bigger and more numerous crystals grew preferentially in acidic pH between 5 and 6 and at PEG3350 concentrations varying between 19-22% (Figure 13).

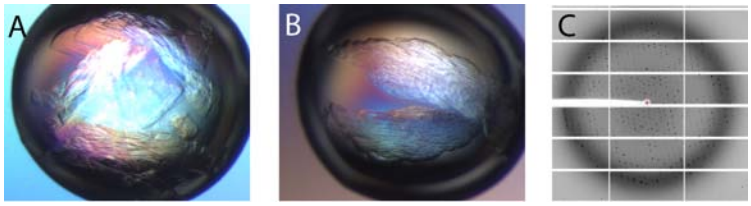

Figure 13. Crystals of tmRad50^{NBD}-Mre11^{HLH} -DNA (A and B) and their diffraction pattern (C). Crystals formed big intergrown and fragile plates of a highly irregular shape.

Processing of the diffraction data collected from these crystals revealed that the electron density accounted for DNA was not very clear. Although the overall geometry and shape of this positive difference density resembled DNA shape, it was difficult to trace the sugar-phosphate backbone and many of the bases were not visible.

In order to find out if the data quality could be improved, refinement screens with a higher molar excess of DNA were performed. Simultaneously, other DNAs were tested (13 bp, 17 bp, 19 bp, 21 bp). Unfortunately, these modifications did not bring any improvement to the diffraction quality and the recurring problem of the poor density for the DNA was due to the flexibility of the DNA molecule, rather than insufficient saturation of the protein with DNA. Other DNA species had only negative effect on the crystal quality. 13 bp and 21 bp DNA failed to yield any crystals whereas 17 bp and 19 bp DNA formed crystals of extremely poor order. As a consequence, very few of them showed any diffraction and these datasets failed during processing. 15 bp DNA with 1 nt overhang was therefore chosen for further refinements.

Since the 1 nt overhang of the DNA was not recognizable in the positive difference density, it was difficult to assign the base pair registry. Therefore, a modified DNA was used, containing one bromouracil instead of a thymine. Bromouracil is structurally similar to thymine; it also pairs with adenine and therefore can be used to mimic thymine (Figure 14). At the same time, the bromine atom should give an anomalous signal recognizable in the density and help to assign the registry and sequence of the DNA.

Crystals with the brominated DNA appeared in the same conditions that yielded crystals with non-modified DNA. Analysis of the anomalous difference density revealed however, that the anomalous signal was scattered and not restrained to one particular position (Figure 14).

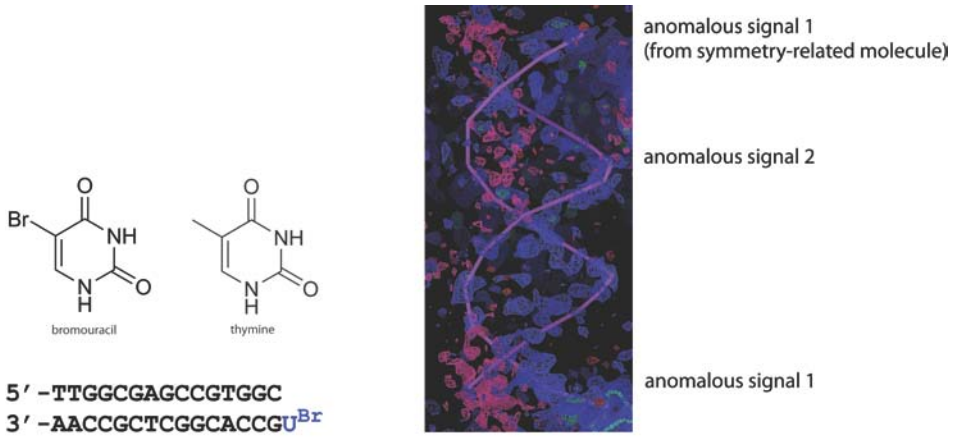

Figure 14. Brominated DNA in crystallization and structure refinement. Left panel: structures of bromouracil, thymine and brominated DNA used in crystallization trials. Right panel: anomalous difference electron density map (in purple) calculated for bromine. Two anomalous signals might result from binding of the DNA molecule in two opposite orientations.

Based on this outcome, it was concluded that the DNA is very flexible in the crystal (anomalous signal is locally scattered) and hypothesized that the DNA can be bound in two 180°-opposite orientations (as there are two anomalous and locally scattered signals) (Figure 15). To test this hypothesis, a palindromic DNA was used for subsequent refinements and indeed a partial improvement of the positive difference density was observed. In the next attempt, a refinement with a PAGE-purified ds15 palindromic DNA was performed. This however did not help any further and it was assumed that the flexibility of the DNA was an intrinsic property of the tmRad50^{NBD}-Mre11^{HLH}-DNA crystals.

TmRad50^{NBD}-Mre11^{HLH}-DNA crystals grew big and relatively thin, often as many irregular plates grown together. They fractured and broke easily upon touching and transfer to cryoprotectants. However, in most cases this fragility did not seem to affect diffraction overall; a bigger obstacle was twinning and multiple diffraction patterns observed in the data of a single crystal, coming from intergrown lattices.

The best initial dataset recorded at SLS (2.4 Å) was indexed and integrated with XDS (Kabsch 1993). The crystal formed in space group P2 with one molecule in the asymmetric unit and the

structure could be determined with molecular replacement with PHASER (McCoy et al. 2007), using the apo tmRad50^{NBD}-Mre11^{HLH} structure as a search model (PDB entry: 3QF7). Most of the model fit well to the calculated electron density and only a few segments of the structure had to be rebuilt manually. Most changes were observed at the coiled-coil domain of Rad50 and at the HLH motif of Mre11. After fitting in a whole B-form 15 bp DNA molecule, the model was subjected to limited rigid-body refinement. This re-built structure was later used as a model for molecular replacement of another dataset that showed clearer positive difference electron density for the DNA molecule (dataset collected at SLS, 2.7 Å). This time the crystal formed in P1 space group, with two molecules in the asymmetric unit. A number of cycles including manual model building and refinement in Phenix (Adams et al. 2002) led to final R-factor values of 21.54% for R_{work} and 27.04% for R_{free}. Table 18 summarizes crystallographic data and refinement statistics.

Table 18. Summary of crystallographic data and refinement statistics of the tmRad50^{NBD}-Mre11^{HLH}-DNA complex. Numbers in parenthesis correspond to the highest resolution shell (2.82-2.67 Å).

tmRad50^{NBD}-Mre11^{HLH}-DNA

Data collection		**Refinement**	
Space group	P1	Resolution (Å)	47.685-2.700
Cell dimensions		No. reflections	51439
a, b, c (Å)	a=50.2	R_{work} / R_{free}	21.54 / 27.04
	b=107.6	**No. atoms**	
	c=97.1	Overall	14169
α, β, γ (°)	α=90.6	Protein	12556
	β=98.3	DNA	1218
	γ=89.4	AMPPNP	124
Wavelength (Å)	1.000020	Magnesium	4
Resolution (Å)	50.2-2.7 (2.7)	Water	267
R_{sym} (%)	13.5 (68.6)	**B-factors** (Å^2)	
I/σI	9.26 (1.89)	Overall	43.37
Completeness (%)	93.8 (80.5)	Protein	35.05
Redundancy	3.43 (3.10)	DNA	146.11
		AMPPNP	19.34
		R. m. s deviations	
		Bond lengths (Å)	0.010
		Bond angles (°)	1.405

4.2.2. Crystal structure of the tmRad50^{NBD}-Mre11^{HLH}-DNA

The new tmRad50^{NBD}-Mre11^{HLH}-DNA structure retains the architecture of the previously reported apo structure (Lammens et al. 2011). Rad50 forms a compact dimer of overall dimensions of 40 x 70 x 100 Å. Roots of the coiled-coil domains protrude from the globular core of the protein, forming an angle of approximately 60°. Similarly to the archeal protein, NBDs of the Rad50 associate in the head-to-tail orientation, where lobe 1 makes contacts to lobe 2 of the opposing monomer (Hopfner et al. 2000). This arrangement sandwiches two AMPPNP molecules and two Mg^{2+} cations, both coordinated by a number of conserved residues (Hopfner et al. 2000; Lammens et al. 2011) (Figure 16).

The Mre11-Rad50 association interface is also clearly visible in the structure and as previously reported, is based on hydrophobic interactions mediated by the conserved residues in the root of the coiled-coil domain and the HLH motif of Mre11 (Figure 15).

The structure shows one DNA molecule bound per Rad50 dimer. In particular, the 15 bp DNA binds asymmetrically to only one Rad50 monomer. Inspection of the binding interface shows that DNA is relatively loosely associated with the protein. The binding is mediated by the interaction of three lysine residues with the sugar-phosphate backbone. Primarily, K115 reaches towards the phosphate group at a distance of 2.8 Å. The interaction is further supported by an analogous lysine-phosphate interaction at residues K175 and K182 within distances of 3.9 Å and 3.5 Å, respectively. This particular arrangement shows the involvement of the coiled-coil domain in the DNA binding. In the structure, only one helix of the coiled-coil domain contacts the DNA. The structure does not imply any particular involvement of the minor/major groove of the DNA to have impact on the binding mode. Also, few crystal contacts at the protein-DNA interface explain why the DNA is flexible in the crystal, especially at the region distal from the globular ATPase domain.

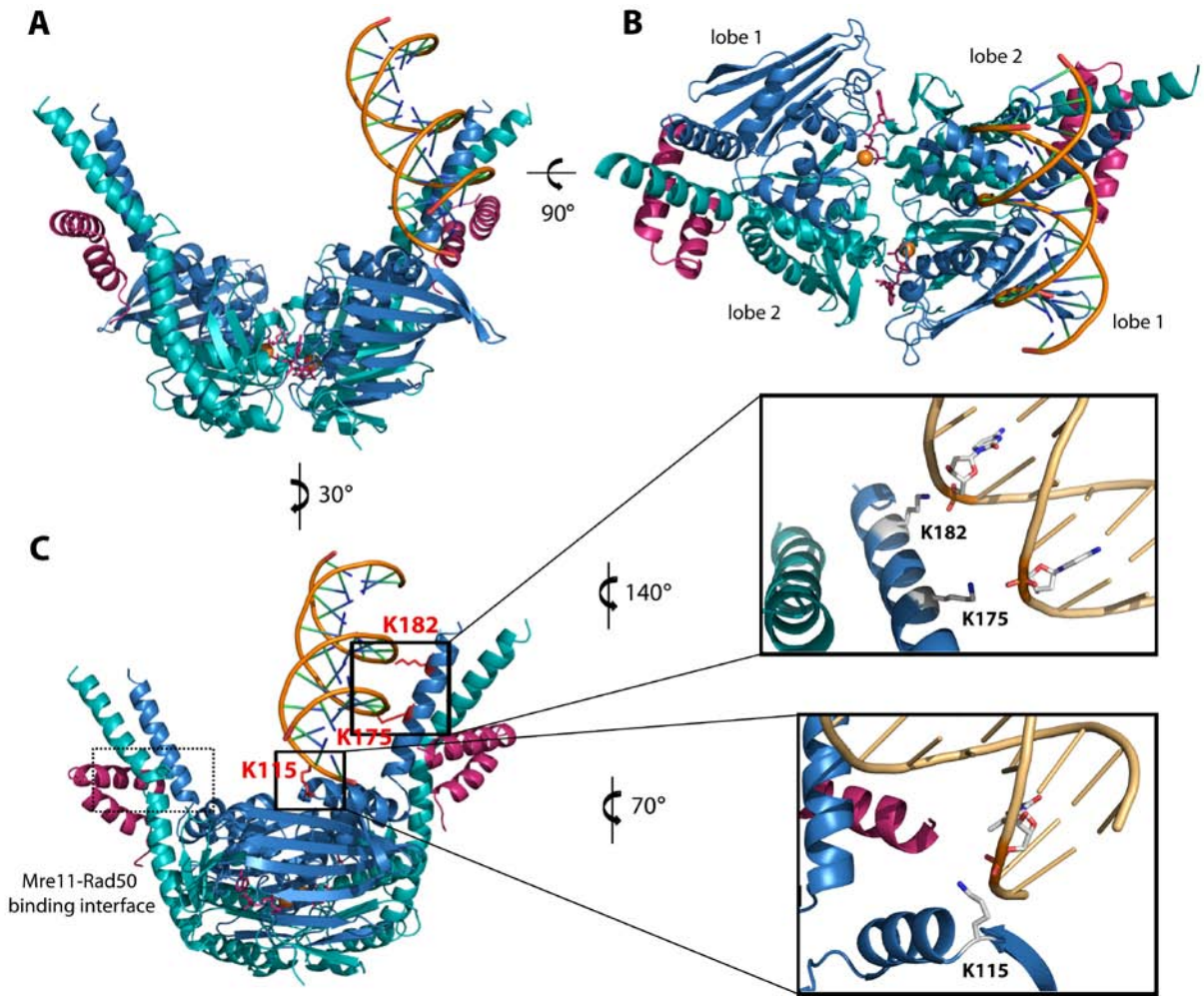

Figure 15. Atomic models of tmRad50^{NBD}-Mre11^{HLH} bound to 15 bp DNA. A: front view, B: top view; Rad50 dimer exhibits the typical head-to-tail monomer arrangement and coordinates two AMPPNP molecules and two Mg^{2+}. C: Rad50 coiled-coil domains mediate Mre11 and DNA binding. The DNA molecule is bound asymmetrically via three lysine residues: K115, K175 and K182.

Comparison of the tmRad50^{NBD}-Mre11^{HLH} and tmRad50^{NBD}-Mre11^{HLH} -DNA structures shows that the DNA binding does not induce conformational changes on the Rad50 dimer or the Rad50-Mre11 interaction interface. The new structure remains largely unaltered, with the globular part exhibiting identical architecture. Changes are visible at the coiled-coil domains and the HLH motifs. DNA-bound model is slightly less compact, with parts of the coiled-coil domains and HLH motifs repositioned 1.8-3.4 Å relative to the apo structure (Figure 16).

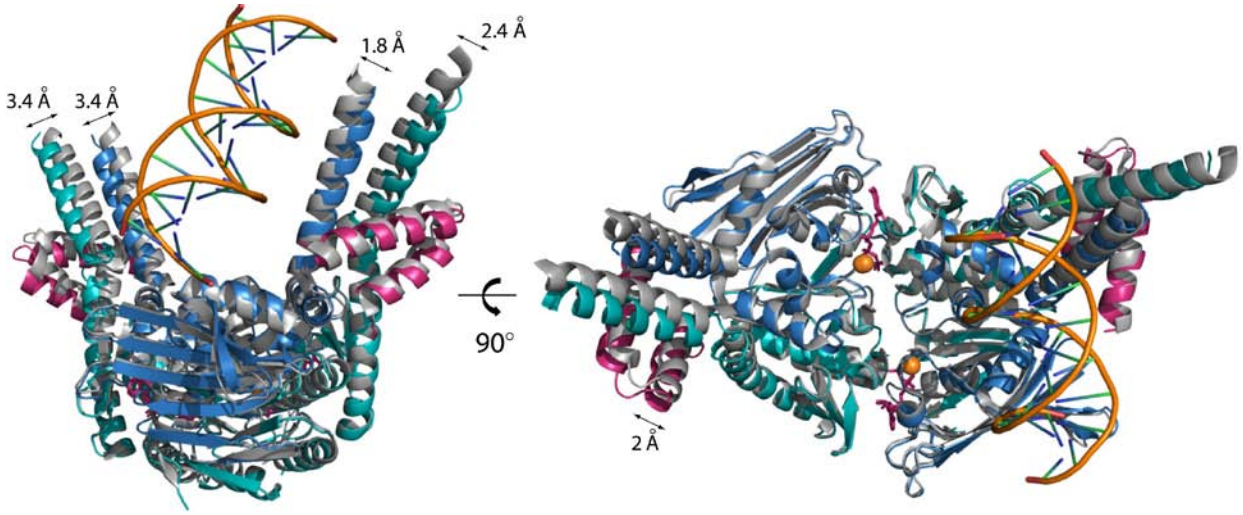

Figure 16. Overlay of tmRad50^{NBD}-Mre11^{HLH} apo and DNA-bound structures. Both structures show almost identical architecture. The biggest repositioning is visible at the coil-coil domains and HLH motifs.

4.3. Characterization of the tmRad50^{NBD}-Mre11^{HLH} *in vitro*

4.3.1. DNA binding properties of the wild-type tmRad50^{NBD}-Mre11^{HLH}

As discussed in the introduction to this work, both eukaryotic MRN/MRNX and prokaryotic MR complexes exhibit DNA-binding activity and multiple nucleolytic activities on different DNA substrates. To gain insight into the DNA-binding activities of the tmRad50^{NBD}-Mre11^{HLH} *in vitro*, the purified and dimerized complex was assayed with different DNA species by EMSA.

The first characteristic feature of the tmRad50^{NBD}-Mre11^{HLH} complex is that it exhibits enhanced DNA binding on longer DNA substrates (Figure 17). Clearly, a 60 bp-DNA is bound more efficiently than a 30 bp-DNA. In order to reach the same binding efficiency for these two DNA species, approximately 10 times more 30 bp-DNA would be required.

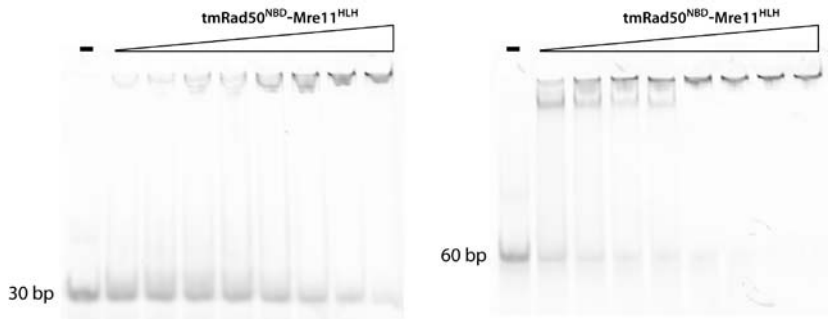

Figure 17. DNA-binding activity of the wild-type tmRad50^{NBD}-Mre11^{HLH}. The complex exhibits higher affinity to longer substrates as compared between 30 bp and 60 bp DNA.

Current understanding of the MRN activity during DSB processing postulates that at least during the initial steps of HR, the complex is responsible for the recognition of the broken DNA. To test this hypothesis *in vitro*, an EMSA with intact and nicked 60 bp-DNA species was performed. The nicked DNA was designed in such a way that the 5' end carried a phosphate moiety and the 3' end was hydroxylated. This type of a single-stranded break could be introduced *in vivo* during DNA end processing by *e. g.* Mre11 owing to its endonuclease activity or by other enzymes of the resection machinery. In this case, the nick would not only mimic a physiologically occurring endonucleolytic cleavage but also relax the DNA, rendering its structure more flexible. However, the DNA-binding efficiency is equally good on both tested substrates (Figure 18), which argues that the tmRad50^{NBD}-Mre11^{HLH} complex shows a preferential binding to modified DNA structures *in vitro*.

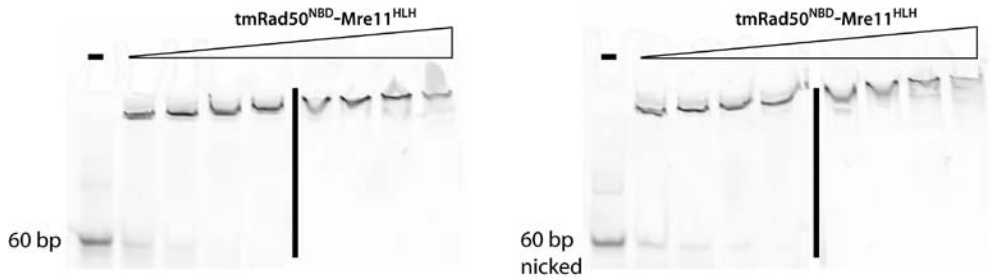

Figure 18. DNA-binding activity of the wild-type tmRad50^{NBD}-Mre11^{HLH}. The complex does not exhibit preference towards nucleolitically modified DNA as compared between intact and nicked 60 bp DNA.

To follow up on the idea of the DNA form affecting the DNA binding by the tmRad50^{NBD}-Mre11^{HLH} *in vitro*, 4 different plasmid species were used in EMSA: closed nicked (circular,

relaxed DNA with one single-stranded break), closed nicked and religated (circular, relaxed but intact DNA), closed supercoiled (circular, supercoiled), and linearized. Figure 19 summarizes the binding activity to all of these DNA species.

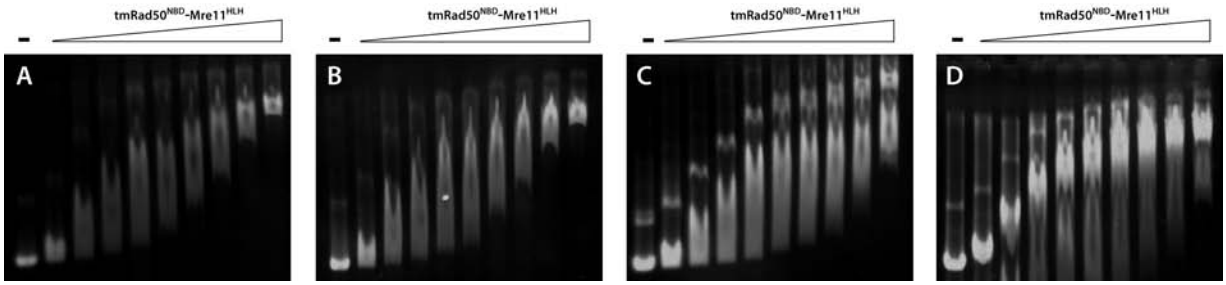

Figure 19. DNA-binding activity of the wild-type tmRad50^{NBD}-Mre11^{HLH} on plasmid substrates. A: closed nicked, B: closed intact, C: supercoiled, D: linearized.

In this experiment no evident preference of the tmRad50^{NBD}-Mre11^{HLH} complex towards topologically changed DNA was detected. Comparison of panels A and B, as already shown on intact ds60 and nicked ds60 DNA (Figure 18), argues that the complex exhibits higher affinity to the endonucleolytically modified DNA. Furthermore, panels B and C show that the topology of the DNA also does not play a role in DNA binding: the tmRad50^{NBD}-Mre11^{HLH} complex binds both supercoiled and relaxed plasmid forms equally well. At the same time, results in B and D show that the complex does not exhibit higher affinity to DNA with exposed ends, since no difference in DNA binding activity is visible between closed and linearized plasmid species.

4.3.2. Model of DNA binding and DNA-binding properties of the tmRad50^{NBD}-Mre11^{HLH} point mutants

Since the DNA visible in the structure does not clearly point out towards the location of the Mre11 active site in the full-length complex (Figure 38, Discussion), it is still not clear how it could be processed by Mre11 *in vivo*. For this reason, in order to shed more light onto DNA-binding properties of the protein *in vitro*, a number of point mutations were introduced into the tmRad50 gene (Figure 20).

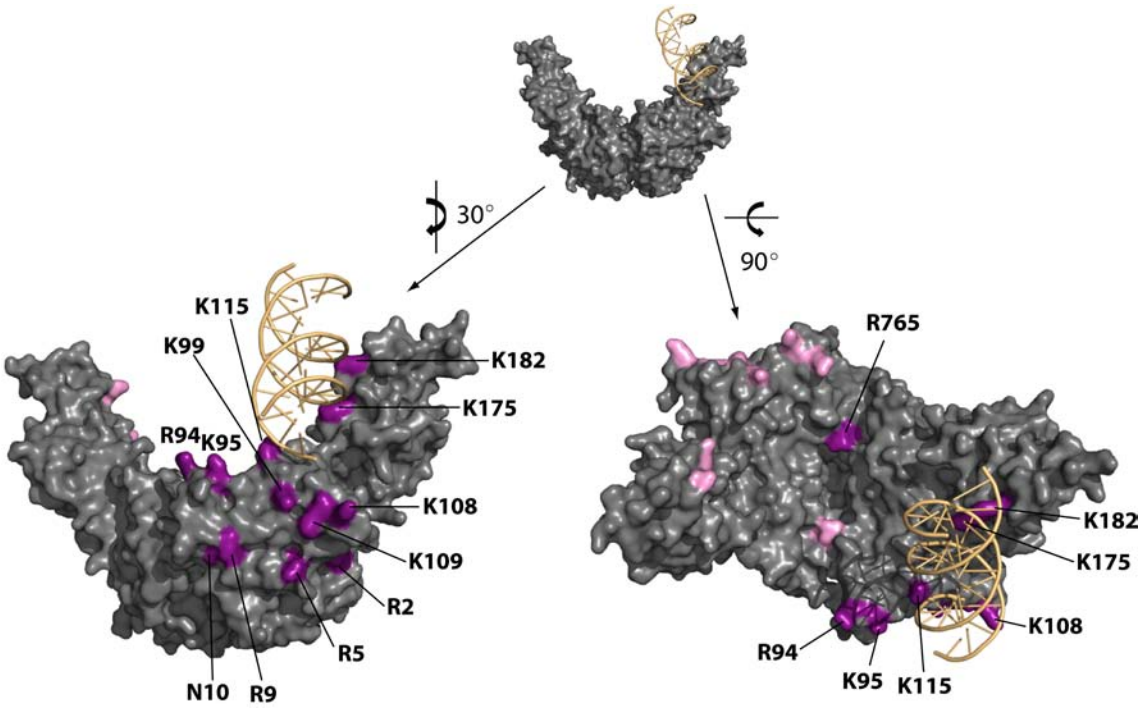

Figure 20. Surface representation of the tmRad50^{NBD}-Mre11^{HLH} complex (grey) with DNA helix (wheat, stick representation). Top panel: front view. Residues chosen for site-mutagenesis located on the opposite monomers are marked in purple and pink, respectively. Residues S768 and E798 are buried and therefore not visible in the picture.

The three lysine residues revealed in the structure to form protein-DNA contacts (K115, K175, K182) were the first choice and at all these positions the lysine was substituted by glutamic acid. In the light of previous studies, it was suggested that the DNA-binding interface might be located on the surface formed in the Rad50 dimer between the coiled-coils domains. According to the calculated surface potential of the tmRad50^{NBD}-Mre11^{HLH} complex, this particular interface encompasses a positively charged patch that could mediate DNA binding *in vivo* (Mockel et al. 2012) (Figure 21). In order to determine if some conserved residues belonging to this putative binding groove would affect DNA binding *in vitro*, mutations R94E, K95E and R765E were introduced.

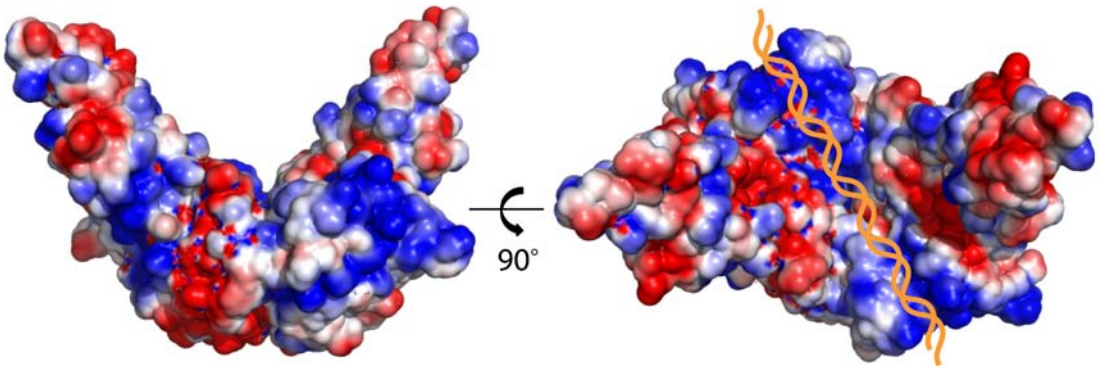

Figure 21. Representation of the surface charge of the tmRad50^{NBD}-Mre11^{HLH} (PDB entry: 3QF7). Interface located at the Rad50^{NDB} dimer between coiled-coil domains is positively charged and could be involved in DNA binding.

Assuming that the DNA-binding interface would involve K115 and the positive residues of the putative binding groove, other positively charged residues at the lateral side of the globular ATPase domain could also play a role in the DNA binding. To test this hypothesis, several conserved lysines (K99, K108, K109) were mutated to glutamic acid.

DNA could also bind from the K115 residue along the surface of the globular ATPase domain towards the Mre11 active site. Therefore, a number of conserved residues localized centrally and at the base of the ATPase domain were introduced: R2Q, R5Q, R9E and N10D. These residues were also described as Rad50S (separation of function) mutants in *S. cerevisiae* (Alani, Padmore, and Kleckner 1990), exhibiting chronic ATM-checkpoint activation.

Two conserved residues: S768 and E798 involved in ATP binding and hydrolysis, respectively, were mutated to serve as an internal control. The signature motif S768R mutant was previously shown to be deficient in ATP binding and therefore Rad50 dimerization, whereas Walker B E798Q mutant should similarly to Walker A mutant impair ATP hydrolysis with no effect on ATP binding and Rad50 dimerization (Moncalian et al. 2004; Bhaskara et al. 2007).

All residues mutated for the *in vitro* DNA-binding analysis were checked for conservation in eukaryotes (in particular in *S. cerevisiae*), so that subsequent *in vivo* analysis could be performed to complement the study. The coiled-coil residues K175 and K182 showed only partial conservation. However, both of these residues were still tested in DNA-binding assay *in vitro* on the assumption that the DNA-coiled-coil association is conserved but guided by other residues in other species.

Preparation and dimerization of tmRad50^{NBD}-Mre11^{HLH} point mutants

Point mutations in the tmRad50^{NBD}-Mre11^{HLH} construct were introduced by site-directed mutagenesis. Mutants were expressed and purified according to the protocol used in the preparation of the wild-type protein. All point mutants were expressed equally well as the wild-type protein and did not show any enhanced instability. In order to confirm that the introduction of mutations would not impair dimer formation of the Rad50 monomers, AMPPNP was added to protein preparation and dimerization was monitored in gel filtration, as described for the wild-type protein. The majority of the mutants showed the same dimerization efficiency as the wild-type protein, including the speed rate of the dimer formation. This was also true for R94E+K115E and K95E+K115E double mutants.

Different behaviour was observed for mutants R765E, S768R and E798Q. As expected, signature motif mutant (S768R) remained in the monomeric form. This particular mutation was showed before to impair ATP binding and dimer formation. Walker D mutant (E798Q) dimerized at a slower rate, with the final dimerization efficiency of approximately 75%. In case of this mutant, ATP-binding and subsequent dimer formation are expected. The mutant should however exhibit no ATP hydrolysis. R765E mutant showed also a slightly slower dimerization rate, but the final efficiency reached the maximum of approximately 85%, comparable with the wt protein (Figure 22).

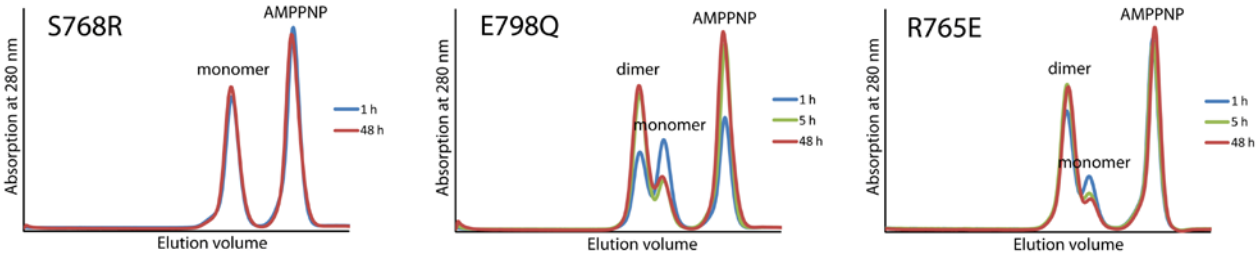

Figure 22. AMPPNP-induced dimerization of selected tmRad50^{NBD}-Mre11^{HLH} mutants. Signature motif mutant S768R remains in a monomeric form. Walker B mutant E798Q shows slower dimerization compared to the wild-type protein, with the maximum efficiency of approximately 75%. R765E mutant also dimerizes at a slower rate but reaches 85% dimerization efficiency, comparable to the wild-type protein.

DNA binding properties of the tmRad50^{NBD}-Mre11^{HLH} point mutants

DNA-binding activity of tmRad50^{NBD}-Mre11^{HLH} point mutants was analyzed and compared to the wild-type protein (Figure 23). In this assay, binding of a circular nicked plasmid was tested.

The wild-type protein, as already shown before, exhibited high binding affinity already in the nanomolar range. Clearly, among the structure-based mutants, the K115 residue showed the strongest effect on the DNA binding. In particular, K115E mutant was unable to bind DNA; an insignificant shift could only be observed at extreme protein molar excess. Two other mutants based on the protein-DNA contacts visible in the crystal structure, K172E and K185E, showed only partial inhibition of the DNA binding, much less pronounced than K115E.

In case of the residues involved in the proposed DNA-binding groove (R94, K95 and R765), R94E and K95E mutants exhibited a dramatic decrease of the DNA-binding activity, comparable with the K115E mutant. R765E mutant also strongly impaired DNA binding but not as severely as the R94E, K95E and K115E mutants. Double-mutants R94E+K115E and K95E+K115E caused a strong inhibition of DNA binding, comparable to the K115E single mutant.

Conserved residues (K99, K108 and K109), that were hypothesized to play a role in forming the DNA-binding path between K115 and the putative binding groove, also strongly affected DNA binding. In particular, K99E mutant showed significantly low DNA-binding activity.

Rad50S mutants (R2Q, R5Q, R9E and N10D) had on the other hand a rather mild effect, with the R9E mutant showing the strongest inhibition of the DNA binding, comparable with the structure-based K182E mutant.

Mutations of residues involved in ATP binding and hydrolysis (signature motif mutant S768R and Walker B mutant E798Q) also had a pronounced effect on DNA binding. S768R mutant strongly impaired the binding in a manner comparable with the mutants K99E and R765E. S768R still exhibited a higher affinity towards DNA than a monomeric tmRad50^{NBD}-Mre11^{HLH} assayed in the absence of AMPPNP. This result confirmed previously published observations that the DNA binding also partially stimulates dimerization, but the full dimer formation is dependent on ATP and Mg^{2+} (Lammens et al. 2011). E798Q bound DNA readily in the nanomolar range like the wild-type protein but the binding was less efficient.

In summary, most of the tested mutations disturbed DNA-binding activity of the tmRad50^{NBD}-Mre11^{HLH} dimeric complex and the strength of this effect varied among distinct mutants.

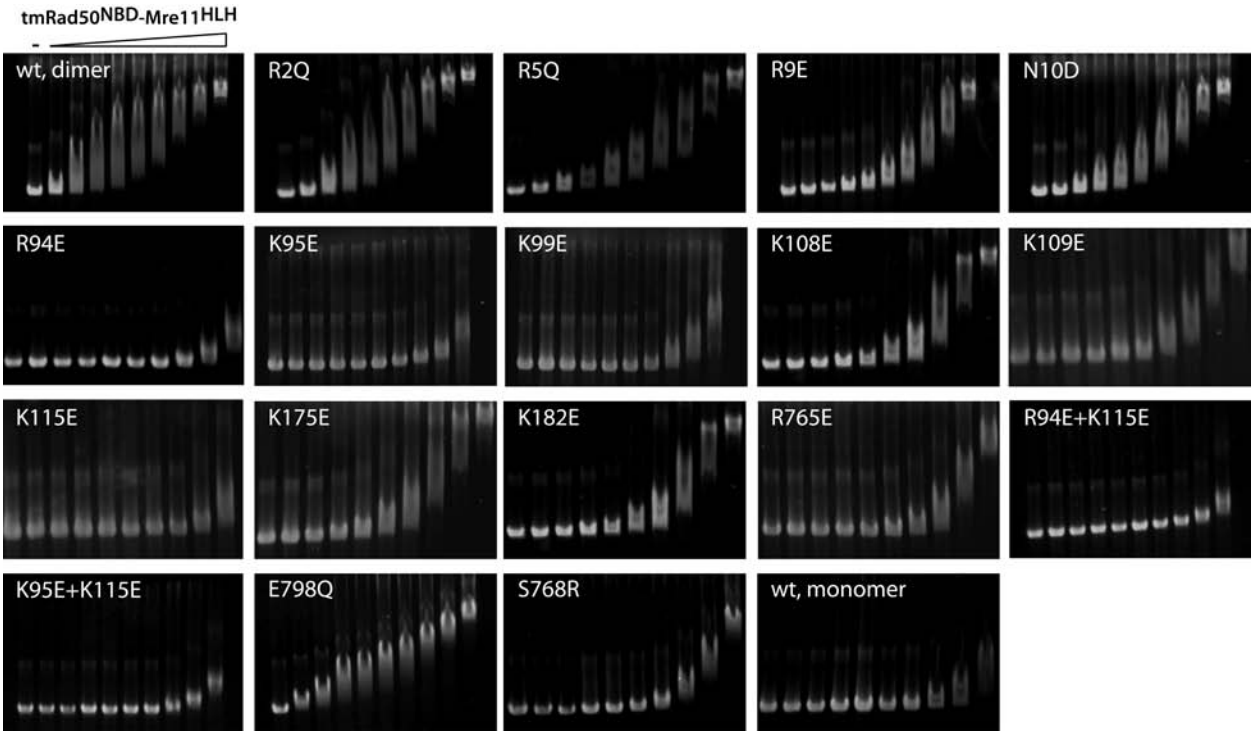

Figure 23. Comparison of the DNA-binding activity of the wild-type (wt) and mutant tmRad50^{NBD}-Mre11^{HLH} complexes. Details in text.

4.4. Structure-based characterization of Rad50 point mutations in *S. cerevisiae*

The structure of the tmRad50^{NBD}-Mre11^{HLH}-DNA together with the *in vitro* analysis of DNA binding does not evidently explain how the complex would recognize and bind DNA in the physiological context of chromatin and two free DNA ends at a DSB site. In order to verify the significance of the features in DNA-protein interface revealed by the structure together with other Rad50 residues tested for the involvement in DNA binding, a number of mutations were introduced into Rad50 gene and tested *in vivo* in *S. cerevisiae*. Conserved residues that showed strongest DNA-binding inhibition *in vitro* were selected for this assay. Figure 24 shows the sequence alignment between bacterial (*T. maritima*), human (*H. sapiens*) and yeast (*S. cerevisiae* and *S. pombe*) Rad50 orthologues. Almost all chosen residues showed conservation in these species, pointing towards their potential importance across all domains of life.

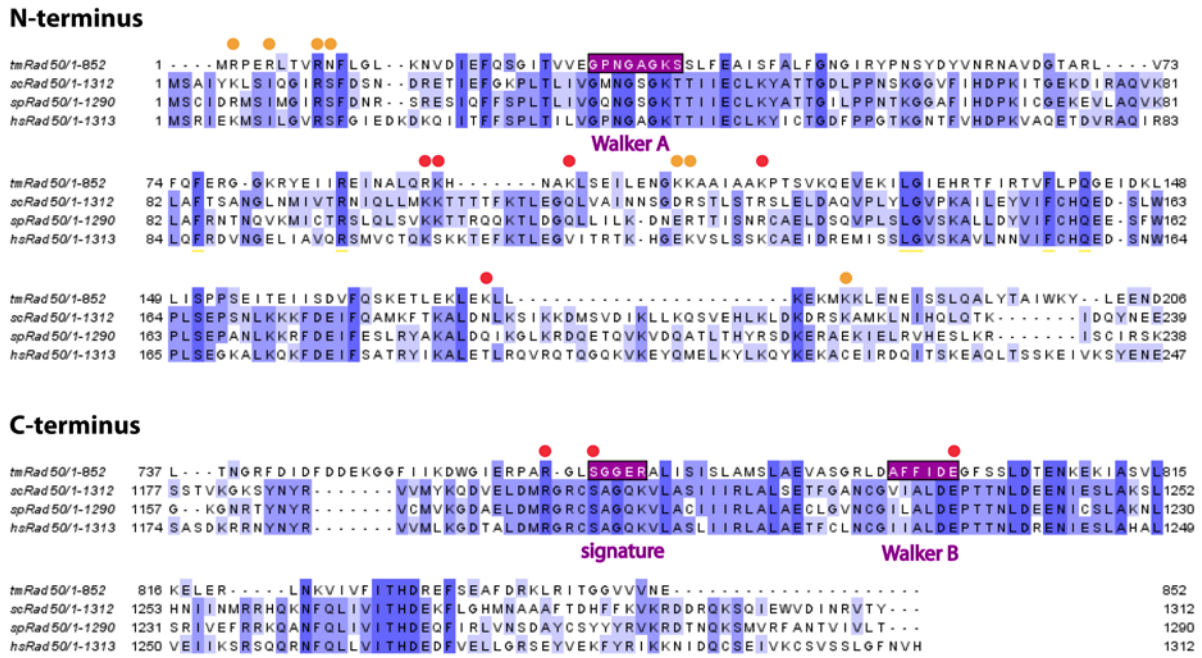

Figure 24. Sequence conservation of N- and C-terminal segments of Rad50 orthologues from *T. maritima, S. cerevisiae, S. pombe* and *H. sapiens*. Walker A, Walker B and signature motif are marked in purple. Orange dots mark residues mutated only in tmRad50^{NBD}, red dot marks residues mutated in tmRad50 and scRad50.

4.4.1. Response to DNA damage

In order to compare the effect of Rad50 point mutations *in vivo*, a complementation assay with the Δrad50 *S. cerevisiae* strain was employed. The knock-out strain is viable in complete medium (YPD), although it grows slower compared to the wild-type strain.

One way to determine whether residues found to be critical for DNA binding *in vitro* would also mediate DNA recognition *in vivo* is to monitor the survival of Rad50 mutants on DNA-damaging agents in comparison to the wild-type cells. To this end, *S. cerevisiae* W303-1a wild-type and W303-1a Δrad50 strains were transformed with an empty pRS313 vector (centromeric plasmid with His marker). W303-1a Δrad50 was also transformed with pRS313 carrying a wild-type scRad50 allele. Growth of these transformants was monitored on the synthetic medium without histidine (control) and on the medium containing camptothecin (CPT), methyl methanesulfonate (MMS) and hydroxyurea (HU) as DNA-damaging agents (Figure 26). Δrad50 retained viability on the complete medium but its growth was retarded. On the contrary, supplementation of the medium with DNA-damaging agents severely impaired Δrad50 survival, confirming the

requirement of the functional MRX complex in DSB repair *in vivo*. Complementation of the Δrad50 strain with a wild-type allele of Rad50 restored the phenotype to the level of wild-type strain. This result also indirectly confirmed that the scRad50 gene introduced on a plasmid was properly expressed and retained its function *in vivo* (Figure 25).

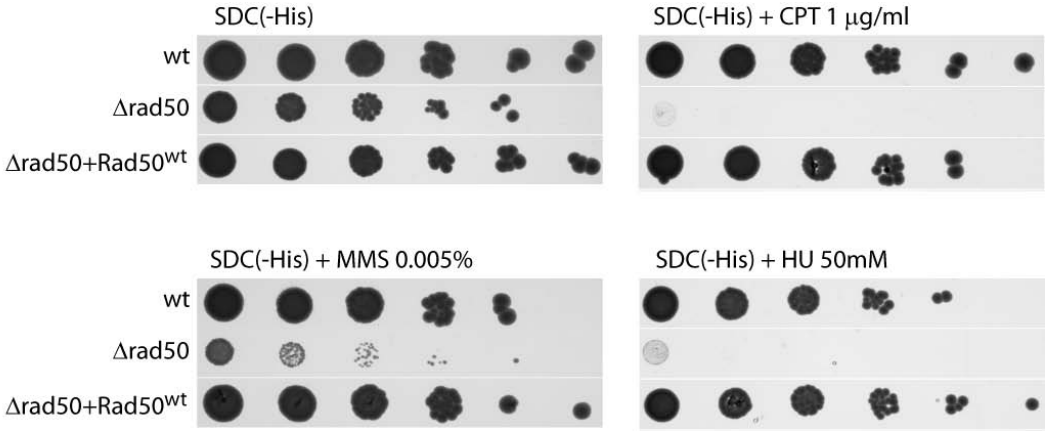

Figure 25. Growth behaviour of *S. cerevisiae* transformants on regular medium SDC(-His) and medium supplemented with DNA-damaging agents. Δrad50 strain transformed with empty pRS313 plasmid does not survive genotoxic stress (Δrad50) caused by captothecin (CPT), methyl methanesulfonate (MMS) or hydroxyurea (HU). Transformation of the Δrad50 strain with the wild-type allele of scRad50 (Δrad50+Rad50^{wt}) rescues the phenotype to the wild-type level (wt).

Based on previous studies (D'Amours and Jackson 2001), observed phenotypes were expected and allowed to employ this assay for monitoring the DNA damage response in *S. cerevisiae* Rad50 mutants. To this end, the Δrad50 strain was transformed with the pRS313 constructs carrying mutated scRad50 alleles and the survival of the transformants was monitored as described before on media supplemented with DNA-damaging agents.

Interestingly, only several of tested mutations showed an altered phenotype compared to Δrad50 and Δrad50+wtRad50 transformants (Figure 26). Clear phenotypic effect was observed for the mutant R1201E and as expected for the signature motif mutant S1205R and Walker B mutant E1235Q. These mutants exhibited partially retarded growth already on complete medium, resembling the Δrad50 strain. In the view of the DNA damage response, R1201E, S1205S and E1235Q were again phenotypically similar to the Δrad50 strain, showing strongly impaired growth on DNA-damaging agents. Out of the three used genotoxins, CPT induced the strongest phenotype, rendering the transformants almost inviable. MMS had a more pronounced effect on

the R1201E mutant than on S1205S and E1235Q mutants, but all these mutants responded better to MMS-induced DNA damage than the Δrad50 strain.

Response to HU affected the signature motif S1205R mutant in the most severe manner. Under these conditions, S1205R was phenotypically identical with the Δrad50 strain. R1201E and E1235Q mutants showed better survival on HU-supplemented medium than S1205S, but their growth was still severely impaired, when compared to the wild-type and rescued Δrad50 transformants.

A weak but still persistent effect on growth and DNA damage response was observed for the double-mutant K103E+R131E. This mutant exhibited slight growth retardation already on the complete medium. This behaviour was manifested also on the CPT-supplemented medium, and to a lesser degree on the HU-supplemented medium.

The rest of the tested mutations did not induce phenotypic effect on growth and response to DNA damage *in vivo*. K103E, K104E, R131E and K104E+R131E mutants, analogous to the DNA-binding deficient mutants of tmRad50^{NBD}-Mre11^{HLH} (R94E, K95E, K115E, K95E+K115E), showed unaffected growth on SDC(-His) medium and normal DNA damage response, comparable to Δrad50+Rad50. Similarly, the structure-based mutant N190D (tmRad50 K175E that showed partially impaired DNA binding *in vitro*), did not show any growth retardation or impair in DNA damage response in *S. cerevisiae*.

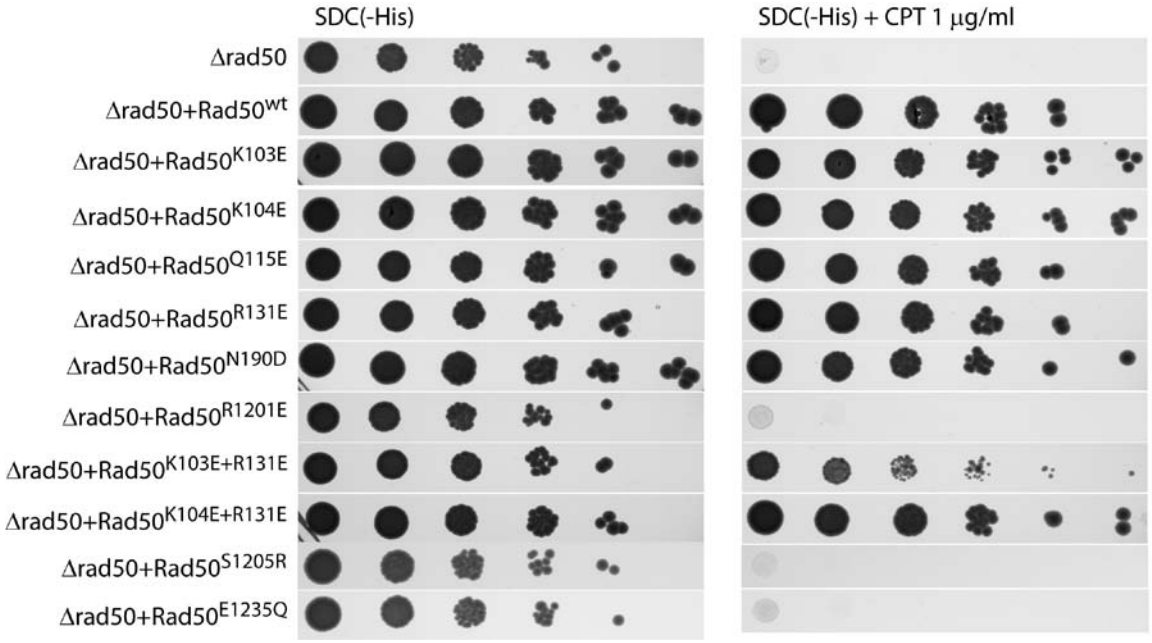

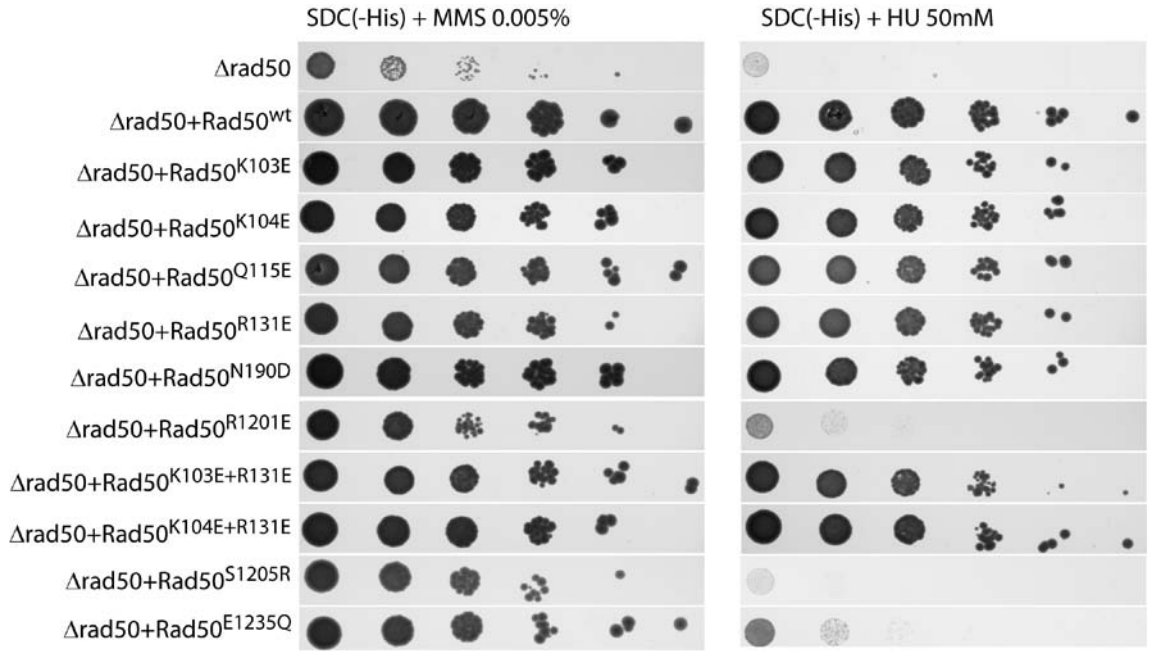

Figure 26. **Growth behaviour of *S. cerevisiae* transformants on regular medium SDC(-His) and medium supplemented with DNA damaging agents.** Transformation of the Δrad50 strain with most of the mutated alleles of scRad50 rescues the phenotype to the wild-type level (Δrad50+ Rad50^{wt}). R1201E, S1205R and E1235Q show strongly impaired DNA damage response, comparable to Δrad50 strain. K103E+R131E double mutant shows partially impaired DNA damage response.

In order to check if the observed phenotypes did not arise as the cause of a decreased cellular level of Rad50, the expression level of Rad50 allele was monitored by Western blot on yeast whole-cell lysates. As shown in (Figure 27), all transformants expressed Rad50 normally.

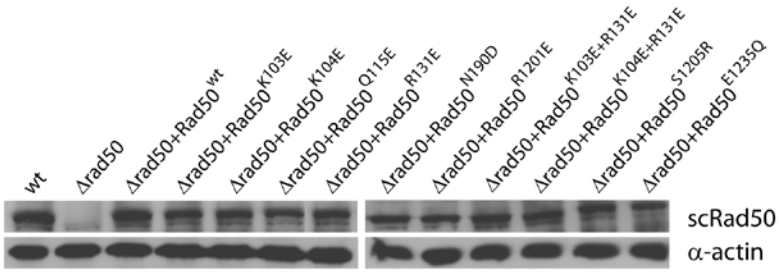

Figure 27. Rad50 expression level in *S. cerevisiae* transformants. All of the mutated Rad50 alleles are well expressed, with the expression level comparable to the wild-type and rescued Δrad50 strains.

4.4.2. End-joining activity

The significance of different Rad50 motifs was further investigated *in vivo* in an end-joining analysis. Interestingly, this experiment revealed that in addition to residues determined to be crucial for DNA-damage response (R1201E, S1205R and E1235Q), mutants K103E and K104E exhibited partial decrease in end-joining efficiency with a linearized plasmid (Figure 28). Moreover, this effect was enhanced in K103E+R131E, but not K104E+R131E double-mutant, although the R131E mutant remained unaffected. End-joining activity was also severely affected in the coiled-coil mutant N190D, although this mutation did not influence response to DNA damage.

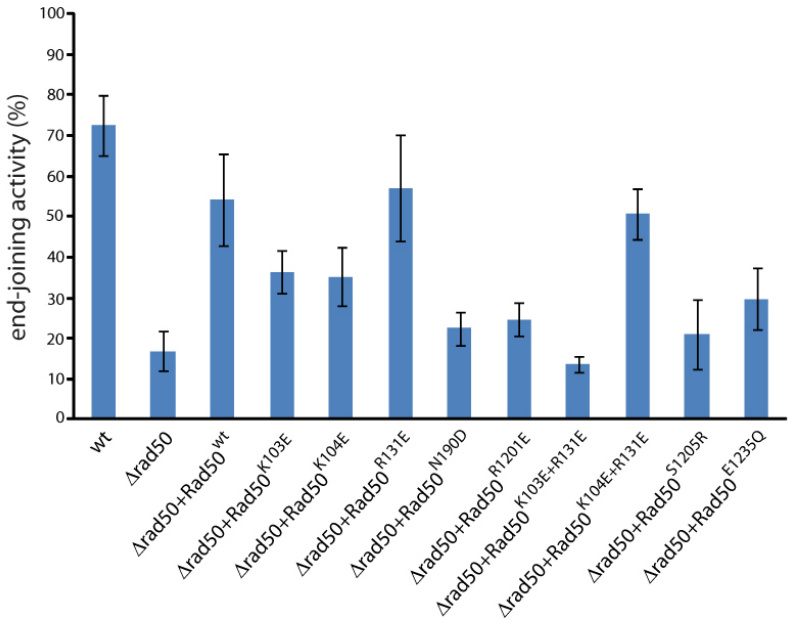

Figure 28. End-joining activity of *S. cerevisiae* Rad50 mutants. All residues determined to be important for DNA-damage response are also significant for end-joining repair (mutants R1201, S1205R, E1235Q, K103E+R131E). In addition, coiled-coil mutant N190D exhibits a strong defect whereas mutants K103E and K104E a partial defect in end-joining.

4.4.3. Telomere maintenance

Yeast telomeres consist of poly(GT) repeats (300 bp), located downstream from the conserved X or XY' elements. Y' element includes a conserved XhoI restriction site and the genomic DNA isolated from wild-type *S. cerevisiae* strains treated with this restrictase generates a 1-1.3 kbp fragment containing the poly(GT) repeat. The repeat can be visualized by Southern blot, using a radioactively labelled hybridization probe that anneals to the repeat. This particular assay was

employed to determine if the Rad50 mutations tested for DNA damage response would show an altered phenotype in maintaining telomeres when compared to the wild-type and Δrad50 strains. As depicted in Figure 29, the Δrad50 strain had significantly shorter telomeres but complementation with the wild-type scRad50 allele restored its phenotype to the wild-type level. K103E and K104E mutants showed a partial impair of telomere maintenance. Interestingly, this effect was enhanced in the K103E+R131E double mutant and comparable to the Δrad50 strain, although the single R131E mutant exhibited the wild-type phenotype. Signature motif mutant S1205R was strongly defective in telomere maintenance, confirming again the significance of the Rad50 dimerization in distinct functions of the MRN complex. The same phenotype was observed for the R1201E mutant. Notably, Walker B mutant E1235Q showed an unaltered phenotype, which argues against the role of the ATP hydrolysis in the MRN function at telomeres.

Interestingly, it is possible that the coiled-coil mutant N190D formed longer telomeres compared to the wild-type strain. In order to verify this, telomere maintenance in this strain would have to be thoroughly investigated over the time span of more generations.

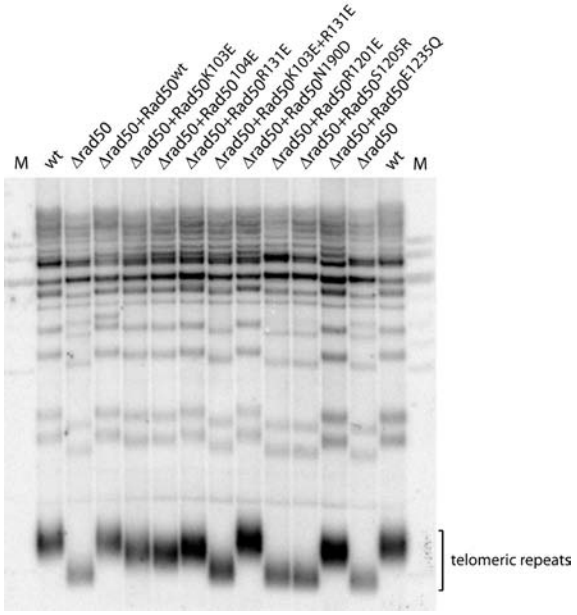

Figure 29. Analysis of telomere maintenance in the wild-type, Δrad50 and rescued Δrad50 strains. Strongest telomere shortening, comparable to Δrad50 strain is exhibited by single mutants R1201E, S1205R and double mutant K103E+R131E. Mild effect is observed for K103E and K104E mutants.

4.5. Establishment of the hMRN-induced ATM activation in *Xenopus laevis* interphase egg extract

Interphase egg extract from *X. laevis* can recapitulate a number of cellular events, including replication, DNA repair, checkpoint control and chromatin remodelling and has been therefore widely used to study molecular principles of these processes. In particular, DNA-induced ATM signalling can be reconstituted in interphase extracts depleted of the endogenous xlMRN complex and supplemented with the wild-type recombinant human complex (Costanzo et al. 2001). This experimental set-up could be employed to monitor ATM signalling in the presence of the mutant hMRN complex and determine the link between structural features of the complex and its function as the signalling mediator.

4.5.1. Preparation of the recombinant hMRN

Expression and purification of the full-length recombinant human MRN complex was first reported in 1999 (Paull and Gellert 1999). This protocol, with minor modifications, was used to prepare the hMRN complex in this work. In contrast to the original protocol, the complex carried only one polyhistidine tag at the C-terminus of Rad50. It was shown though, that this modification did not affect complex formation and purification. Also, hMRN was expressed in HighFive insect cells for 72 hours, rather than in Sf9 insect cells for 48 hours and the cells were infected with a single baculovirus carrying all three genes of the MRN complex. In the original work cells were co-infected with three separate baculoviruses. Again, it was shown that this modification did not alter the expression level or the behaviour of the complex during purification.

The complex was first purified on NiNTA resin. High DNA contamination could be easily removed during the ion exchange step and finally the complex was subjected to gel filtration on Superose 6 column. As shown in the gel filtration elution profile (Figure 30), the complex formed a number of species. This result was contradictory to the previously published study where the authors claimed to obtain a complex of approximately 1.2 MDa (Paull and Gellert 1999). Furthermore, the stoichiometry of the complex was clearly disturbed, with Nbs1 being underexpressed relative to Mre11 and Rad50 (Figure 30).

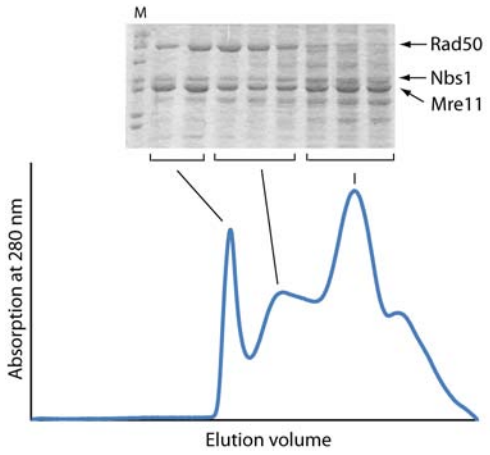

Figure 30. Elution profile of the recombinant human full-length MRN complex in gel filtration. The complex forms several oligomeric species. Nbs1 is at substoichiometric level.

Attempts to obtain a more homogenous sample with less impurities and an elevated Nbs1 level failed. These included expression of the complex in HighFive cells co-infected with separate Mre11/Rad50- and Nbs1-baculoviruses at a high excess of the latter one. Also, placing the polyhistidine tag at the C-terminus of Nbs1 instead of Rad50 or Mre11 did not improve the purity and stoichiometry of the complex.

4.5.2. Interphase *X. laevis* egg extracts

X. laevis egg extract suitable for studies of mitotic DSBs should be blocked at the early stage of interphase, preferably in phase G1. Such extracts are still able to proceed to S- and G2-phases of the cell cycle. In order to test whether extracts were indeed halted in G1 phase, demembrated sperm nuclei were introduced to the extract. Responsive extracts (*i. e.* G1-phase extracts of good quality) should in this case recapitulate replication. As shown in Figure 31, extract prepared in this work were fully capable of restoring replication on sperm DNA, as monitored by incorporation of the Cy3-labelled dCTP in the newly synthesized DNA.

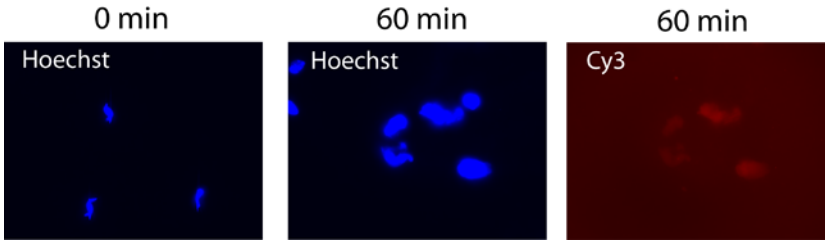

Figure 31. Replication of demembrated sperm nuclei in *X. laevis* egg extract. Chromatin in sperm nuclei changes from compact (A) towards a more loose and relaxed form (B and C). Incorporation of the Cy3-dCTP into the newly synthesized DNA is well visible after 60 min upon the nuclei addition.

4.5.3. DNA-induced ATM activation in interphase *X. laevis* egg extracts

In order to monitor checkpoint signalling elicited by hMRN mutants, interphase extract from *Xenopus laevis* unfertilized eggs was used. In the assay, the extract was first depleted of the endogenous cellular MRN complex with the anti-xlMre11 polyclonal serum. The efficiency of the immunodepletion was very high, as monitored by Western blot analysis (Figure 32).

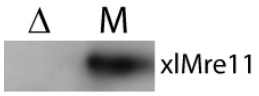

Figure 32. Immunodepletion of the endogenous MRN complex from *X. laevis* egg extract. Immunodepletion efficiency with polyclonal anti-xlMre11 serum is very high as monitored by a Western blot analysis performed against xlMre11. Δ: depleted extract, M: mock extract.

DNA damage was mimicked by the introduction of exogenous blunt-ended DNA to the extract and the signalling response was monitored by the appearance of the phopshorylated species of ATM (autophosphorylation site S1981). Optimization of this experimental setup included type of DNA to induce the response (poly(A)/poly(T) duplex, phage λ DNA-BstEII digest, 200 bp blunt-ended PCR product), DNA concentration in the extract, reaction time and reaction temperature. In established conditions, a clear phosphorylation of the ATM was detected in mock extract, whereas no ATM phosphorylation could be visible in the xlMRN-depleted extract (Figure 33). The response was very fast, with a partial ATM-phosphorylation already detectable after 2 minutes upon stimulation with DNA.

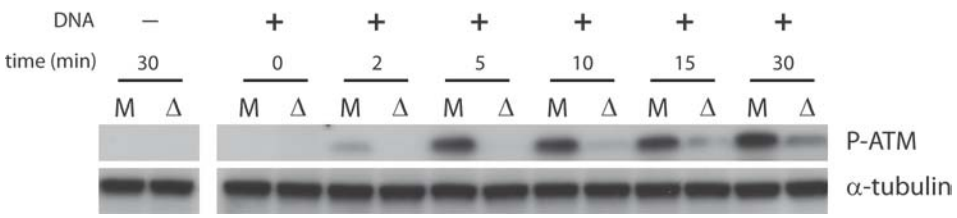

Figure 33. ATM phosphorylation in *X. laevis* egg extract. DNA-induced ATM phosphorylation is visible only in mock extract (M), but not in xlMRN-immunodepleted extract (Δ). ATM is also not phosphorylated in extract not stimulated with DNA.

4.6. Rescue of ATM activation by the hMRN complex

ATM signalling in Mre11-depleted *X. laevis* egg extract was shown before to be recapitulated by addition of recombinant hMRN (Costanzo et al. 2001). In order to see whether the hMRN complex prepared in this work would also restore ATM phophorylation upon DNA damage, the optimized assay (paragraph 4.4.3.) was employed. It was expected that supplementation of the xlMRN-depleted extract with the hMRN complex would result in ATM phosphorylation upon addition of DNA. Unfortunately, this result was never observed in the extract (Figure 34).

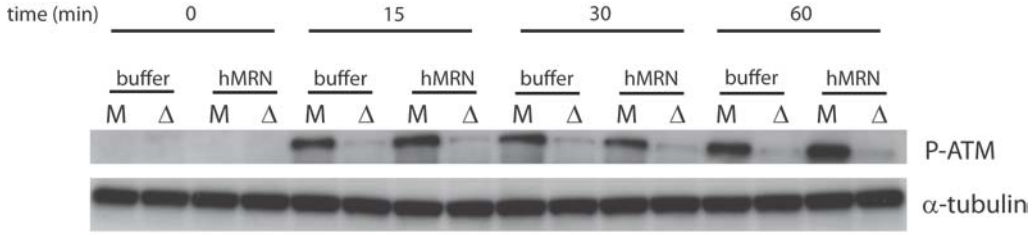

Figure 34. Rescue experiment in *X. laevis* egg extract. Recombinant hMRN does not restore DNA-induced ATM phosphorylation in xlMRN-immunodepleted egg extract (Δ) even after 60 min from reaction start. At the same time, hMRN storage buffer does not affect ATP phosphorylation in the mock extract (M).

To rule out that the activity of the hMRN is affected by its oligomerization state, distinct species of the complex formed in gel filtration were tested separately. Moreover, attempts were made to enrich the sample with the signalling subunit Nbs1. However, they turned out to be unsuccessful. As the extract is extremely sensitive to dilution and addition of certain buffers, the hMRN complex was dialysed to buffer containing 10 mM Hepes-KOH pH 7.5, 100mM KCl and 1 mM DTT (V. Costanzo, personal communication) or 10 mM Hepes-KOH pH 7.7, 50 mM KCl, 2.5 mM $MgCl_2$, 250 mM sucrose (Dupre, Boyer-Chatenet, and Gautier 2006) prior to rescue

experiments. These buffer conditions are believed to be more suitable for the work with the *X. laevis* egg extracts as they do not affect the behaviour of the extract if added in small amounts (V. Constanzo, J. Gautier, personal communication). Again, these attempts also did not improve the DNA damage response in the depleted extract and eventually no rescue of ATM signalling was observed. For this reason, further experiments including mutants of the hMRN complex could not be performed.

5. Discussion

Double-strand breaks and their repair

Double-strand breaks are one of the most deleterious DNA lesions and pose a severe threat to genome stability. DSBs appear as a result of DNA exposure to a number of damaging agents of both physical and chemical nature. The most harmful factors responsible for the DSB formation are ionizing radiation, reactive oxygen species and genotoxic agents. Moreover, factors that interfere with progression of replication often result in stalling and subsequent collapse of the replication fork, exposing “naked” DNA ends and eliciting a response similar to DSBs.

Many of the DNA modifying or damaging agents lead to damage formation of nature different to DSBs. These lesions are recognized by distinct repair systems but, unless repaired, they are often transformed into DSBs. Furthermore, certain cellular events include generation of programmed DSBs. Such physiological breaks are formed in a tightly regulated manner and are crucial to crossing-over events during meiosis, mating-type switching in *S. cerevisiae* or V(D)J recombination fundamental to the development of adaptive immune system in vertebrates.

Both spontaneous and programmed DSBs pose a threat to genome stability and their accumulation can lead to severe genetic disorders including cancer. A single DSB is sufficient to induce checkpoint activation, assuring that the cell cycle halts in order to give the repair machinery time to respond to the lesion. However, if this repair mechanism fails, continuous DSB signalling promotes shutdown of the cellular metabolism followed by programmed cell death (Friedberg 2003).

There are two alternative DSB repair pathway: homologous recombination and non-homologous end joining. The HR system is considered accurate and mostly error-free and bases on an extensive resection of the DNA ends followed by a replication-governed repair and use of homology segments available on the lesion-free sister chromatid. On the other hand, the NHEJ system is characterized by a limited DNA end resection followed by a direct end joining, usually not accompanied by a large-scale replication-governed repair. For this reason, NHEJ is considered a more error-prone repair pathway, leading to possible deletions (Hartlerode and Scully 2009).

HR and NHEJ systems are employed by yeast and higher eukaryotes with different preference. Yeast repair their DSBs predominantly via HR, whereas mammalian genomes are protected

mostly by NHEJ-associated factors. The reason for this discrepancy and the principles governing the repair pathway choice are so far not entirely clear. A number of recently published studies reports many of the DSBR and cell cycle control factors to play a role in balancing HR/NHEJ pathways (Chapman, Taylor, and Boulton 2012).

Mre11-Rad50-Nbs1 complex: facts and open questions

Protein landscape of the DSB repair and signalling is very complex but largely conserved throughout the domains of life. One of the key players in this plethora of factors is the Mre11-Rad50-Nbs1 (Xrs2) complex, with the highly conserved Mre11-Rad50 enzymatic core. MRN/X plays a multifaceted role in the repair of mitotic breaks but is also indispensible for other cellular events (Figure 35). These include telomere maintenance, V(D)J recombination, repair of meiotic DSBs and DNA damage induced checkpoint activation. More recently, new functions of the MRN complex in the progression of mitosis and innate immunity response to viral infection were reported (Kondo et al. 2013; Rozier et al. 2013). The complex is required for both DSB repair pathways but its function has been best described for homologous recombination. In the course of HR, the MRN is believed to recognize and bind to the damage site, form a structural scaffold for other repair proteins and interact with ATM checkpoint kinase, mediating the damage event to the cell cycle control machinery. The complex plays an important mechanistic role at the damage site: it is able to tether DNA ends together and participate in bridging distal homologous DNA segments. Due to its enzymatic activities, it also takes part in early resection events (Stracker and Petrini 2011).

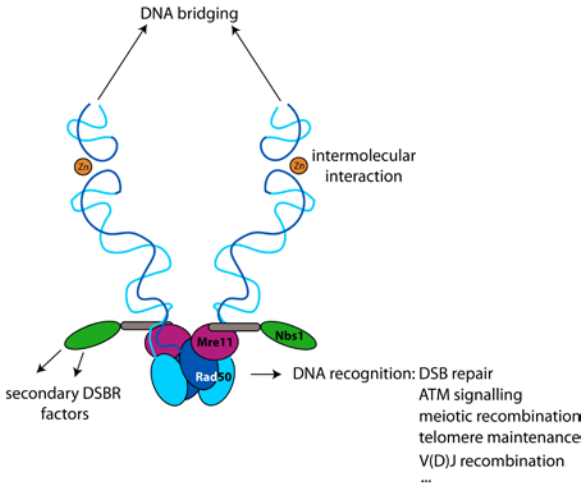

Figure 35. Model of the MRN complex and its implications for MRN functions.

Extensive studies of the diverse roles of the MRN complex have greatly contributed to the current understanding of the functional features governing its function in distinct cellular processes. However, many fundamental characteristics still await clarification. One of the most fundamental questions was to mechanistically understand how the complex senses DNA breaks. It was proposed that the DNA-binding interface is located on the enzymatic core of the complex, *i. e.* Rad50 ATPase and Mre11 nuclease domains. Archeal Mre11 structure bound to DNA gave first insight into the mechanism of DNA binding (Williams et al. 2009) but became later difficult to interpret in the context of the full-length Mre11-Rad50 complex. Namely, the initially determined DNA-binding pocket at the Mre11 active site was later found to be closed off by the Rad50 ATPase domain (Figure 7, Introduction) (Lim et al. 2011; Mockel et al. 2012).

To address molecular principles of the DNA recognition, the catalytic domain of the bacterial orthologue of Rad50 together with a short interacting motif of Mre11 was crystallized in complex with 15 bp DNA. In the attempt of verifying structural information and understanding the significance of structural features of the Rad50-DNA assembly, extensive mutagenesis studies were performed both *in vitro* in DNA-binding assays and *in vivo* in DNA damage response in *S. cerevisiae*.

Towards the structure of Rad50-DNA assembly

The Mre11-Rad50 subcomplex exhibits a high degree of sequence and structural conservation throughout species. Preparation of the recombinant eukaryotic Mre11-Rad50-Nbs1 complex, including its individual subunits and subcomplexes, suitable for X-ray diffraction studies posed a lot of difficulty. Attempts of expressing the MRN complex, both full-length and truncated constructs, from four different eukaryotic species (*S. pombe*, *D. melanogaster*, *H. sapiens*, *E. cuniculi*) were mostly unsuccessful (data not shown). Recombinant expression was performed in *E. coli* and in baculovirus-infected insect cells and in the end only the full-length hMRN complex could be purified from insect cells. The quality of this protein sample was however not high enough to pursue further structural studies. For this reason, a bacterial orthologue of Rad50 from *T. maritima* was chosen to be used in the structural studies presented in this work. In fact, archeal and bacterial orthologues of both Mre11 and Rad50 have been widely employed before in structural investigations of the MR complex and largely contributed to the understanding of

the subunit arrangement in the complex and the structural-functional relation between its enzymatic activities.

Since the MR complex from *T. maritima* has been such a potent tool in recent studies, tmRad50 catalytic head composed of the nucleotide-binding domain (tmRad50^{NBD}) together with a short interacting helix-loop-helix motif of Mre11 (tmMre11^{HLH}) was chosen for crystallization with DNA. *T. maritima* belongs to hyperthermophilic organisms, thereby being an attractive species for structural studies. The proteome of thermophilic organisms exhibits high stability and compactness, both being of preferential characteristics in the choice for crystallization experiments. Moreover, optimal living temperature of *T. maritima* ranges between 55-90°C. Due to this fact, the *E. coli* cell lysate containing recombinant tmRad50^{NBD}-Mre11^{HLH} complex could be precleared by incubation at 60°C. This additional purification step can often be taken advantage of while working with recombinant proteins from thermophilic species.

The minimal tmRad50^{NBD}-Mre11^{HLH} protein construct suitable for bicistronic expression was readily crystallized before and therefore chosen as a minimal subcomplex for further studies of the DNA recognition. The construct lacked the long coiled-coil domain. This large helical segment of Rad50 is characterized by high intrinsic flexibility and is therefore not suitable for crystallization purposes. Also, the Mre11 construct included only the C-terminal helix-loop-helix motif that was identified as the minimal part to interact with the root of the Rad50 coiled-coil domain. Due to the fact that previous attempts of crystallizing tmRad50^{NBD} together with the full-length Mre11 and DNA were unsuccessful (C. Möckel, personal communication), the N-terminal nuclease and capping domains were excluded from the expression construct.

As reported before, the minimal tmRad50^{NBD}-Mre11^{HLH} protein construct was highly stable during purification procedure and the final yield, purity and homogeneity of the protein facilitate crystallization trials. The protein, although eluting in gel filtration as a monomeric species (*i. e.* comprising only one Rad50 molecule with one helix-loop-helix motif of Mre11), efficiently formed a stable dimer upon AMPPNP addition.

The tmRad50^{NBD}-Mre11^{HLH} complex, together with DNA and AMPPNP, was subjected to extensive crystallization trials. DNA of different length was tested and the sample was screened against various conditions. Several conditions yielded crystals but the processing of diffraction data revealed that most of them contained only tmRad50^{NBD}-Mre11^{HLH} dimer. Only one of the initial conditions turned out to yield DNA-bound tmRad50^{NBD}-Mre11^{HLH} complex.

DNA-containing crystals that gave diffraction data suitable for the structure determination contained a 15 bp DNA duplex. At the stage of initial data analysis, the difference density coming from the DNA molecule was not very clear and a number of attempts was undertaken to improve DNA binding in the crystal. Screening DNA of varying lengths and "saturating" the protein-DNA crystallization solution with DNA did not bring clear improvement and at that stage it was already postulated that the DNA does not form very tight contacts to the protein. In order to recognize and assign the DNA registry, further refinements included co-crystallization with brominated DNA. The bromine atom provided possibility of calculating the anomalous electron density. Although this attempt did allow for assigning the DNA sequence, the locally scattered anomalous signal proved again that the DNA molecule was a highly flexible element in the structure. Moreover, observation of clear two anomalous signals calculated for a molecule containing one bromine atom only suggested that the DNA molecule could orient in two opposite directions within protein molecules of the same crystal. This would then mean that the electron difference density represented an average of the two possible DNA positions in the crystal and be therefore poor in details. In order to verify this possibility, palindromic DNA was used and indeed this approach significantly improved data quality.

Rad50-DNA structure

In the last years, a number of atomic models of prokaryotic MR orthologues have been published, including the tmRad50^{NBD}-Mre11^{HLH} (apo) structure (Lammens et al. 2011). The new tmRad50^{NBD}-Mre11^{HLH}-DNA model largely depicts all the structural features reported for the apo structure. The Rad50 NBDs arrangement is preserved, with the classical head-to-tail dimer interface, encompassing bipartite ATPase domains. Similarly, AMPPNP and Mg^{2+} binding is again clearly visible in the structure and maintained by the already described conserved motifs: Walker A and B motifs together with the signature motif. Also, the Rad50-Mre11 interaction interface exhibits no changes.

Most notable differences between the DNA-bound and the apo structures are visible at the coiled-coil domain. Within this region a shift of 1.8-3.8 Å is observed. These conformational changes can be induced by the DNA-binding. However, such alterations might also arise due to the molecule arrangement in the crystal, especially that they appear at the part of the protein proved to be prone to higher flexibility (coiled-coils) rather than more compact globular

enzymatic core of the complex. Furthermore, the change of conformation can result from DNA binding and be further intensified by the position, orientation and intramolecular contact within the crystal structure.

The new tmRad50^{NBD}-Mre11^{HLH}-DNA structure may have trapped a very initial state of the Rad50-DNA assembly. A tempting hypothesis would be that once the DNA is bound, Rad50 hydrolyses ATP and undergoes a conformational rearrangement that in turn affects DNA location on the complex and/or DNA structure. This ATP-induced DNA relocation could deliver DNA at the nuclease site of the Mre11, influencing also the cross-talk between enzymatic processing of the break and Nbs1-mediated signalling.

DNA recognition

The DNA-bound structure shows only one DNA molecule associated with a Rad50 dimer. Binding is asymmetrical and coordinated by only one Rad50 monomer. Moreover, the DNA shows a loose association with the protein. Three residues on the protein side could be clearly identified to mediate the DNA binding (K115, K175 and K182). These lysines contact phosphate moieties of the sugar-phosphate backbone (Figure 15, Results). Other than that, the model gives no evidence of other type of the DNA-protein interaction, such as minor/major groove recognition or end recognition. The binding is sequence independent which can be inferred from the fact that the crystals were formed with almost all types of tested DNA. In particular, 15 bp DNA with 1 nt overhang had an entirely different sequence from the palindromic 15 bp duplex and yet both crystals yielded comparable electron densities for the DNA. Sequence-independent binding is expected since a DSB can occur at any locus and the repair machinery should be equally efficient at the whole DNA span, irrespective of the sequence.

The DNA binding is coordinated in the structure also via the coiled-coil residues. Both of them (K175 and K182) are semi-conserved in higher eukaryotes. It is however possible that the coiled-coils-supported DNA binding occur in all species, but is coordinated by different positively charged residues, depending on the species. The structure shows that only one out of the two helices of the coiled-coil domain supports DNA binding. *In vivo*, binding could be mediated by more distal segments of the coiled-coil domain involving both helices. Such hypothesis would support the already observed significance of the coiled-coil domain in many MRX/MRN functions (Hohl et al. 2011). This report clearly shows that the full-length coiled-coil domain is

absolutely indispensable for preserving healthy cellular physiology, including telomere maintenance, repair of meiotic breaks and homologous recombination. It has been proposed that the flexible coiled-coil domain might participate in the proper arrangement of the ATPase domains of Rad50 and that even subtle alterations at distal segments of the coiled-coils could affect the catalytic activity of the whole complex. Coiled-coils-coordinated DNA recognition and binding would nicely complement this hypothesis.

Although the electron density accounted for the DNA molecule was not very clear, it is most likely an undistorted B-form DNA. There is no evident evidence that Rad50 elicited any changes in DNA topology: no DNA melting or bending can be deduced based on the electron density. However, it still cannot be excluded that such activity on DNA is indeed performed *in vivo*. It would likely be linked to ATP hydrolysis and in that case, a number of atomic models of the intermediate states of the Mre11-Rad50-DNA assembly should be investigated in order to gain insight into mechanistic details of this process.

Although the atomic model of DNA-bound tmRad50^{NBD}-Mre11^{HLH} is not very intuitive, mutational analysis supported the significance of the DNA binding residues revealed by the structure as assayed *in vitro* in DNA-binding experiments. Particularly, the K115 residue turned out to play a fundamental role in this activity. Impair of the DNA binding was also visible to a degree for the coiled-coil mutants K175E and K182E. Their effect was not as strong as observed for the K115E mutant, but as deduced from the poor electron density for the DNA in this region, the coiled-coil domain might play a supportive role in DNA binding.

DNA binding models

Several DNA recognition models have so far been proposed based on atomic models of separate subunits or subcomplexes of the MRN complex. All of them postulated that the DNA-binding interface is located on the catalytic core of the complex. A few possible locations of this interface have been under consideration. The DNA is recognized by the Mre11 nuclease domain and the binding could be further supported by Rad50 ATPase domains (Williams et al. 2009). Alternatively, both proteins could participate in forming one DNA-binding interface. This last hypothesis was proposed in a recent report showing tmRad50^{NBD}-Mre11^{FL} (Mre11 full-length) and tmRad50^{NBD}-Mre11^{HLH} structures (Lammens et al. 2011). The ATP-free “open” extended Mre11-Rad50 complex would recognize DNA ends via distantly located Rad50 monomers.

Subsequently, DNA-stimulated and ATP-dependent dimerization would result in closing of the whole complex on the DNA in such a way, that the catalytic domains of Rad50 and Mre11 would form a clamp around the DNA duplex (Figure 36).

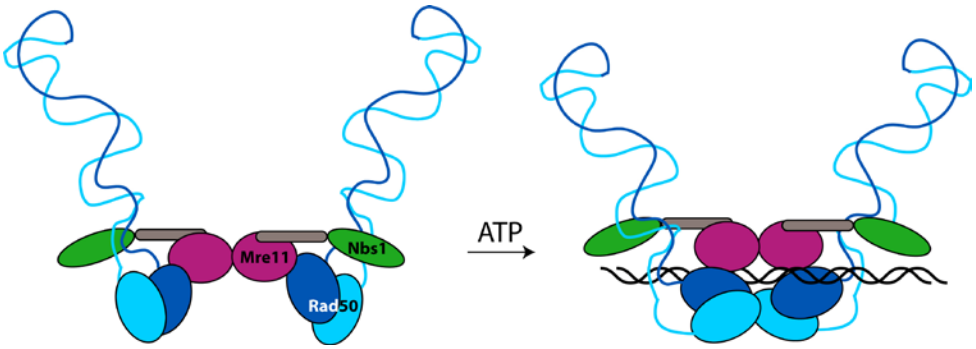

Figure 36. Clamp model of DNA recognition by the Mre11-Rad50-Nbs1 complex. ATP binding induces dimerization of Rad50 monomers into a "closed" form where nuclease and ATPase domains of Mre11 and Rad50, respectively, would form a ring-shaped DNA-binding tunnel. Based on: (Lammens et al. 2011).

More recent results, however, strongly argue against the "clamp" model. Structures of tmRad50^{NBD}-Mre11^{FL} in closed conformation from two prokaryotic species clearly show that in the fully dimerized MR assembly there is no channel wide enough to accommodate a DNA duplex (Lim et al. 2011; Mockel et al. 2012). These structures are contradictory not only to the "clamp" model but also to the DNA-bound pfMre11 structure published earlier (Williams et al. 2008). In particular, the Rad50 dimer tightly associates with the Mre11 dimer and blocks the access to the Mre11 active site at the same position that was identified to form the DNA-binding pocket in the pfMre11-DNA model (Figure 7, Introduction). This outcome already showed that the mechanism of DNA binding might be much more complex as initially expected. Moreover, ATP binding and hydrolysis induces clear conformational changes in the Rad50 dimer that are transmitted to Mre11 and possibly to Nbs1 (Mockel et al. 2012). One could expect that DNA also induces conformational changes within the whole complex and perhaps together with ATP in a cooperative manner. This could mean that the DNA-binding interface is flexible rather that rigid and a number of distinct motifs on the MR assembly might govern the binding in an alternating manner. Furthermore, it was observed that the interface built up by the dimerizing Rad50 monomers located between the coiled-coil domains is positively charged and could serve as a DNA-binding platform (Figure 22, Introduction). This hypothesis was further complemented

with a postulation that the DNA duplex bound to MRN is partially unwound during ATP hydrolysis (Paull and Gellert 1999) and that one strand on the duplex could freely migrate through the Mre11/Rad50 clamp and be enzymatically processed by Mre11 (Mockel et al. 2012) (Figure 37).

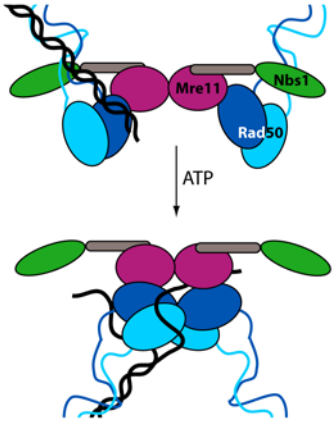

Figure 37. ATP-induced conformational change of the Mre11-Rad50 complex and its implication for DNA binding. In the ATP-bound ("closed") form, Rad50 ATPase domains sterically seclude the Mre11 active site and impair postulated clamp formation around dsDNA. dsDNA could undergo partial unwinding and then be accessible to the Mre11 active site. Based on: (Mockel et al. 2012).

Although the new tmRad50^{NBD}-Mre11^{HLH}-DNA structure does not clearly prove any of the previously postulated models of DNA binding, it also does not exclude some of these hypotheses. Firstly, the new structure definitely does not argue against the tempting idea of DNA passing along the positively charged groove located between the coiled-coils (Figure 22, Results). As visible in the arrangement of the molecules in the crystal lattice, this particular interface is occupied by a symmetry-related molecule of Rad50, which does not leave space for the DNA (Figure 38). Furthermore, several residues located on the groove were found to be crucial for DNA-binding activity *in vitro* and for telomere maintenance *in vivo*. Taken together, the putative binding groove is a strong candidate for a DNA-binding interface.

The arrangement of the symmetry-related molecules in the crystal lattice is also most probably the reason why DNA binding is asymmetrical in the crystal. Crystal packing clearly shows that in each Rad50 dimer one coiled-coil domain supports DNA binding and the other is involved in crystal contacts to a neighbouring Rad50 molecule. Therefore, it is still be possible that *in vivo* the complex recognizes DNA in a symmetrical way.

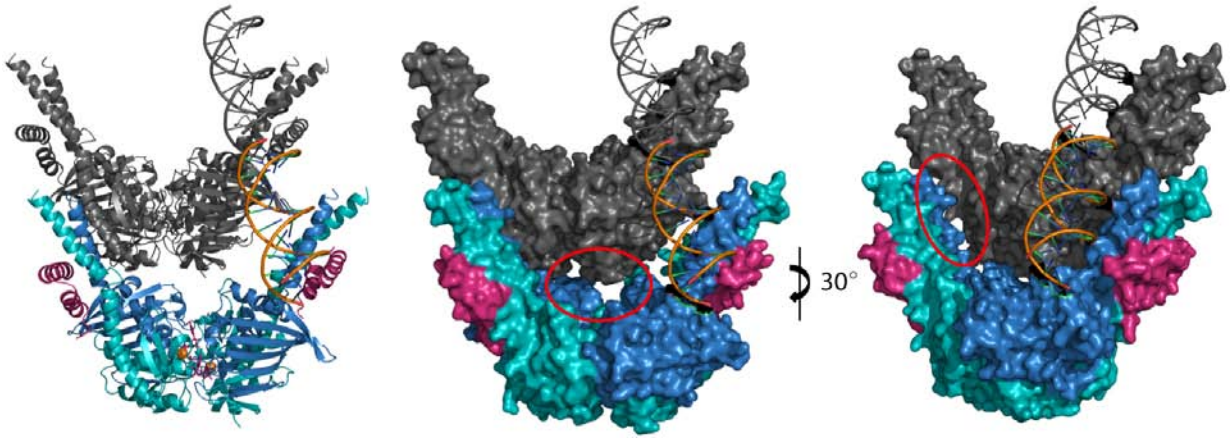

Figure 38. Arrangement of the symmetry-related molecules in the crystal lattice. Left panel: cartoon representation, middle and right panels: surface representation. Red rings mark the putative the DNA-binding groove (middle panel) and the DNA-free coiled-coil domain (right panel). Both positions are occupied by the symmetry-related molecule (shown in grey).

Insights from *in vitro* functional studies

In vitro studies showed that the structurally determined residues on Rad50 responsible for contacting DNA were indeed involved in DNA-binding activity of the protein. It could be also assumed that DNA-binding activity would depend on the DNA form, as *in vivo* the complex should recognize broken DNA ends. One could expect that nicked and most likely linearized plasmid would be bound by the protein more efficiently. Surprisingly, no difference in DNA binding-activity was observed for topologically different DNA forms. The tmRad50^{NBD}-Mre11^{HLH} complex bound circular, linearized, supercoiled and relaxed DNA with comparable efficiency and did not show exhibit preference for binding to the exposed DNA ends. One explanation could be that the protein exhibits weak preference for certain forms of DNA *in vitro* and these could not be observed with the sensitivity of EMSA. Alternatively, it is be possible that the minimal subunit of the complex used in *in vitro* assays does not exhibit the full potential of the tmMR complex on DNA. It was shown before with the purified human MRN that the most efficient DNA binding is observed for the full-length complex containing all subunits (Paull and Gellert 1999). Following this notion, the situation *in vivo* might be even more complex, with other repair factors modulating DNA binding activity of the MRN (Limbo et al. 2007; Richard et al. 2011; Polo et al. 2012). Taken together, although no preference for binding certain DNA forms was observed *in vitro*, such divergent behaviour *in vivo* cannot be excluded. The

experimental setup employed for *in vitro* assays is very simplified and certainly does not reflect the complexity of the cellular system. At the same time, performed EMSAs could only provide qualitative and not quantitative information on the DNA-binding activity.

Notably, the longer DNA used in DNA-binding tests, the better activity did the tmRad50^{NBD}-Mre11^{HLH} exhibit. Significant difference was readily observed between 30 bp and 60 bp DNAs. This result suggests that that the DNA-binding interface is much more complex compared to what was determined by the atomic model of the tmRad50^{NBD}-Mre11^{HLH}-DNA and involves other motifs on the Mre11-Rad50 catalytic head. This hypothesis is further supported by the fact that the DNA used for crystallization is very short and does not reflect the high complexity if the chromatin structure – a physiological context in which the MRN complex has to recognize the damage site.

Further mutational analyses *in vitro* showed that almost all point mutants of the tmRad50^{NBD}-Mre11^{HLH} complex exhibited lower DNA-binding activity when compared to the wild-type protein. These residues are irregularly scattered on the surface of the globular Rad50 catalytic core and at first glance form a rather random interface (Figure 21, Results). It can be that already single substitutions change the surface potential of the whole construct so strongly that the DNA binding is affected even if a given residue does not participate in forming the DNA-binding interface. However, taking into consideration the position of the DNA in the crystal and that *in vivo* the DNA has to contact the nuclease domain of Mre11, it is possible that a number of residues on the globular Rad50 ATPase domain would mediate DNA binding. *In vitro* data where tmRad50^{NBD}-Mre11^{HLH} point mutants were tested for DNA-binding activity strongly support this notion. Conserved lysines R94 and K95 seem to have a special importance. These residues on both Rad50 monomers mark distant edges of the putative DNA-binding groove. Mutating these residues strongly impairs DNA binding and this effect is comparable with the K115E mutant identified as a direct protein-DNA contact in the structure. This result would on one hand support the notion that the positively charged groove extended between the coiled-coil domains of Rad50 is indeed responsible for DNA binding and on the other hand would point towards the idea, that a number of positively charged residues on the globular Rad50 catalytic head support this binding. It can be therefore postulated that the DNA binding through the positive patch or coordinated via the coiled-coil domain is guided along the side located centrally on the ATPase domains towards Mre11 active site (Figure 39). Also, one needs to consider that

the protein construct used for these studies represents only a small fraction of the full-length complex and therefore the details of the DNA binding cannot be extrapolated globally on the behaviour of the MRN *in vivo*. Taken together, mutational studies clearly show that the DNA-binding interface is complex, dynamic and coordinated by many distinct motifs of the Mre11-Rad50 catalytic head.

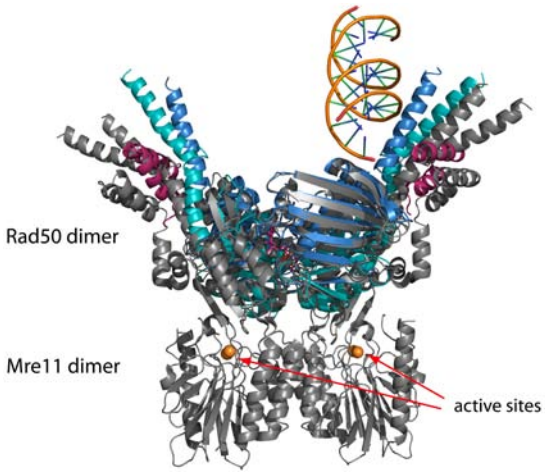

Figure 39. Overlay of the tmRad50^{NBD}-Mre11^{HLH}-DNA (in colour) and fully dimerized tmRad50^{NBD}-Mre11^{FL} structures (in grey; PDB entry: 3THO). DNA is located far from the Mre11 active sites.

Insights from *in vivo* functional studies

Conserved residues identified in the structure and in *in vitro* binding assays to play a role in the DNA-binding activity of the tmRad50^{NBD}-Mre11^{HLH} complex were also mutated in yeast *S. cerevisiae*. Further *in vivo* studies revealed the significance of these residues in DNA damage response, end joining and telomere maintenance. In the assays, the wild-type and knockout strain Δrad50 was compared to the Δrad50 strain rescued with wild-type and mutated Rad50 alleles.

DNA damage response was dramatically impaired in mutants involved in ATP binding and hydrolysis (S1205R and E1235Q, respectively) to have a dramatic impact on cell survival on DNA-damaging agents. This was already reported together with the observation that inhibition of ATP binding has even more severe effect in DNA damage response (Moncalian et al. 2004; Bhaskara et al. 2007). An equally strong phenotype was also observed for the R1201E mutant. R1201 is one of the conserved residues of the putative binding groove on Rad50 dimer interface. This mutation showed already an effect in DNA binding activity *in vitro*. Its action *in vivo* is even more pronounced, with survival capability comparable to Δrad50 strain. In the

tmRad50^{NBD}-Mre11^{HLH} structure R765 is relatively deeply buried in the groove and it is not clear if it could be directly involved in DNA binding unless the DNA molecule would be bent. At the same time R765 is located just a few aminoacids upstream from the signature motif and it is plausible that the mutation of this residue gives such a strong phenotype because of affecting the proper arrangement of the ATP binding cleft. However, the recombinant tmRad50^{NBD}-Mre11^{HLH} R765E mutant showed an insignificantly slower dimer formation upon AMPPNP addition and dimerized with the same efficiency as the wild-type protein. One possible explanation could be that *in vivo* the R1201E mutation (tmRad50 R765) strongly affects the surface charge of the groove, suggesting that this residue is crucial to the formation of the positively charged DNA-binding interface. Alternatively, the R1201E mutation could have to no effect on ATP binding *in vivo*, but rather impair its hydrolysis, resulting in a phenotype almost identical to the E1235Q mutant. The R1201E mutation could also affect the proper arrangement of the Rad50 dimer rather than the dimer formation itself, which would in turn impair the MRX complex formation and/or function *in vivo*. One way to exclude the possibility of defects in the complex formation due to R1201E mutation would be to perform co-immunoprecipitation experiments and verify if all subunits of the complex are still present interacting.

Other point mutations, including residues shown to be important for DNA binding in the structure and in *in vitro* assays did not affect *S. cerevisiae* survival on DNA-damaging agents. Changes in the phenotype were visible in the double-mutant K103E+R131E, combining residues responsible for most dramatic effect in EMSA. This effect can on one hand support *in vitro* data and on the other be in favour of the notion that the DNA binding is further mediated by a combination of the Rad50-Mre11motifs.

Interestingly, some of the residues identified to be important for DNA binding *in vitro* but not exhibiting an altered phenotype in yeast response to DNA damage significantly affected telomere maintenance and end-joining activity. The two lysine residues K103 and K104 (R94 and K95 in tmRad50) marking the exits of the putative DNA-binding groove exhibited partially shorter telomeres and partially impaired end-joining repair. Interestingly, this effect was strongly enhanced in the K103E+R131E double mutant, but not in the K104E+R131E double mutant, and comparable to the Rad50 knock-out strain, although R131E single mutant showed normal telomere maintenance and end joining. Notably, the signature motif S1205R mutant was

deficient in all three analyzed *in vivo* processes: DNA-damage response, end-joining activity and telomere maintenance, whereas the Walker B E1235Q mutant exhibited defects in DNA-damage response and end joining but was fully proficient in telomere metabolism. Remarkably, the coiled-coil mutant N190D also showed separation-of-function, being proficient in DNA-damage response but defective in end joining. This result again points out that activities of the MRN complex are distinctly employed for different cellular processes and therefore it is possible that DNA binding mode depends on the process.

An informative complement to the *in vitro* and *in vivo* studies would have been analyses of other MRN-dependent functions. This was attempted in ATM signalling experiment in *X. laevis* egg extract. Although it had been shown before that recombinant hMRN complex restores ATM signalling in xlMRN-immunodepleted extract (Costanzo et al. 2001), this result could never be reproduced in this work and for this reason structure-based mutations could not be checked for the importance in ATM signalling. Preparation of the responsive egg extract and the optimization of the immunodepletion and reaction conditions were successful. It was therefore assumed that the experiment failed either due to the substoichiometric Nbs1 concentration in the sample or low activity of the complex due to partial oligomerization or aggregation of the protein sample. This negative result was however surprising, since the procedure was carried out strictly according to previously published protocols.

Summary and future perspectives

In summary, presented structural and functional results give first insight into DNA binding by Rad50. The tmRad50^{NBD}-Mre11^{HLH}-DNA structure identified residues on the Rad50 catalytic head important to DNA binding. Additionally, involvement of the coiled-coil domain in supporting DNA binding was determined. Extensive mutational studies *in vitro* and *in vivo* not only supported these structural findings but also shed more light on other Rad50 motifs important to DNA recognition in different cellular processes.

It became apparent that the DNA-binding interface is complex and involves a number of residues/motifs, likely to be located both on Rad50 and Mre11. Presumably, the DNA binding is dynamic and involved in a cross-talk between ATP binding and hydrolysis. DNA recognition and the binding mode can be also dependent on distinct cellular process accompanied by the MRN complex. As already emphasized, some particular residues in the scRad50 that did not turn

out to be crucial to the response to DNA damage had significant importance in telomere maintenance and end-joining repair. It would be interesting to look closely at the role of these residues in other cellular events employing the MRN complex such as meiosis and signalling. Different modes of DNA binding could be also supported by the MRN-associating factors that would modulate the binding mechanism and the activity of the complex, depending of the process.

At the moment it is still difficult to fully understand which exactly structural features of the complex govern DNA recognition at the DSB site. In particular, it is not clear how the complex would sense a DNA end. More details would need to be obtained also to determine how exactly the coiled-coil domain contributes to DNA binding in different species since this segment of Rad50 is poorly conserved in sequence. It would be extremely insightful to have DNA-bound structures of larger subcomplexes of the MRN and be able to identify DNA-binding motifs on eukaryotic orthologues. Since the recent structures of fully dimerized prokaryotic Mre11-Rad50 complexes argue against previously published pfMre11-DNA bound model, structure of a more complete catalytic head of the complex bound to DNA would help to determine the role of distinct subunits in forming the DNA-binding interface and address the hypothesis of the existence of two independent DNA-binding pockets: one located on Rad50 and the other on Mre11.

Having all this information in hand, structure-guided functional studies would certainly contribute to dissecting individual MRN features responsible for the distinct roles in DNA repair, telomere maintenance, meiosis an many other cellular processes accompanied by MRN complex.

6. References

Adams, P. D., R. W. Grosse-Kunstleve, L. W. Hung, T. R. Ioerger, A. J. McCoy, N. W. Moriarty, R. J. Read, J. C. Sacchettini, N. K. Sauter, and T. C. Terwilliger. 2002. PHENIX: building new software for automated crystallographic structure determination. *Acta Crystallogr D Biol Crystallogr* 58 (Pt 11):1948-54.

Ajimura, M., S. H. Leem, and H. Ogawa. 1993. Identification of new genes required for meiotic recombination in Saccharomyces cerevisiae. *Genetics* 133 (1):51-66.

Alani, E., R. Padmore, and N. Kleckner. 1990. Analysis of wild-type and rad50 mutants of yeast suggests an intimate relationship between meiotic chromosome synapsis and recombination. *Cell* 61 (3):419-36.

Aravind, L., D. R. Walker, and E. V. Koonin. 1999. Conserved domains in DNA repair proteins and evolution of repair systems. *Nucleic Acids Res* 27 (5):1223-42.

Bakkenist, C. J., and M. B. Kastan. 2003. DNA damage activates ATM through intermolecular autophosphorylation and dimer dissociation. *Nature* 421 (6922):499-506.

Ball, H. L., M. R. Ehrhardt, D. A. Mordes, G. G. Glick, W. J. Chazin, and D. Cortez. 2007. Function of a conserved checkpoint recruitment domain in ATRIP proteins. *Mol Cell Biol* 27 (9):3367-77.

Becker-Catania, S. G., G. Chen, M. J. Hwang, Z. Wang, X. Sun, O. Sanal, E. Bernatowska-Matuszkiewicz, L. Chessa, E. Y. Lee, and R. A. Gatti. 2000. Ataxia-telangiectasia: phenotype/genotype studies of ATM protein expression, mutations, and radiosensitivity. *Mol Genet Metab* 70 (2):122-33.

Bhaskara, V., A. Dupre, B. Lengsfeld, B. B. Hopkins, A. Chan, J. H. Lee, X. Zhang, J. Gautier, V. Zakian, and T. T. Paull. 2007. Rad50 adenylate kinase activity regulates DNA tethering by Mre11/Rad50 complexes. *Mol Cell* 25 (5):647-61.

Borde, V., and J. Cobb. 2009. Double functions for the Mre11 complex during DNA double-strand break repair and replication. *Int J Biochem Cell Biol* 41 (6):1249-53.

Bosco, E. E., C. N. Mayhew, R. F. Hennigan, J. Sage, T. Jacks, and E. S. Knudsen. 2004. RB signaling prevents replication-dependent DNA double-strand breaks following genotoxic insult. *Nucleic Acids Res* 32 (1):25-34.

Boulton, S. J., and S. P. Jackson. 1996. Saccharomyces cerevisiae Ku70 potentiates illegitimate DNA double-strand break repair and serves as a barrier to error-prone DNA repair pathways. *EMBO J* 15 (18):5093-103.

Boulton, S. J., and S. P. Jackson. 1998. Components of the Ku-dependent non-homologous end-joining pathway are involved in telomeric length maintenance and telomeric silencing. *EMBO J* 17 (6):1819-28.

Breen, A. P., and J. A. Murphy. 1995. Reactions of oxyl radicals with DNA. *Free Radic Biol Med* 18 (6):1033-77.

Buis, J., Y. Wu, Y. Deng, J. Leddon, G. Westfield, M. Eckersdorff, J. M. Sekiguchi, S. Chang, and D. O. Ferguson. 2008. Mre11 nuclease activity has essential roles in DNA repair and genomic stability distinct from ATM activation. *Cell* 135 (1):85-96.

Capp, J. P., F. Boudsocq, P. Bertrand, A. Laroche-Clary, P. Pourquier, B. S. Lopez, C. Cazaux, J. S. Hoffmann, and Y. Canitrot. 2006. The DNA polymerase lambda is required for the repair of non-compatible DNA double strand breaks by NHEJ in mammalian cells. *Nucleic Acids Res* 34 (10):2998-3007.

Carney, J. P., R. S. Maser, H. Olivares, E. M. Davis, M. Le Beau, J. R. Yates, 3rd, L. Hays, W. F. Morgan, and J. H. Petrini. 1998. The hMre11/hRad50 protein complex and Nijmegen breakage syndrome: linkage of double-strand break repair to the cellular DNA damage response. *Cell* 93 (3):477-86.

Cejka, P., E. Cannavo, P. Polaczek, T. Masuda-Sasa, S. Pokharel, J. L. Campbell, and S. C. Kowalczykowski. 2010. DNA end resection by Dna2-Sgs1-RPA and its stimulation by Top3-Rmi1 and Mre11-Rad50-Xrs2. *Nature* 467 (7311):112-6.

Chalker, A. F., D. R. Leach, and R. G. Lloyd. 1988. Escherichia coli sbcC mutants permit stable propagation of DNA replicons containing a long palindrome. *Gene* 71 (1):201-5.

Chan, D. W., B. P. Chen, S. Prithivirajsingh, A. Kurimasa, M. D. Story, J. Qin, and D. J. Chen. 2002. Autophosphorylation of the DNA-dependent protein kinase catalytic subunit is required for rejoining of DNA double-strand breaks. *Genes Dev* 16 (18):2333-8.

Chapman, J. R., M. R. Taylor, and S. J. Boulton. 2012. Playing the end game: DNA double-strand break repair pathway choice. *Mol Cell* 47 (4):497-510.

Chappell, C., L. A. Hanakahi, F. Karimi-Busheri, M. Weinfeld, and S. C. West. 2002. Involvement of human polynucleotide kinase in double-strand break repair by non-homologous end joining. *EMBO J* 21 (11):2827-32.

Chen, L., C. J. Nievera, A. Y. Lee, and X. Wu. 2008. Cell cycle-dependent complex formation of BRCA1.CtIP.MRN is important for DNA double-strand break repair. *J Biol Chem* 283 (12):7713-20.

Choi, M., J. Shi, S. H. Jung, X. Chen, and K. H. Cho. 2012. Attractor landscape analysis reveals feedback loops in the p53 network that control the cellular response to DNA damage. *Sci Signal* 5 (251):ra83.

Ciccia, A., and S. J. Elledge. 2010. The DNA damage response: making it safe to play with knives. *Mol Cell* 40 (2):179-204.

Coic, E., G. F. Richard, and J. E. Haber. 2006. Saccharomyces cerevisiae donor preference during mating-type switching is dependent on chromosome architecture and organization. *Genetics* 173 (3):1197-206.

Connelly, J. C., E. S. de Leau, and D. R. Leach. 1999. DNA cleavage and degradation by the SbcCD protein complex from Escherichia coli. *Nucleic Acids Res* 27 (4):1039-46.

Connelly, J. C., E. S. de Leau, E. A. Okely, and D. R. Leach. 1997. Overexpression, purification, and characterization of the SbcCD protein from Escherichia coli. *J Biol Chem* 272 (32):19819-26.

Connelly, J. C., L. A. Kirkham, and D. R. Leach. 1998. The SbcCD nuclease of Escherichia coli is a structural maintenance of chromosomes (SMC) family protein that cleaves hairpin DNA. *Proc Natl Acad Sci U S A* 95 (14):7969-74.

Connelly, J. C., and D. R. Leach. 1996. The sbcC and sbcD genes of Escherichia coli encode a nuclease involved in palindrome inviability and genetic recombination. *Genes Cells* 1 (3):285-91.

Costanzo, V., K. Robertson, M. Bibikova, E. Kim, D. Grieco, M. Gottesman, D. Carroll, and J. Gautier. 2001. Mre11 protein complex prevents double-strand break accumulation during chromosomal DNA replication. *Mol Cell* 8 (1):137-47.

Cox, B. S., and J. M. Parry. 1968. The isolation, genetics and survival characteristics of ultraviolet light-sensitive mutants in yeast. *Mutat Res* 6 (1):37-55.

D'Amours, D., and S. P. Jackson. 2001. The yeast Xrs2 complex functions in S phase checkpoint regulation. *Genes Dev* 15 (17):2238-49.

D'Amours, D., and S. P. Jackson. 2002. The Mre11 complex: at the crossroads of dna repair and checkpoint signalling. *Nat Rev Mol Cell Biol* 3 (5):317-27.

Davis, A. P., and L. S. Symington. 2004. RAD51-dependent break-induced replication in yeast. *Mol Cell Biol* 24 (6):2344-51.

de Jager, M., K. M. Trujillo, P. Sung, K. P. Hopfner, J. P. Carney, J. A. Tainer, J. C. Connelly, D. R. Leach, R. Kanaar, and C. Wyman. 2004. Differential arrangements of conserved building blocks among homologs of the Rad50/Mre11 DNA repair protein complex. *J Mol Biol* 339 (4):937-49.

de Jager, M., J. van Noort, D. C. van Gent, C. Dekker, R. Kanaar, and C. Wyman. 2001. Human Rad50/Mre11 is a flexible complex that can tether DNA ends. *Mol Cell* 8 (5):1129-35.

DeFazio, L. G., R. M. Stansel, J. D. Griffith, and G. Chu. 2002. Synapsis of DNA ends by DNA-dependent protein kinase. *EMBO J* 21 (12):3192-200.

Delia, D., M. Piane, G. Buscemi, C. Savio, S. Palmeri, P. Lulli, L. Carlessi, E. Fontanella, and L. Chessa. 2004. MRE11 mutations and impaired ATM-dependent responses in an Italian family with ataxia-telangiectasia-like disorder. *Hum Mol Genet* 13 (18):2155-63.

Desai-Mehta, A., K. M. Cerosaletti, and P. Concannon. 2001. Distinct functional domains of nibrin mediate Mre11 binding, focus formation, and nuclear localization. *Mol Cell Biol* 21 (6):2184-91.

Difilippantonio, S., A. Celeste, M. J. Kruhlak, Y. Lee, M. J. Difilippantonio, L. Feigenbaum, S. P. Jackson, P. J. McKinnon, and A. Nussenzweig. 2007. Distinct domains in Nbs1 regulate irradiation-induced checkpoints and apoptosis. *J Exp Med* 204 (5):1003-11.

Dupre, A., L. Boyer-Chatenet, and J. Gautier. 2006. Two-step activation of ATM by DNA and the Mre11-Rad50-Nbs1 complex. *Nat Struct Mol Biol* 13 (5):451-7.

Eker, A. P., C. Quayle, I. Chaves, and G. T. van der Horst. 2009. DNA repair in mammalian cells: Direct DNA damage reversal: elegant solutions for nasty problems. *Cell Mol Life Sci* 66 (6):968-80.

Emsley, P., and K. Cowtan. 2004. Coot: model-building tools for molecular graphics. *Acta Crystallogr D Biol Crystallogr* 60 (Pt 12 Pt 1):2126-32.

Escribano-Diaz, C., A. Orthwein, A. Fradet-Turcotte, M. Xing, J. T. Young, J. Tkac, M. A. Cook, A. P. Rosebrock, M. Munro, M. D. Canny, D. Xu, and D. Durocher. 2013. A cell cycle-dependent regulatory circuit composed of 53BP1-RIF1 and BRCA1-CtIP controls DNA repair pathway choice. *Mol Cell* 49 (5):872-83.

Eykelenboom, J. K., J. K. Blackwood, E. Okely, and D. R. Leach. 2008. SbcCD causes a double-strand break at a DNA palindrome in the Escherichia coli chromosome. *Mol Cell* 29 (5):644-51.

Falck, J., J. Coates, and S. P. Jackson. 2005. Conserved modes of recruitment of ATM, ATR and DNA-PKcs to sites of DNA damage. *Nature* 434 (7033):605-11.

Ferguson, D. O., and W. K. Holloman. 1996. Recombinational repair of gaps in DNA is asymmetric in Ustilago maydis and can be explained by a migrating D-loop model. *Proc Natl Acad Sci U S A* 93 (11):5419-24.

Fernet, M., M. Gribaa, M. A. Salih, M. Z. Seidahmed, J. Hall, and M. Koenig. 2005. Identification and functional consequences of a novel MRE11 mutation affecting 10 Saudi Arabian patients with the ataxia telangiectasia-like disorder. *Hum Mol Genet* 14 (2):307-18.

Friedberg, E. C. 2003. DNA damage and repair. *Nature* 421 (6921):436-40.

Game, J. C., T. J. Zamb, R. J. Braun, M. Resnick, and R. M. Roth. 1980. The Role of Radiation (rad) Genes in Meiotic Recombination in Yeast. *Genetics* 94 (1):51-68.

Garcia, V., S. E. Phelps, S. Gray, and M. J. Neale. 2011. Bidirectional resection of DNA double-strand breaks by Mre11 and Exo1. *Nature* 479 (7372):241-4.

Gasior, S. L., A. K. Wong, Y. Kora, A. Shinohara, and D. K. Bishop. 1998. Rad52 associates with RPA and functions with rad55 and rad57 to assemble meiotic recombination complexes. *Genes Dev* 12 (14):2208-21.

Gatti, R. A. 2001. The inherited basis of human radiosensitivity. *Acta Oncol* 40 (6):702-11.

Gibson, F. P., D. R. Leach, and R. G. Lloyd. 1992. Identification of sbcD mutations as cosuppressors of recBC that allow propagation of DNA palindromes in Escherichia coli K-12. *J Bacteriol* 174 (4):1222-8.

Gilad, S., L. Chessa, R. Khosravi, P. Russell, Y. Galanty, M. Piane, R. A. Gatti, T. J. Jorgensen, Y. Shiloh, and A. Bar-Shira. 1998. Genotype-phenotype relationships in ataxia-telangiectasia and variants. *Am J Hum Genet* 62 (3):551-61.

Goodsell, D. S. 2001. The molecular perspective: ultraviolet light and pyrimidine dimers. *Oncologist* 6 (3):298-9.

Gottlieb, T. M., and S. P. Jackson. 1993. The DNA-dependent protein kinase: requirement for DNA ends and association with Ku antigen. *Cell* 72 (1):131-42.

Gu, J., H. Lu, A. G. Tsai, K. Schwarz, and M. R. Lieber. 2007. Single-stranded DNA ligation and XLF-stimulated incompatible DNA end ligation by the XRCC4-DNA ligase IV complex: influence of terminal DNA sequence. *Nucleic Acids Res* 35 (17):5755-62.

Halazonetis, T. D., V. G. Gorgoulis, and J. Bartek. 2008. An oncogene-induced DNA damage model for cancer development. *Science* 319 (5868):1352-5.

Hartlerode, A. J., and R. Scully. 2009. Mechanisms of double-strand break repair in somatic mammalian cells. *Biochem J* 423 (2):157-68.

Hohl, M., Y. Kwon, S. M. Galvan, X. Xue, C. Tous, A. Aguilera, P. Sung, and J. H. Petrini. 2011. The Rad50 coiled-coil domain is indispensable for Mre11 complex functions. *Nat Struct Mol Biol* 18 (10):1124-31.

Hopfner, K. P., L. Craig, G. Moncalian, R. A. Zinkel, T. Usui, B. A. Owen, A. Karcher, B. Henderson, J. L. Bodmer, C. T. McMurray, J. P. Carney, J. H. Petrini, and J. A. Tainer. 2002. The Rad50 zinc-hook is a structure joining Mre11 complexes in DNA recombination and repair. *Nature* 418 (6897):562-6.

Hopfner, K. P., A. Karcher, L. Craig, T. T. Woo, J. P. Carney, and J. A. Tainer. 2001. Structural biochemistry and interaction architecture of the DNA double-strand break repair Mre11 nuclease and Rad50-ATPase. *Cell* 105 (4):473-85.

Hopfner, K. P., A. Karcher, D. S. Shin, L. Craig, L. M. Arthur, J. P. Carney, and J. A. Tainer. 2000. Structural biology of Rad50 ATPase: ATP-driven conformational control in DNA double-strand break repair and the ABC-ATPase superfamily. *Cell* 101 (7):789-800.

Hopfner, K. P., and J. A. Tainer. 2003. Rad50/SMC proteins and ABC transporters: unifying concepts from high-resolution structures. *Curr Opin Struct Biol* 13 (2):249-55.

Hopkins, B. B., and T. T. Paull. 2008. The P. furiosus mre11/rad50 complex promotes 5' strand resection at a DNA double-strand break. *Cell* 135 (2):250-60.

Huertas, P., F. Cortes-Ledesma, A. A. Sartori, A. Aguilera, and S. P. Jackson. 2008. CDK targets Sae2 to control DNA-end resection and homologous recombination. *Nature* 455 (7213):689-92.

Kabsch, W. 1993. Automatic processing of rotation diffraction data from crystals of initially unknown symmetry and cell constants. *J Appl Crystallogr* 26 (6):795-800.

Karlseder, J., D. Broccoli, Y. Dai, S. Hardy, and T. de Lange. 1999. p53- and ATM-dependent apoptosis induced by telomeres lacking TRF2. *Science* 283 (5406):1321-5.

Keeney, S. 2008. Spo11 and the Formation of DNA Double-Strand Breaks in Meiosis. *Genome Dyn Stab* 2:81-123.

Kerzendorfer, C., and M. O'Driscoll. 2009. Human DNA damage response and repair deficiency syndromes: linking genomic instability and cell cycle checkpoint proficiency. *DNA Repair (Amst)* 8 (9):1139-52.

Kironmai, K. M., and K. Muniyappa. 1997. Alteration of telomeric sequences and senescence caused by mutations in RAD50 of Saccharomyces cerevisiae. *Genes Cells* 2 (7):443-55.

Kondo, T., J. Kobayashi, T. Saitoh, K. Maruyama, K. J. Ishii, G. N. Barber, K. Komatsu, S. Akira, and T. Kawai. 2013. DNA damage sensor MRE11 recognizes cytosolic double-stranded DNA and induces type I interferon by regulating STING trafficking. *Proc Natl Acad Sci U S A* 110 (8):2969-74.

Krejci, L., V. Altmannova, M. Spirek, and X. Zhao. 2012. Homologous recombination and its regulation. *Nucleic Acids Res* 40 (13):5795-818.

Kubota, Y., and H. Takisawa. 1993. Determination of initiation of DNA replication before and after nuclear formation in Xenopus egg cell free extracts. *J Cell Biol* 123 (6 Pt 1):1321-31.

Kunz, C., Y. Saito, and P. Schar. 2009. DNA Repair in mammalian cells: Mismatched repair: variations on a theme. *Cell Mol Life Sci* 66 (6):1021-38.

Kuzminov, A. 2001. DNA replication meets genetic exchange: chromosomal damage and its repair by homologous recombination. *Proc Natl Acad Sci U S A* 98 (15):8461-8.

Laemmli, U. K. 1970. Cleavage of structural proteins during the assembly of the head of bacteriophage T4. *Nature* 227 (5259):680-5.

Lammens, K., D. J. Bemeleit, C. Mockel, E. Clausing, A. Schele, S. Hartung, C. B. Schiller, M. Lucas, C. Angermuller, J. Soding, K. Strasser, and K. P. Hopfner. 2011. The Mre11:Rad50 structure shows an ATP-dependent molecular clamp in DNA double-strand break repair. *Cell* 145 (1):54-66.

Leach, D. R., R. G. Lloyd, and A. F. Coulson. 1992. The SbcCD protein of Escherichia coli is related to two putative nucleases in the UvrA superfamily of nucleotide-binding proteins. *Genetica* 87 (2):95-100.

Lee, J. H., R. Ghirlando, V. Bhaskara, M. R. Hoffmeyer, J. Gu, and T. T. Paull. 2003. Regulation of Mre11/Rad50 by Nbs1: effects on nucleotide-dependent DNA binding and association with ataxia-telangiectasia-like disorder mutant complexes. *J Biol Chem* 278 (46):45171-81.

Lee, J. H., and T. T. Paull. 2004. Direct activation of the ATM protein kinase by the Mre11/Rad50/Nbs1 complex. *Science* 304 (5667):93-6.

Lempiainen, H., and T. D. Halazonetis. 2009. Emerging common themes in regulation of PIKKs and PI3Ks. *EMBO J* 28 (20):3067-73.

Lim, H. S., J. S. Kim, Y. B. Park, G. H. Gwon, and Y. Cho. 2011. Crystal structure of the Mre11-Rad50-ATPgammaS complex: understanding the interplay between Mre11 and Rad50. *Genes Dev* 25 (10):1091-104.

Limbo, O., C. Chahwan, Y. Yamada, R. A. de Bruin, C. Wittenberg, and P. Russell. 2007. Ctp1 is a cell-cycle-regulated protein that functions with Mre11 complex to control double-strand break repair by homologous recombination. *Mol Cell* 28 (1):134-46.

Limoli, C. L., E. Giedzinski, W. M. Bonner, and J. E. Cleaver. 2002. UV-induced replication arrest in the xeroderma pigmentosum variant leads to DNA double-strand breaks, gamma -H2AX formation, and Mre11 relocalization. *Proc Natl Acad Sci U S A* 99 (1):233-8.

Liu, J., L. Renault, X. Veaute, F. Fabre, H. Stahlberg, and W. D. Heyer. 2011. Rad51 paralogues Rad55-Rad57 balance the antirecombinase Srs2 in Rad51 filament formation. *Nature* 479 (7372):245-8.

Lloyd, J., J. R. Chapman, J. A. Clapperton, L. F. Haire, E. Hartsuiker, J. Li, A. M. Carr, S. P. Jackson, and S. J. Smerdon. 2009. A supramodular FHA/BRCT-repeat architecture mediates Nbs1 adaptor function in response to DNA damage. *Cell* 139 (1):100-11.

Lombard, D. B., and L. Guarente. 2000. Nijmegen breakage syndrome disease protein and MRE11 at PML nuclear bodies and meiotic telomeres. *Cancer Res* 60 (9):2331-4.

Luo, G., M. S. Yao, C. F. Bender, M. Mills, A. R. Bladl, A. Bradley, and J. H. Petrini. 1999. Disruption of mRad50 causes embryonic stem cell lethality, abnormal embryonic development, and sensitivity to ionizing radiation. *Proc Natl Acad Sci U S A* 96 (13):7376-81.

Ma, Y., U. Pannicke, K. Schwarz, and M. R. Lieber. 2002. Hairpin opening and overhang processing by an Artemis/DNA-dependent protein kinase complex in nonhomologous end joining and V(D)J recombination. *Cell* 108 (6):781-94.

Mahajan, K. N., L. Gangi-Peterson, D. H. Sorscher, J. Wang, K. N. Gathy, N. P. Mahajan, W. H. Reeves, and B. S. Mitchell. 1999. Association of terminal deoxynucleotidyl transferase with Ku. *Proc Natl Acad Sci U S A* 96 (24):13926-31.

Mahajan, K. N., S. A. Nick McElhinny, B. S. Mitchell, and D. A. Ramsden. 2002. Association of DNA polymerase mu (pol mu) with Ku and ligase IV: role for pol mu in end-joining double-strand break repair. *Mol Cell Biol* 22 (14):5194-202.

Mahaney, B. L., K. Meek, and S. P. Lees-Miller. 2009. Repair of ionizing radiation-induced DNA double-strand breaks by non-homologous end-joining. *Biochem J* 417 (3):639-50.

Mari, P. O., B. I. Florea, S. P. Persengiev, N. S. Verkaik, H. T. Bruggenwirth, M. Modesti, G. Giglia-Mari, K. Bezstarosti, J. A. Demmers, T. M. Luider, A. B. Houtsmuller, and D. C. van Gent. 2006. Dynamic assembly of end-joining complexes requires interaction between Ku70/80 and XRCC4. *Proc Natl Acad Sci U S A* 103 (49):18597-602.

Maser, R. S., R. Zinkel, and J. H. Petrini. 2001. An alternative mode of translation permits production of a variant NBS1 protein from the common Nijmegen breakage syndrome allele. *Nat Genet* 27 (4):417-21.

McBlane, J. F., D. C. van Gent, D. A. Ramsden, C. Romeo, C. A. Cuomo, M. Gellert, and M. A. Oettinger. 1995. Cleavage at a V(D)J recombination signal requires only RAG1 and RAG2 proteins and occurs in two steps. *Cell* 83 (3):387-95.

McCoy, A. J., R. W. Grosse-Kunstleve, P. D. Adams, M. D. Winn, L. C. Storoni, and R. J. Read. 2007. Phaser crystallographic software. *J Appl Crystallogr* 40 (Pt 4):658-674.

Meek, K., P. Douglas, X. Cui, Q. Ding, and S. P. Lees-Miller. 2007. trans Autophosphorylation at DNA-dependent protein kinase's two major autophosphorylation site clusters facilitates end processing but not end joining. *Mol Cell Biol* 27 (10):3881-90.

Metcalfe, J. A., J. Parkhill, L. Campbell, M. Stacey, P. Biggs, P. J. Byrd, and A. M. Taylor. 1996. Accelerated telomere shortening in ataxia telangiectasia. *Nat Genet* 13 (3):350-3.

Mockel, C., K. Lammens, A. Schele, and K. P. Hopfner. 2012. ATP driven structural changes of the bacterial Mre11:Rad50 catalytic head complex. *Nucleic Acids Res* 40 (2):914-27.

Moncalian, G., B. Lengsfeld, V. Bhaskara, K. P. Hopfner, A. Karcher, E. Alden, J. A. Tainer, and T. T. Paull. 2004. The rad50 signature motif: essential to ATP binding and biological function. *J Mol Biol* 335 (4):937-51.

Naom, I. S., S. J. Morton, D. R. Leach, and R. G. Lloyd. 1989. Molecular organization of sbcC, a gene that affects genetic recombination and the viability of DNA palindromes in Escherichia coli K-12. *Nucleic Acids Res* 17 (20):8033-45.

Neale, M. J., J. Pan, and S. Keeney. 2005. Endonucleolytic processing of covalent protein-linked DNA double-strand breaks. *Nature* 436 (7053):1053-7.

Nouspikel, T. 2009. DNA repair in mammalian cells : Nucleotide excision repair: variations on versatility. *Cell Mol Life Sci* 66 (6):994-1009.

Orr-Weaver, T. L., and J. W. Szostak. 1983. Yeast recombination: the association between double-strand gap repair and crossing-over. *Proc Natl Acad Sci U S A* 80 (14):4417-21.

Park, Y. B., J. Chae, Y. C. Kim, and Y. Cho. 2011. Crystal structure of human Mre11: understanding tumorigenic mutations. *Structure* 19 (11):1591-602.

Paull, T. T., and M. Gellert. 1998. The 3' to 5' exonuclease activity of Mre 11 facilitates repair of DNA double-strand breaks. *Mol Cell* 1 (7):969-79.

Paull, T. T., and M. Gellert. 1999. Nbs1 potentiates ATP-driven DNA unwinding and endonuclease cleavage by the Mre11/Rad50 complex. *Genes Dev* 13 (10):1276-88.

Polo, S. E., A. N. Blackford, J. R. Chapman, L. Baskcomb, S. Gravel, A. Rusch, A. Thomas, R. Blundred, P. Smith, J. Kzhyshkowska, T. Dobner, A. M. Taylor, A. S. Turnell, G. S. Stewart, R. J. Grand, and S. P. Jackson. 2012. Regulation of DNA-end resection by hnRNPU-like proteins promotes DNA double-strand break signaling and repair. *Mol Cell* 45 (4):505-16.

Rahal, E. A., L. A. Henricksen, Y. Li, R. S. Williams, J. A. Tainer, and K. Dixon. 2010. ATM regulates Mre11-dependent DNA end-degradation and microhomology-mediated end joining. *Cell Cycle* 9 (14):2866-77.

Richard, D. J., L. Cubeddu, A. J. Urquhart, A. Bain, E. Bolderson, D. Menon, M. F. White, and K. K. Khanna. 2011. hSSB1 interacts directly with the MRN complex stimulating its recruitment to DNA double-strand breaks and its endo-nuclease activity. *Nucleic Acids Res* 39 (9):3643-51.

Robertson, A. B., A. Klungland, T. Rognes, and I. Leiros. 2009. DNA repair in mammalian cells: Base excision repair: the long and short of it. *Cell Mol Life Sci* 66 (6):981-93.

Rozier, L., Y. Guo, S. Peterson, M. Sato, R. Baer, J. Gautier, and Y. Mao. 2013. The MRN-CtIP pathway is required for metaphase chromosome alignment. *Mol Cell* 49 (6):1097-107.

Sanal, O., F. Ersoy, L. Yel, I. Tezcan, A. Metin, H. Ozyurek, S. Gariboglu, S. Fikrig, A. I. Berkel, G. T. Rijkers, and B. J. Zegers. 1999. Impaired IgG antibody production to pneumococcal polysaccharides in patients with ataxia-telangiectasia. *J Clin Immunol* 19 (5):326-34.

Sartori, A. A., C. Lukas, J. Coates, M. Mistrik, S. Fu, J. Bartek, R. Baer, J. Lukas, and S. P. Jackson. 2007. Human CtIP promotes DNA end resection. *Nature* 450 (7169):509-14.

Savitsky, K., A. Bar-Shira, S. Gilad, G. Rotman, Y. Ziv, L. Vanagaite, D. A. Tagle, S. Smith, T. Uziel, S. Sfez, M. Ashkenazi, I. Pecker, M. Frydman, R. Harnik, S. R. Patanjali, A. Simmons, G. A. Clines, A. Sartiel, R. A. Gatti, L. Chessa, O. Sanal, M. F. Lavin, N. G. Jaspers, A. M. Taylor, C. F. Arlett, T. Miki, S. M. Weissman, M. Lovett, F. S. Collins, and Y. Shiloh. 1995. A single ataxia telangiectasia gene with a product similar to PI-3 kinase. *Science* 268 (5218):1749-53.

Schiller, C. B., K. Lammens, I. Guerini, B. Coordes, H. Feldmann, F. Schlauderer, C. Mockel, A. Schele, K. Strasser, S. P. Jackson, and K. P. Hopfner. 2012. Structure of Mre11-Nbs1 complex yields insights into ataxia-telangiectasia-like disease mutations and DNA damage signaling. *Nat Struct Mol Biol* 19 (7):693-700.

Sharples, G. J., and D. R. Leach. 1995. Structural and functional similarities between the SbcCD proteins of Escherichia coli and the RAD50 and MRE11 (RAD32) recombination and repair proteins of yeast. *Mol Microbiol* 17 (6):1215-7.

Shim, E. Y., W. H. Chung, M. L. Nicolette, Y. Zhang, M. Davis, Z. Zhu, T. T. Paull, G. Ira, and S. E. Lee. 2010. Saccharomyces cerevisiae Mre11/Rad50/Xrs2 and Ku proteins regulate association of Exo1 and Dna2 with DNA breaks. *EMBO J* 29 (19):3370-80.

Shinohara, A., and T. Ogawa. 1998. Stimulation by Rad52 of yeast Rad51-mediated recombination. *Nature* 391 (6665):404-7.

Shrivastav, M., L. P. De Haro, and J. A. Nickoloff. 2008. Regulation of DNA double-strand break repair pathway choice. *Cell Res* 18 (1):134-47.

Sievers, F., A. Wilm, D. Dineen, T. J. Gibson, K. Karplus, W. Li, R. Lopez, H. McWilliam, M. Remmert, J. Soding, J. D. Thompson, and D. G. Higgins. 2011. Fast, scalable generation of high-quality protein multiple sequence alignments using Clustal Omega. *Mol Syst Biol* 7:539.

Singer, B. 1986. O-alkyl pyrimidines in mutagenesis and carcinogenesis: occurrence and significance. *Cancer Res* 46 (10):4879-85.

Stewart, G. S., R. S. Maser, T. Stankovic, D. A. Bressan, M. I. Kaplan, N. G. Jaspers, A. Raams, P. J. Byrd, J. H. Petrini, and A. M. Taylor. 1999. The DNA double-strand break repair gene hMRE11 is mutated in individuals with an ataxia-telangiectasia-like disorder. *Cell* 99 (6):577-87.

Stracker, T. H., M. Morales, S. S. Couto, H. Hussein, and J. H. Petrini. 2007. The carboxy terminus of NBS1 is required for induction of apoptosis by the MRE11 complex. *Nature* 447 (7141):218-21.

Stracker, T. H., and J. H. Petrini. 2011. The MRE11 complex: starting from the ends. *Nat Rev Mol Cell Biol* 12 (2):90-103.

Sullivan, K. D., C. L. Gallant-Behm, R. E. Henry, J. L. Fraikin, and J. M. Espinosa. 2012. The p53 circuit board. *Biochim Biophys Acta* 1825 (2):229-44.

Sung, P., L. Krejci, S. Van Komen, and M. G. Sehorn. 2003. Rad51 recombinase and recombination mediators. *J Biol Chem* 278 (44):42729-32.

Suslova, N. G., I. V. Fedorova, and NIu Zhelezniakova. 1975. [Effect of uvs1, uvs2 and xrs mutations on the radiosensitivity of and frequency of induced mitotic recombination in diploid yeast cells]. *Genetika* 11 (11):58-66.

Sutherland, B. M., P. V. Bennett, O. Sidorkina, and J. Laval. 2000. Clustered DNA damages induced in isolated DNA and in human cells by low doses of ionizing radiation. *Proc Natl Acad Sci U S A* 97 (1):103-8.

Takai, H., A. Smogorzewska, and T. de Lange. 2003. DNA damage foci at dysfunctional telomeres. *Curr Biol* 13 (17):1549-56.

Takata, H., Y. Tanaka, and A. Matsuura. 2005. Late S phase-specific recruitment of Mre11 complex triggers hierarchical assembly of telomere replication proteins in Saccharomyces cerevisiae. *Mol Cell* 17 (4):573-83.

Taylor, A. M., D. G. Harnden, C. F. Arlett, S. A. Harcourt, A. R. Lehmann, S. Stevens, and B. A. Bridges. 1975. Ataxia telangiectasia: a human mutation with abnormal radiation sensitivity. *Nature* 258 (5534):427-9.

Tornaletti, S. 2009. DNA repair in mammalian cells: Transcription-coupled DNA repair: directing your effort where it's most needed. *Cell Mol Life Sci* 66 (6):1010-20.

Tsai, C. J., S. A. Kim, and G. Chu. 2007. Cernunnos/XLF promotes the ligation of mismatched and noncohesive DNA ends. *Proc Natl Acad Sci U S A* 104 (19):7851-6.

Uchisaka, N., N. Takahashi, M. Sato, A. Kikuchi, S. Mochizuki, K. Imai, S. Nonoyama, O. Ohara, F. Watanabe, S. Mizutani, R. Hanada, and T. Morio. 2009. Two brothers with ataxia-telangiectasia-like disorder with lung adenocarcinoma. *J Pediatr* 155 (3):435-8.

Uematsu, N., E. Weterings, K. Yano, K. Morotomi-Yano, B. Jakob, G. Taucher-Scholz, P. O. Mari, D. C. van Gent, B. P. Chen, and D. J. Chen. 2007. Autophosphorylation of DNA-PKCS regulates its dynamics at DNA double-strand breaks. *J Cell Biol* 177 (2):219-29.

Usui, T., T. Ohta, H. Oshiumi, J. Tomizawa, H. Ogawa, and T. Ogawa. 1998. Complex formation and functional versatility of Mre11 of budding yeast in recombination. *Cell* 95 (5):705-16.

van Gent, D. C., and M. van der Burg. 2007. Non-homologous end-joining, a sticky affair. *Oncogene* 26 (56):7731-40.

van Noort, J., T. van Der Heijden, M. de Jager, C. Wyman, R. Kanaar, and C. Dekker. 2003. The coiled-coil of the human Rad50 DNA repair protein contains specific segments of increased flexibility. *Proc Natl Acad Sci U S A* 100 (13):7581-6.

Varon, R., C. Vissinga, M. Platzer, K. M. Cerosaletti, K. H. Chrzanowska, K. Saar, G. Beckmann, E. Seemanova, P. R. Cooper, N. J. Nowak, M. Stumm, C. M. Weemaes, R. A. Gatti, R. K. Wilson, M. Digweed, A. Rosenthal, K. Sperling, P. Concannon, and A. Reis. 1998. Nibrin, a novel DNA double-strand break repair protein, is mutated in Nijmegen breakage syndrome. *Cell* 93 (3):467-76.

Verkaik, N. S., R. E. Esveldt-van Lange, D. van Heemst, H. T. Bruggenwirth, J. H. Hoeijmakers, M. Z. Zdzienicka, and D. C. van Gent. 2002. Different types of V(D)J recombination and end-joining defects in DNA double-strand break repair mutant mammalian cells. *Eur J Immunol* 32 (3):701-9.

Walker, J. R., R. A. Corpina, and J. Goldberg. 2001. Structure of the Ku heterodimer bound to DNA and its implications for double-strand break repair. *Nature* 412 (6847):607-14.

Waltes, R., R. Kalb, M. Gatei, A. W. Kijas, M. Stumm, A. Sobeck, B. Wieland, R. Varon, Y. Lerenthal, M. F. Lavin, D. Schindler, and T. Dork. 2009. Human RAD50 deficiency in a Nijmegen breakage syndrome-like disorder. *Am J Hum Genet* 84 (5):605-16.

Waris, G., and H. Ahsan. 2006. Reactive oxygen species: role in the development of cancer and various chronic conditions. *J Carcinog* 5:14.

Williams, G. J., R. S. Williams, J. S. Williams, G. Moncalian, A. S. Arvai, O. Limbo, G. Guenther, S. SilDas, M. Hammel, P. Russell, and J. A. Tainer. 2011. ABC ATPase signature helices in Rad50 link nucleotide state to Mre11 interface for DNA repair. *Nat Struct Mol Biol* 18 (4):423-31.

Williams, R. S., G. E. Dodson, O. Limbo, Y. Yamada, J. S. Williams, G. Guenther, S. Classen, J. N. Glover, H. Iwasaki, P. Russell, and J. A. Tainer. 2009. Nbs1 flexibly tethers Ctp1 and Mre11-Rad50 to coordinate DNA double-strand break processing and repair. *Cell* 139 (1):87-99.

Williams, R. S., G. Moncalian, J. S. Williams, Y. Yamada, O. Limbo, D. S. Shin, L. M. Groocock, D. Cahill, C. Hitomi, G. Guenther, D. Moiani, J. P. Carney, P. Russell, and J. A. Tainer. 2008. Mre11 dimers coordinate DNA end bridging and nuclease processing in double-strand-break repair. *Cell* 135 (1):97-109.

Williams, R. S., J. S. Williams, and J. A. Tainer. 2007. Mre11-Rad50-Nbs1 is a keystone complex connecting DNA repair machinery, double-strand break signaling, and the chromatin template. *Biochem Cell Biol* 85 (4):509-20.

Wiltzius, J. J., M. Hohl, J. C. Fleming, and J. H. Petrini. 2005. The Rad50 hook domain is a critical determinant of Mre11 complex functions. *Nat Struct Mol Biol* 12 (5):403-7.

Wolner, B., S. van Komen, P. Sung, and C. L. Peterson. 2003. Recruitment of the recombinational repair machinery to a DNA double-strand break in yeast. *Mol Cell* 12 (1):221-32.

Xiao, Y., and D. T. Weaver. 1997. Conditional gene targeted deletion by Cre recombinase demonstrates the requirement for the double-strand break repair Mre11 protein in murine embryonic stem cells. *Nucleic Acids Res* 25 (15):2985-91.

Xie, A., A. Kwok, and R. Scully. 2009. Role of mammalian Mre11 in classical and alternative nonhomologous end joining. *Nat Struct Mol Biol* 16 (8):814-8.

Xu, C., L. Wu, G. Cui, M. V. Botuyan, J. Chen, and G. Mer. 2008. Structure of a second BRCT domain identified in the nijmegen breakage syndrome protein Nbs1 and its function in an MDC1-dependent localization of Nbs1 to DNA damage sites. *J Mol Biol* 381 (2):361-72.

Yaffe, M. P., and G. Schatz. 1984. Two nuclear mutations that block mitochondrial protein import in yeast. *Proc Natl Acad Sci U S A* 81 (15):4819-23.

Yan, C. T., C. Boboila, E. K. Souza, S. Franco, T. R. Hickernell, M. Murphy, S. Gumaste, M. Geyer, A. A. Zarrin, J. P. Manis, K. Rajewsky, and F. W. Alt. 2007. IgH class switching and translocations use a robust non-classical end-joining pathway. *Nature* 449 (7161):478-82.

You, Z., C. Chahwan, J. Bailis, T. Hunter, and P. Russell. 2005. ATM activation and its recruitment to damaged DNA require binding to the C terminus of Nbs1. *Mol Cell Biol* 25 (13):5363-79.

Zhang, X., and T. T. Paull. 2005. The Mre11/Rad50/Xrs2 complex and non-homologous end-joining of incompatible ends in S. cerevisiae. *DNA Repair (Amst)* 4 (11):1281-94.

Zhu, J., S. Petersen, L. Tessarollo, and A. Nussenzweig. 2001. Targeted disruption of the Nijmegen breakage syndrome gene NBS1 leads to early embryonic lethality in mice. *Curr Biol* 11 (2):105-9.

Zhu, X. D., B. Kuster, M. Mann, J. H. Petrini, and T. de Lange. 2000. Cell-cycle-regulated association of RAD50/MRE11/NBS1 with TRF2 and human telomeres. *Nat Genet* 25 (3):347-52.

Zhuang, J., G. Jiang, H. Willers, and F. Xia. 2009. Exonuclease function of human Mre11 promotes deletional nonhomologous end joining. *J Biol Chem* 284 (44):30565-73.

Zimmermann, M., F. Lottersberger, S. B. Buonomo, A. Sfeir, and T. de Lange. 2013. 53BP1 regulates DSB repair using Rif1 to control 5' end resection. *Science* 339 (6120):700-4.

Zou, L., and S. J. Elledge. 2003. Sensing DNA damage through ATRIP recognition of RPA-ssDNA complexes. *Science* 300 (5625):1542-8.

7. Abbreviations

°C	degree Celcius
2-ME	β-mercaptoethanol
3D	three-dimension
6-FAM	6-carboxyfluorescein
6His	6-histidine tag
aa	aminoacid
Å	angstrom
AMPPNP	adenosine 5´(ß,γ-imido)triphosphate
A-T	adenine-thymine pair
ATLD	ataxia-telangiectasia like disease
ATM	ataxia telangiectasia mutated
ATP	adenosine-5'-triphosphate
BER	base excision repair
bp	base pair (base pairs)
BRCT	breast cancer carboxy-terminus
C-terminus	carboxy-terminus
CPT	camptothecin
CV	colume volume
Cy3-dCTP	Cy3-labelled deoxycytidine triphosphate
D. melanogaster	*Drosophila melanogaster*
DDR	direct damage reversal
DNA	doexyribonucleic acid
DNA-PK	DNA-dependent protein kinase
dNTP	deoxyribonucleotide
DSB	double-strand break
DSBR	double-strand break repair
dsDNA	double-stranded DNA
DTT	dithiotreitol
ECL	enhanced chemoluminiscence
E. coli	*Escherichia coli*
E. cuniculi	*Encephalitozoon cuniculi*
EDTA	ethylenediaminetetraacetic acid
e. g.	*exempli gratia* (for example)
EMSA	electrophoretic mobility shift assay
ESRF	European Synchrotron Radiation Facility
EtOH	ethanol
FHA	forkhead associated
FL	full-length
Fw	forward
G-C	guanine-cytosine
h	hour (hours)

H. sapiens	*Homo sapiens*
HLH	helix-loop-helix
hMRN	human MRN
HPLC	high performance liquid chromatography
HPSF	high purity salt free
HR	homologous recobination
HU	hydroxyurea
i. e.	*id est* (that is)
Ig	immunoglobulin
IPTG	isopropyl-ß-D-thiogalactopyranosid
IR	ionizing radiation
kDa	kilo Dalton
LB	lysogeny broth
M	molar
mA	miliampere
MDa	mega dalton
Mg	magnesium
min	minute (minutes)
MMEJ	microhomology-mediated end joining
MMS	methyl methanesulfonate
Mn	manganese
MR	Mre11-Rad50
MRN/MRX	Mre11-Rad50-Nbs1 (Mre11-Rad50-Xrs2 in *S. cerevisiae*)
N-terminus	amino-terminus
nt	nucleotide
NER	nucleotide excision repair
NBD	nucleotide binding domain
NBS	Nijmegen breakage syndrome
NBSLD	Nijmegen breakage syndrome like disease
NHEJ	non homologous end joining
Ni-NTA	nickel-nitrilotriacetic acid
No.	number
nt	nucleotide
OD_{600}	optical density at 600nm
ORF	open reading frame
PAGE	polyacrylamide gel electrophoresis
PBS	phosphate-buffered saline
PCR	polymerase chain reaction
PDB	protein data bank
PEG	polyethylene glycol
P. furiosus	*Pyrococcus furiosus*
pfRad50	Rad50 from *P. furiosus*
pH	potential of hydrogen
PVDF	polyvinylidene difluoride

R. m. s	root mean square
rcf	relative centrifugal force
ROS	reactive oxygen species
RPA	replication protein A
rpm	rotation per min
Rv	reverse
s	second
S. cerevisiae	*Saccharomyces cerevisiae*
S. frugiperda	*Spodoptera frugiperda*
S. pombe	*Schizosaccharomyces pombe*
scRad50	Rad50 from *S. cerevisiae*
SDS	sodium dodecyl-sulfate
SLS	Swiss Light Source
SMC	structural maintenance of chromosome
ssDNA	single-stranded DNA
TA	Tris-acetate
TBST	Tris buffered saline with Tween20
TCA	trichloroacetic acid
Tcr	T-cell receptor
T. maritima	*Termothoga maritima*
tmMre11	Mre11 from *T. maritima*
tmRad50	Rad50 from *T. maritima*
T. ni	*Trichoplusia ni*
Tris	tris(hydroxymethyl)aminomethane
UV	ultraviolet radiation
V(D)J recombination	variable-diverse-joining recombination
WT	wild-type
X. laevis	*Xenopus laevis*
xlMre11	Mre11 from *X. laevis*
xlMRN	MRN from *X. laevis*
YPD	yeast extract peptone dextrose
YT	yeast extract tryptone
Zn	zinc

8. Curriculum vitae

Personal details

Name	Anna Maria Rojowska
Date of birth	01. 02. 1984
Place of birth	Krakow, Poland
Nationality	Polish

Education

Oct 2004-Jun 2009	Studies in Biotechnology Jagiellonian University, Krakow, Poland
Sep 1999-Jun 2003	A. Witkowski High School No. 5, Krakow, Poland

Academic training

Sep 2009-now	PhD Thesis in Structural Biology group of Prof. Dr. Karl-Peter Hopfner, Gene Center, Department of Biochemistry, Faculty for Chemistry and Pharmacy Ludwig-Maximilians-Universität München, Germany
Oct 2004-Jun 2009	Master Thesis in Biotechnology group of Prof. A. Dubin, Department of Analytical Biochemistry Jagiellonian University, Krakow, Poland
Feb 2008-Aug 2008	Internship (Socrates/Erazmus Exchange Program) group of Dr. Tad. A. Holak, Department of Cell Structure Biology, Max-Planck Institute for Biochemistry, Martinsried, Germany

9. Acknowledgements

Foremost, I would like to thank Prof. Karl-Peter Hopfner for providing me with a generous possibility of working in his research group on a challenging and exciting project. I am thankful for his support and advice and for the opportunity to develop my own ideas and interests.

I thank Prof. Mario Halic for agreeing to be the second evaluator of this thesis.

My special acknowledgements are directed to Katja Lammens for her interest and close assistance at every stage of this thesis. I greatly appreciate her involvement in the project, constructive discussions and fruitful ideas. Last, but not least, I thank her for being a patient and inspiring teacher of crystallography, always ready to support me with her broad expertise.

Many thanks go to Carolin Möckel who introduced me to the project and was always ready to share her vast experience on the prokaryotic Mre11-Rad50 complex and various biochemical techniques. I would also like to thank Christian Schiller for his help with *S. cerevisiae* specific methods. I thank Brigitte Kessler for assisting me with protein biochemistry and *in vivo* experiments and all members of the Hopfner group for a nice and stimulating atmosphere at work.

I thank Heidi Feldmann for performing telomere assays and invaluable support in planning experiments in *S. cerevisiae*.

I would like to express my appreciation to Vincenzo Costanzo for hosting me in his laboratory in Clare Hall, South Mimms, and giving me a chance to work with the *Xenopus laevis* egg extract system. My thanks go also to Esben Lorentzen and Harald Dürr for being part of my Thesis Advisory Committee and providing me with support and advice.

I deeply thank my family in Poland and all my friends. I cannot imagine pulling through without you!

Finally, my special thanks go to Marcelino; I cannot emphasize enough how much I appreciate your patience, caring and support. Thank you for standing by me, you are absolutely the best.